AD-A070 994 NOTTINGHAM UNIV (ENGLAND) DEPT OF METALLURGY AND MAT--ETC F/G 11/6
METALLURGICAL CHANGES IN THE HIGH TEMPERATURE FRETTING OF NI AN--ETC(U)
FEB 79 R B WATERHOUSE, M M HAMDY DAJA37-75-R-0649

UNCLASSIFIED NL

1 OF 2
AD A070994

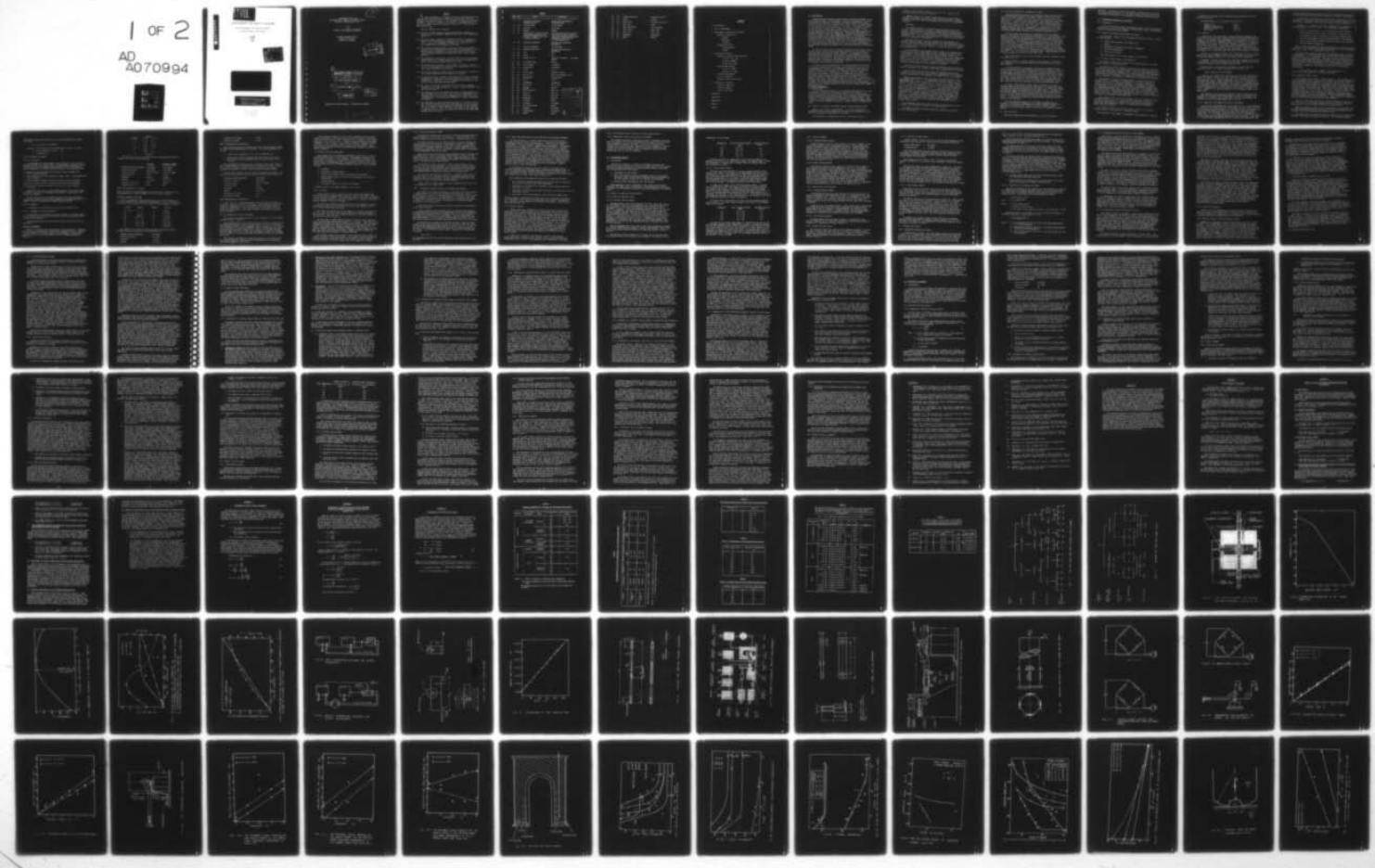

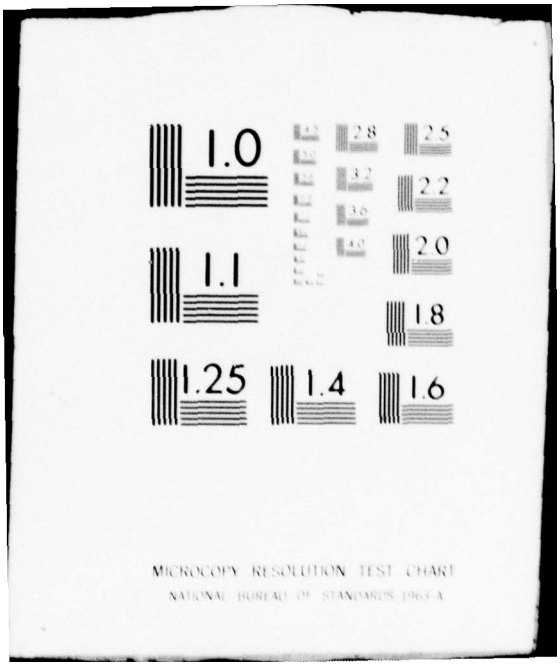
1.0
1.1
1.25
1.4
1.6
2.8
3.2
3.6
4.0
2.5
2.2
2.0
1.8
MICROCOPY RESOLUTION TEST CHART
NATIONAL BUREAU OF STANDARDS 1963-A

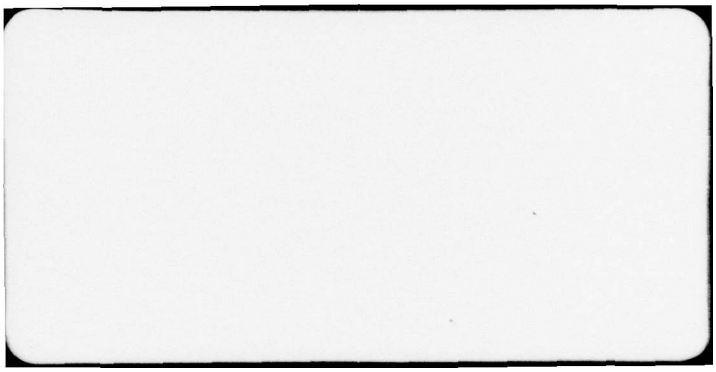

(11)

Department of the Army
Army Materials & Mechanics Research Center
Watertown, Massachusetts 02172

(15) Contract Number DAJA37-75-R-0649

European Research Office
United States Army
London W.1., England

(6) METALLURGICAL CHANGES IN THE HIGH TEMPERATURE FRETTING OF Ni and Ti ALLOYS,

(9) Final Technical Report,

by

(10) R.B. Waterhouse and M.M. Hamdy

(11) February 1979

(12) 149 p.

Approved for public release; distribution unlimited

SUMMARY

The report describes an investigation into the fretting-fatigue and fretting wear of two materials: Ti-6Al-4V, of which there were two supplies from different sources - IMI and AMMRC, and Inconel 718 supplied by AMMRC. Tests were carried out in normal air at temperatures up to 600 C in the case of the IMI Ti-6Al-4V, and up to 700 C in the case of the Inconel 718.

The main findings are as follows:

(1) The plain fatigue strength, the fretting-fatigue strength, and fretting wear of Ti-6Al-4V (AMMRC) are the same at room temperature and 100 C.

(2) The plain fatigue strength of Ti-6Al-4V (IMI 318) is reduced by a factor of 3.3 on raising the temperature from room temperature to 600 C. The fatigue strength is reduced by a factor of 5.1 at room temperature by the presence of fretting.

(3) The fretting-fatigue strength of Ti-6Al-4V (IMI 318) is reduced slightly as the temperature is raised from room temperature to 600 C. This reduction is thought to be due to the deterioration in the fatigue strength rather than any specific effect on the fretting behaviour.

(4) The fretting-wear behaviour of Ti-6Al-4V (IMI 318) does not change significantly as the temperature is raised from room temperature to 600 C. No evidence of glaze formation is found.

(5) The plain fatigue strength of aged Inconel 718 rose by a factor of 1.2 as the temperature was raised from room temperature to 540 C. At 700 C creep interfered with the tests.

(6) The fatigue strength of aged Inconel 718 was reduced by a factor of 2.3 at room temperature in the presence of fretting.

(7) The fretting-fatigue strength of aged Inconel 718 was not altered by increasing the temperature from room temperature to 280 C, but was increased by a factor of 2.1 as the temperature was raised to 540 C. At 700 C creep interfered with the tests.

(8) The lives of specimens of aged Inconel 718, tested in fretting-fatigue at 280 C, were increased by a factor of ten at stresses above the fatigue strength.

(9) The fretting wear of aged Inconel 718 showed a marked decrease at a slip amplitude of 40 μm at 280 C and at all slip amplitudes at 540 C compared with the wear at room temperature and at 280 C at 10 μm slip amplitude. The changes were mirrored in a reduced coefficient of friction.

(10) The improvement in fretting-fatigue strength of aged Inconel 718 at 540 C and the increased life in fretting-fatigue at 280 C, together with the reduction in wear damage, are attributed to the formation of a glaze oxide. At 540 C the glaze oxide forms at all amplitudes of slip, but at 280 C the glaze oxide only forms at slip amplitudes greater than 20 to 22 μm.

ERRATA

Page	Line	Error	Correction
2	9	having two different microstructures	having some difference in microstructure
2	47	in this range	in the range
3	35	was room	were room
6	40	prings	prongs
8	9	IMI 318 was in the hot rolled and annealed condition and Ti-6Al-4V (AMMRC) was in the β worked condition.	The two alloys were in the hot rolled and annealed condition with the following physical and mechanical properties for 9.5 mm diameter rod:
8	36	physical properties	physical and mechanical properties
9	4	the two specimens	the specimens
9	16	physical properties	physical and mechanical properties
9	29	Mo C	M_6 C
13	15	three	two
13	20	lines 20 to 24	delete "3. Surface ... fretting parts"
14	19	the table below	table 6
14	23	in the table	in table 6
15	8	conclusions	conclusion
17	2	35 mm	35 μm
17	8	at 10 cycles	after one cycle
17	28	scar to be	scar on the sphere to be
18	17	demonstrate	demonstrates
18	21	10 mm	10 μm
19	34	increased.	increased,
19	38	10^4 to 10^5	10^4 to 10^6
20	28	depends	depend
21	19	28°C tested at	280 C at
21	40	plate 14	plate 12
21	41	plate 12	plate 14
22	33	specimens	specimen
23	26	of while	while
26	44	in higher	at higher
28	42	into small flakes	delete
30	5	fragment	fragments
31	11	corresponded	correspond
31	23	Partlo	Bartlo

36	55	Figures 60 and 61	Figures 44 and 45
37	10	early	steady
38	13	their alloy	the alloy in ref. 23
38	22	the creep	creep
39	4	This conclusion	The conclusion
39	13	>550 ± 260	≥550 ± 260
39	14	<550 ± 215	≤550 ± 215
43	33	condition	conditions
44	41	Partlo	Bartlo

CONTENTS

1. Introduction

Complex machines comprise a large number of separate components in contact with each other. If the machine is subject to vibration or if certain of the parts are cyclically stressed it is possible that periodic small relative movement typical of fretting will occur at areas of contact unless this has been foreseen and overcome in the design. The result of fretting is the production of wear debris which if it escapes can lead to loss of fit and may also initiate wear in other parts of the machine. A more serious consequence is the initiation of fatigue cracks which may propagate causing failure of one of the components. Fatigue strength reduction factors of between 2 and 3 are common where fretting is concerned, and they tend to be higher for the high strength materials. In the authors' experience with a wide variety of materials from high strength steels to titanium alloys the fatigue strength at 10^7 cycles at room temperature when fretting is present is usually in the region of 150 MN/m^2 although the UTS may be between 800 and 1200 MN/m^2 (1,2). In practice surface treatments are applied to overcome the problem if it cannot be dealt with at the design stage.

At elevated temperatures in oxidising atmospheres oxide films on metal surfaces grow to greater thicknesses and generally have good protective properties where they are not unduly stressed. The suggestion has been made that they may constitute an effective surface treatment in reducing the effects of fretting (3). There is some evidence that fretting wear is reduced on mild steel as the temperature is raised to 500 C (4,5,6), but there is little information on the fatigue behaviour of materials at high temperatures in the presence of fretting.

The most important components in a gas turbine engine are the rotor discs and the turbine blades attached to their peripheries which operate at temperatures up to 600 C in an oxidising atmosphere. The blades are fixed to the disc by dove-tail or fir tree roots and therefore involve contact in this region. Vibration in a rotating disc is a common experience and fretting in the fixings of turbine blades is not unknown. In certain engine designs the disc is bolted to the main shaft via a flange and fretting is also possible under the bolt heads. Initiation of fatigue cracks in the disc at these areas can lead to catastrophic failure of the disc. With these considerations in mind and with the general absence of information on high temperature fretting-fatigue the following investigation was carried out on two alloys, Inconel 718 and Ti-6Al-4V, which are of interest in these applications.

2. Plan of experiments

2.1 Introduction

As one of the main objectives of the present investigation is to study the effect of fretting on the fatigue properties of two alloys, i.e. Ti-6Al-4V and Inconel 718, and how this effect changes with temperature, a series of fretting fatigue tests as well as plain fatigue tests have been conducted to try and elucidate the mechanisms of fretting fatigue. Also, to obtain a better understanding of the processes occurring during fretting fatigue it has been decided to carry out a further series of fretting wear tests.

2.2 Choice of variables for fretting fatigue and plain fatigue tests

There are two series of experiments, the first was performed to construct fretting fatigue curves, and the second was conducted to obtain plain fatigue curves in the absence of fretting.

The experimental schedule given in Fig. 1 summarises the plain

fatigue and the fretting fatigue tests carried out. Details of the testing conditions are given in Table 1.

Number of cycles to failure and amplitude of slip were chosen as dependent variables, whereas mean stress, alternating stress, clamping pressure, test temperature and microstructure were chosen as independent variables.

Materials

Two different batches of Ti-6Al-4V alloy have been used in this series of tests, having two different microstructures and mechanical properties. The first batch was supplied by Army Materials and Mechanics Research Center, U.S.A., and the second one was supplied by Imperial Metal Industries, U.K. The first will be referred to as AMMRC and the latter as IMI 318 in the present investigation.

One batch of Inconel 718 alloy, supplied by Army Materials and Mechanics Research Center, has been tested in the aged condition, as this is the usual condition used in practice, but some tests have been conducted on the material in the annealed condition to study the effect of varying the microstructure.

The mean stress for the fretting fatigue tests at all testing temperatures and for plain fatigue tests at 600 C conducted on IMI 318 alloy was 247 MN/m^2. It was found impossible with the above conditions to obtain fatigue curves in the absence of fretting at any of the temperatures below 600 C. For this reason, the mean stress was increased to enable plain fatigue curves to be obtained. An adjustment for the fatigue strength has been made to enable a comparison between the fatigue and fretting fatigue results at a mean stress of 247 MN/m^2.

The mean stress for the plain fatigue and fretting fatigue tests conducted on Ti-6Al-4V alloy (AMMRC) at all testing temperatures was 400 MN/m^2.

The mean stress for the plain fatigue and fretting fatigue tests conducted on Inconel 718 alloy at all testing temperatures in the annealed condition was 256 MN/m^2, but increased to 550 MN/m^2 in the aged condition.

Testing temperatures for Ti-6Al-4V alloy (IMI 318) were varied from room temperature to 600 C. Four temperature levels were used, i.e. room temperature, 200, 400 and 600 C (273, 473, 673, 873 K). Testing temperatures for Ti-6Al-4V alloy (AMMRC) were room temperature and 100 C (293 and 373 K). Testing temperatures for Inconel 718 alloy in the aged condition were varied from room temperature to 700 C. Four temperature levels were used in the present investigation, i.e. room temperature, 280, 540 and 700 C (293, 553, 813 and 973 K). For Inconel 718 alloy in the annealed condition tests have been conducted at room temperature and 600 C (293 and 873 K). It should be pointed out that 600 C for the titanium alloy and 700 C for Inconel 718 alloy are above the maximum temperatures at which they would normally be used. However, they were chosen to give a clear picture of the effects of raising the test temperature and to magnify these effects.

The alternating stress was varied in order to give numbers of cycles to failure in this range of 100,000 to 10 million cycles.

The clamping pressure has been chosen to be 32 MN/m^2 for all the fretting fatigue tests.

2.3 Choice of variables for fretting wear tests

Many fretting wear tests have been conducted using such contact surface configurations which gave very small initial contact area at the start of the test compared to the final contact area at the end of the fretting test. Moreover, the normal contact loads applied in those tests were small. These two factors resulted in a very high ratio of the initial nominal mean contact pressure at the start of the fretting test to the final pressure at the end of the test. In some cases this ratio ranged between 250 and 750. Consequently, a large portion of the test duration, possibly more than 50% of the test duration, was run at very low nominal mean contact pressure far away from the presumed value.

For this reason, and because it was decided to use such contact surface configurations in the present investigation, i.e. hemispherical ended rider on flat surface; the first series of tests was carried out using different radii for the hemispherical end of the rider and fixing all the other variables. The objective of this series of tests was to determine the optimum radius of the hemispherical rider which would give the minimum ratio of the initial nominal mean contact pressure at the start of the test to the final pressure at the end of the test and which would result in a mean pressure throughout the test as near as possible to the required test pressure. Also as a result of these tests it was possible to determine the normal load to be used in the subsequent tests. These preliminary tests have been conducted on Ti-6Al-4V alloy (IMI 318).

The second series of tests is the fretting wear tests, details of which are shown in Fig. 2.

Due to shortage of material tests were only conducted on Ti-6Al-4V alloy (AMMRC) in the as-received condition and Inconel 718 alloy in the aged condition.

To correlate fretting wear results with those in fretting fatigue some of the variables in the fretting wear tests were chosen to be the same as those found in the fretting fatigue tests. So, the frequency in the fretting wear tests was 50 Hz. As the slip amplitude value (peak to peak) in the fretting fatigue tests varied between 10 and 36 μm, Table 2, it was decided to use two levels for the amplitude of slip, i.e. 10 and 40 μm. The testing temperatures for Ti-6Al-4V (AMMRC) was room temperature and 100 C (293 and 373 K) and for Inconel 718 alloy room temperature, 280 and 540 C (293, 553 and 813 K), the same as in the fretting fatigue tests.

The shape of the fretting fatigue curves determined the number of fretting cycles chosen in the fretting wear tests. Two values for number of cycles were chosen corresponding to the highest and lowest (knee point) alternating stress levels in the fretting fatigue curves. According to this base the number of fretting cycles chosen for the titanium alloy was 10^5 and 3.5×10^6 cycles and for Inconel 718 alloy was 8×10^4 and 10^6 cycles. To gain some knowledge about the processes involved in the early stages of fretting tests, additional tests have been conducted for 6000 cycles on both materials.

Since the processes involved in the fretting mechanism such as adhesion, cold welding at asperities, and debris accumulation should be reflected in the coefficient of friction, it was decided to study coefficient of friction under dynamic conditions as a function of number of cycles.

2.4 Data collection

Data were obtained through experiments for the above mentioned

variables. Observations between the dependent variables and the independent ones were conditional, i.e. data were recorded for variations in one independent variable while other independent variables were kept constant.

3. Experimental equipment and specimens

3.1 Introduction

As it was decided to conduct two different types of test in the present investigation, i.e. fretting fatigue and fretting wear tests, two completely different arrangements were prepared.

3.2 Fatigue and fretting fatigue tests arrangement

The principal elements of the arrangement are shown in Plate 1. These elements include:

1. Fatigue testing machine and dynamometer
2. Furnace
3. Temperature measurement and control arrangement
4. Fretting fatigue device
5. Specimen and bridges.

The detail description of these elements is given below.

3.2.1 Fatigue testing machine and dynamometer:

The fatigue testing machine used for this investigation is the Avery Midget Pulsator, a push-pull machine.

The components of the machine are assembled on a rigid cast iron base. The machine is driven by an electric motor. The motor drives an eccentric with an adjustable throw, linked in turn by means of a connecting rod to an elastic leaf spring which transfers, via a moving headstock, the alternating load produced to the specimen. The value of the alternating load can be varied, according to requirements, by adjusting the driving motor eccentric.

The specimen is secured by suitable grips at one end to the moving headstock and at the other to the dynamometer. The latter comprises an elastic steel ring and a reading microscope. The amount of load being applied at any time is indicated by the amount of dynamometer deflection. The deflection is indicated by a narrow band of light which is superimposed on a magnified graduated scale within the microscope. A calibration chart supplied with the machine allows the microscope reading to be converted into actual load units. A calibration curve has been done on a Mayes testing machine and it was found that the difference between the obtained calibration and that of the supplier is only about 0.5%.

The dynamometer is secured to a crosshead which can be displaced along the machine base by means of a screw and crank mechanism. This device allows the application of a constant static pre-load, either tensile or compressive, and furthermore, allows the accommodation of specimens of widely differing lengths.

An automatic cut-off switch is incorporated adjacent to the moving headstock and this will operate if a specimen breaks.

The indication of the number of reversals of load applied to a specimen

is indicated on a counter which is mounted on the driving motor at the rear of the machine.

The specifications of the machine are as follows:

Maximum load	3000 N
Maximum pulsating load	1500 N
Minimum pulsating load	110 N
Motor speed	3000 rpm

3.2.2 Furnace:

A furnace has been constructed to surround fatigue specimens being tested in the Avery push-pull fatigue testing machine with fretting bridges clamped to the specimen. The experiments have been conducted in ordinary laboratory air, with no atmosphere control. The furnace is a cylindrical one provided with a hole at its centre parallel to its axis to accommodate the specimen and bridges. The furnace is split longitudinally into two halves. The furnace has a radial hole at the midway of its length which is perpendicular to the first hole. The radial hole is used to accommodate the prongs of the proving ring which hold the bridges against the specimen.

Figure 3 is a schematic drawing of the furnace and Plate 2 is a photograph of the furnace assembly with the top half removed, showing the specimen with the bridges clamped on to it by means of the proving ring.

The furnace is heated by means of two resistance elements in each half of the furnace. The four heating elements are made of Ni-Cr alloy and are connected in series to give an output power of 1 kW.

The two halves of the furnace are tightened together with four tightening screws. The outside dimensions of the furnace are:

110 mm diameter and 90 mm length

Initially, the furnace main outside body was made from sindanyo (heat insulating material) backed with heat insulating wool, while the inside surface and the two flat faces of each half of the furnace were made of stainless steel sheet. Careful temperature surveys in both longitudinal and radial directions revealed that at 600 C there was a variation of 34 C over the gauge length of the specimen. Relocation of the heating elements and replacement of the two stainless steel panels by sindanyo panels has reduced the temperature variation over the gauge length to within 3 C at 600 C. Figures 4 to 7 show the results of the temperature surveys after improvement.

The furnace is supported by an adjustable support which allows its position with respect to the specimen when the latter is clamped on the machine to be adjusted in such a way that no contact exists between the specimen or the proving ring prongs and the furnace.

3.2.3. Temperature measurement and control arrangement:

Initially the arrangement used was as shown in Fig. 8. The thermocouple is chromel-alumel which is inserted in the furnace so that the hot junction is very near to the left-hand foot of the fretting bridge. The induced emf from the thermocouple is recorded by a temperature measuring recorder (Speedomax). The terminals of the thermocouple are also connected to a control unit to cut off the electrical power supplied to the heating elements of the furnace when the specimen reaches the test temperature. Also there is a cut-off switch superimposed over the automatic cut-off switch of the

fatigue testing machine and this will operate if a specimen breaks to cut off the electrical power supplied to the heating elements of the furnace.

Unfortunately, this arrangement suffered from a fluctuation in the test temperature. For example, when the control temperature was adjusted to 300 C, the recorded temperature of the specimen fluctuated between 250 and 350 C.

Accordingly, a modification has been introduced in the arrangement. The new arrangement is shown in Figure 9. The modification consists of:

1. Using two thermocouples, one for temperature control which is located radially at the midway of the furnace length with the hot junction as near as possible to the heating element, while the second thermocouple records the temperature of the specimen.
2. Using a variac which controls the input voltage to the furnace to suit the testing temperature.

This modified arrangement reduced the fluctuation in the test temperature to ± 1 C for different test temperatures ranging from room temperature up to 400 C, and ± 2 C for temperatures above 400 C.

The temperature recording instrument was calibrated using a millivolt potentiometer. An emf corresponding to a certain temperature was applied to the Speedomax and the Speedomax reading was recorded. This step was repeated at different temperatures. The emf vs temperature table was taken from the National Bureau of Standards, Circular 561. Emf is expressed on the international temperature scale of 1948. The table used is for reference junction 0 C, so a compensation for room temperature was made before starting the calibration. The calibration resulted in the following relationship:

Recorded temperature = 0.996384 x true temperature + 4.7

where the two temperatures are in degrees centigrade.

3.2.4. Fretting fatigue device:

The fretting fatigue device is shown in Plate 3. The fretting was produced by clamping a pair of bridge pieces 19 mm in length and 3.5 mm wide, each having two feet of dimension 1.5 x 3.5 mm (Figure 10) which were machined from the same material as the specimen and had the same heat treatment condition, and were given the same surface finish on the gauge length of the specimen. The bridges were clamped on to the prepared flats of the specimen by means of a proving ring. The clamping load was applied by means of screwed prongs along one diameter of the ring and measured by the resulting contraction of the perpendicular diameter. Steel balls pressed into the outside of the ring at either end of this perpendicular diameter served as measuring points for a micrometer. Plate 3 shows the proving ring with the prings holding the bridges on to the specimen.

Since the proving ring was located outside the furnace it was made of mild steel, but the prongs were inserted inside the furnace and therefore they were made of creep resistant material - Nimonic 90 alloy.

When the specimen was stressed by a sufficiently high alternating load, tangential movement between the bridge feet and the flat surfaces of the specimen results, which produces the fretting action.

The proving ring was calibrated with dead weights and its diameter was measured. The results are shown in Figure 11. The calibration showed a

linear relationship between applied load and the proving ring diameter as follows:

$$D = D_o + 0.00372 - 0.0005789\ P$$

where D_o = ring diameter at room temperature and zero load in mm.

D = ring diameter at load P, mm

P = clamping load, N

3.2.5 Specimen and bridges

3.2.5.1 Specimens:

The specimens are machined from 4.76 mm diameter rod and they have a length of 150 mm. The centre portion of the specimen, as shown in Plate 3 and Figure 12, has two parallel flats machined on it of 28 mm minimum length, reducing the thickness over this section to the following values:

1.56 mm for all Ti-6Al-4V (IMI 318) fretting fatigue specimens and 600 C fatigue specimens,

0.7 mm for Ti-6Al-4V (IMI 318) fatigue specimens tested at room temperature, 200 C and 400 C,

0.8 mm for Ti-6Al-4V (AMMRC) fatigue and fretting fatigue specimens,

0.5 mm for all tests conducted on Inconel 718 alloy (aged condition),

1.6 and 1 mm for all tests conducted on Inconel 718 alloy (annealed condition).

The ends of the flats are given a 50 mm radius to avoid abrupt change in section. The ends of the specimen are threaded to secure it in the grips of the machine.

Due to the shortage in the materials some of the room temperature Inconel alloy 718 and Ti-6Al-4V alloy (AMMRC) have been made with the flat portion = 12 mm in length and the overall length was 92 mm.

3.2.5.2 Bridges:

A description of the bridges has been given in Section 3.2.4.

3.2.5.3 Specimens and bridges material:

It was decided to fret bridges against specimens of the same material. Also the bridges had the same heat treatment and the same surface finish as those of the specimen.

The materials used in this investigation were Ti-6Al-4V and Inconel alloy 718,

3.2.5.3.1 Ti-6Al-4V .

This α - β titanium alloy was supplied by two suppliers: 1) Imperial Metal Industries (Kynoch) Ltd. (Birmingham), commercially known as IMI 318 2) Army Materials and Mechanics Research Center (AMMRC), both of them in the form of 9.5 mm and 4.7 mm diameter rods, the chemical analysis of which is:

Element	Weight % 9.5 mm	4.7 mm
Al	6.35	6.47
V	4.24	4.15
Fe	0.08	0.05
H	0.003	-
O	0.17	<0.2
Ti	balance	

IMI 318 was in the hot rolled and annealed condition and Ti-6Al-4V (AMMRC) was in the β worked condition.

	IMI 318	Ti-6Al-4V (AMMRC)
Ultimate tensile strength*	1037 MN/m^2	1126 MN/m^2
0.2% proof stress*	966 MN/m^2	1015 MN/m^2
Elastic modulus	106 x 10^3 MN/m^2	106 x 10^3 MN/m^2
Poisson's ratio	0.361	0.361
Hardness*	321 VHN	336 VHN
Density	4.42 g/cm^3	4.42 g/cm^3
Elongaton in 25 mm*	20.6%	20.2%
Reduction in area *	47.4%	46%

NOTE: *Experimentally determined.

Plates 4a-d show the microstructure of the IMI 318 while Plates 5a-d show microstructure of Ti-6Al-4V (AMMRC) in the as received condition.

3.2.5.3.2 Inconel alloy 718:

This is a nickel-base alloy which was supplied by Army Materials and Mechanics Research Center, Watertown, Massachusetts, U.S.A., in the form of 9.5 mm and 4.7 mm diameter rods, the nominal chemical analysis of which is:

Element	Weight %	Element	Weight %
Ni (plus Co)	50 - 55	Co	1.0 max
Cr	17 - 21	C	0.08 max
Fe	Balance	Mn	0.35 max
Nb	4.75 - 5.5	Si	0.35 max
Mo	2.8 - 3.3	P	0.015 max
Ti	0.65 - 1.15	S	0.015 max
Al	0.2 - 0.8	B	0.006 max

The material was in the hot formed and annealed condition with the following physical properties for 9.5 mm diameter rod:

Ultimate tensile strength*	968 MN/m^2
0.2% proof stress*	515 MN/m^2
Hardness*	273 VHN
Density	8.19 g/cm^3

Elongation in 25 mm*	49.9%
Reduction in area*	46.3%

NOTE: *Experimentally determined.

The majority of the two specimens were given a heat treatment process to develop the maximum mechanical properties. The heat treatment was as follows:

1. Solution heat treatment at 954 C for one hour/air cool.

2. Aged at 718 C for 8 h, furnace cooled at the rate of 15 C/h to 620 C, held at this temperature for total ageing time of 18 h, air cool.

This treatment was carried out in a horizontal tube vacuum furnace. Only a limited number of specimens could be treated at any time. A probe was put with each batch and was sectioned and examined for internal structure and hardness in order to check the heat treatment process.

The same heat treatment was used for both specimens and bridges. The final physical properties of the heat treated 4.7 mm rod were as follows:

Ultimate tensile strength*	1316 MN/m^2
0.2% proof stress*	1072 MN/m^2
Elastic modulus	200×10^3 MN/m^2
Poisson's ratio	0.294
Hardness*	450 VHN
Density	8.22 g/cm^3
Elongation in 25 mm*	15.5%
Reduction in area*	40%

NOTE: *Experimentally determined.

Plates 6a,b show the microstructure of Inconel alloy 718 in the aged condition. Plates 6c,d show the difference in microstructure between the as received (annealed) and the aged condition when they were etched to reveal the precipitates. It is noticeable that Ni_3Cb, Laves CbC and MoC phases were precipitated at the grain boundaries and inside the grains in the aged material.

3.2.5.4 Specimen and bridge preparation

The bridges were machined from the 9.5 mm diameter rod to the required dimensions given in Figure 10.

The specimens were cut from the supplied rods into the required length. They were then threaded at their ends and milled to produce the parallel flat surfaces according to the thicknesses given in Section 3.2.5.1 but were 0.3 mm oversized as a grinding allowance. Most of the Inconel 718 specimens were then treated (see Section 2.2) according to that heat treatment given in Section 3.2.5.3.2. After heat treating the Inconel 718 specimens, the flat surfaces of both the Ti-6Al-4V and the Inconel alloy 718 specimens were ground.

The specimen flat surfaces and the feet surfaces of the bridge were then polished through a series of silicon carbide papers of successively increasing fineness up to 600 grid.

Final surface preparation was left until specimens and bridges were required for testing. This preparation consists of polishing the surfaces with 0 and 00 grade emery paper. This stage of preparation gave a surface roughness of 0.1 μm as C.L.A. on a surface roughness measuring instrument (Talysurf). Care was taken to ensure that all visible scratches were removed so as not to provide possible sources of fatigue failure. After that both the specimen and bridges were thoroughly degreased by washing in trichloroethylene.

3.3 Fretting wear test arrangement

The fretting rig was originally constructed by Overs (7) as a cross-cylinders fretting rig, but was adapted for the present investigation to fret a spherical rider on a flat specimen. The modified arrangement has the facility of measuring and recording the friction force as well as the normal contact load simultaneously. The principal elements of the arrangement are shown in Plate 7 and schematically in Figure 13. Those elements include:

1. Specimens
2. Oscillating movement system
3. Oscillating movement control and measuring arrangement
4. Normal contact force and friction force measuring and recording arrangement
5. Heating furnace.
6. Temperature control and recording arrangement.

A detailed description of these elements is given below.

3.3.1 Specimens

It was decided to fret a spherical rider against a stationary flat plate specimen of the same material, with the same heat treatment condition, and the same surface finish. The oscillatory motion of the rider was parallel to the polishing direction of the flat specimen, i.e. parallel to the longitudinal direction of the flat specimen.

The flat plate specimen was machined from 9.5 mm diameter rod and was 50 mm long, 9 mm wide and 3 mm thick. It had two holes drilled in it to fix it in the stainless steel support.

The rider was machined from 9.5 mm diameter rod with a screw thread at one end to fix it into the transmission shaft, and a spherical surface of 100 mm radius at the other end. Detailed drawings of the flat specimen and the rider are shown in Figure 14.

The flats were polished through a series of silicon carbide abrasive papers of successively increasing fineness up to 600 grid. The final surface preparation was left until they were required for testing. This preparation consisted of polishing the surfaces with 0 and 00 grade emery paper. This stage of preparation gave a surface roughness of 0.1 μm as C.L.A. on a surface roughness measuring instrument (Talysurf). Care was taken to ensure that all visible scratches were removed. Finally the flat specimen was thoroughly degreased by washing in trichloroethylene.

The spherical surface of the rider tip was given the same polishing and cleaning procedure as the flat specimen. The polishing was done by placing it in the chuck of a bench drill and it was rotating at 2400 rpm whilst carefully polishing it by hand, taking care not to damage its profile.

3.3.2 Oscillating movement system

This system was constructed to produce oscillatory tangential relative motion between the rider and the flat specimen. A close-up view of the system is shown in Plate 8 while Figure 15 shows a detailed drawing of it.

The system consists of a bent shaft holding at one end the rider and rigidly connected at the other end to the driving spindle of a Goodman's electromagnetic vibration generator, Model 390A. A power amplifier with a built-in, low distortion oscillator drives the vibration generator and so produces the oscillatory motion of the driving spindle, which is transmitted via the transmission shaft to the rider.

Eight strain gauges were fixed on the transmission shaft to measure the frictional force as well as the normal contact force. The shape of the shaft enabled the point of application of the tangential frictional force between the rider and the flat specimen to be aligned with the main centre line of the shaft and the driving spindle.

The transmission shaft was hollow to allow cooling water to pass through it so as to avoid overheating of the shaft and the strain gauges. It reduced the shaft cross-sectional area in the strain gauged zone which allowed measurement of very small forces. Because one end of the shaft was inserted inside the furnace, it was made of stainless steel.

The vibration generator was supported on a horizontal hinged support which could tilt it in a vertical plane to the required position via an adjusting screw and nut mechanism. By this vertical movement the normal contact load could be easily and accurately adjusted.

A steel plate was firmly attached to the transmission shaft to provide a gap between it and a fixed probe.

3.3.3. Oscillating movement control and measuring arrangement

The vibration generator was driven by a Ling Altec 5 VA power oscillator which enabled two of the main variables in fretting wear tests to be controlled, i.e. amplitude of relative motion and frequency. All the tests were performed at 50 Hz, i.e. the same frequency as that previously used in the fretting fatigue tests, see Section 2.3. The frequency was checked by means of a stroboscopic light. Two amplitudes of motion were used, 10 μm and 40 μm, see Section 2.3.

A Wayne Kerr vibration meter model B731B was used for the measurement of the slip amplitude.

A probe connected to the vibration meter was brought into proximity with the steel plate attached to the transmission shaft and the capacitance so formed was displayed in terms of distance and peak to peak vibration amplitude on the two meters of the instrument. The two measurements were not interdependent, i.e. the accuracy of measurement of distance was unaffected by variation in vibration amplitude, within limits, and vice versa.

A calibration was carried out to find the relation between the meter reading and the actual amplitude of motion at the rider. This was done by measuring simultaneously the amplitudes at the steel plate, x_1 μm, and at the end of the transmission shaft near the rider, x μm when the shaft was oscillating. The calibration results showed a straight line relationship as follows:

$$x_1 = 1.09\ x$$

This difference has been taken into consideration when adjusting the slip amplitude.

3.3.4 Normal fore and friction force measuring and recording arrangement

In order to decide on a normal contact force and frictional force measuring method, the usual considerations of sensitivity and independent measurements of both of them were considered. Wire electrical strain gauges offer a convenient means of meeting these requirements. Furthermore, electrical strain gauges make it possible to record forces as a function of time, which in addition to being convenient becomes a real necessity in those instances where forces fluctuate. For these reasons eight electrical resistance wire strain gauges were bonded to the outer cylindrical surface of the transmission shaft at the part where it has a reduced cross-sectional area as shown in Figure 15. The relative position of the strain gauge axis to the transmission shaft axis (Figure 16), and the way in which they were electrically connected in the bridge circuits (Figure 17), enabled them to measure, simultaneously and independently, the frictional force and the normal contact load between the rider and the flat specimen. Further detail of this is given in Appendix A.

As illustrated in Figure 13 the output signals of the strain gauge measuring instrument were amplified using a multi-channel amplifier and fed to a U-V recorder (direct recording Visicorder oscillograph Model 2106). This arrangement provided a means for recording continuously and simultaneously the friction force as well as the normal contact load.

Many calibrations and studies have been done to study the following:

1. The relationship between the normal contact force and the frictional force and the recorder light spot displacement.
2. The effect of the normal force variation on the recorded frictional force and vice versa.
3. The effect of raising the specimen temperature on the recorded normal and frictional forces.
4. The effect of the inertia force on the friction and normal forces.

Details of these calibrations and studies are given in Appendix B illustrating the convenience of this measuring and recording arrangement for the present work. Typical recorded charts for the friction force during a fretting test are shown in Plates 9a,b.

3.3.5 Heating furnace

A furnace previously constructed by Overs (7) was used to surround the rider and the flat specimen during the high temperature fretting wear tests. The furnace was a vertical shaft type one closed from the top side as shown graphically in Figure 26. A slit was cut into the furnace wall to accommodate the transmission shaft. Alumina cement was used to face the sides of this slit and a coating of sodium silicate sealed the pores in the cement preventing any contamination from dust particles. The inside of the furnace was dome-shaped and constructed from a fused alumina tube. This provided an excellent dust-free enclave. A heating element (Pyrobar) of 3 kW capacity was wound around the dome. The outer wall of the furnace was constructed from aluminium sheet while the top and bottom sides of it were closed by sindanyo heat insulating material. The inner space between the dome and the outer surface was filled with heat insulating wool (Triton Kao wool ceramic fibre).

To reduce heat transfer to the vibration generator and the strain gauges during high temperature tests, cooling water was passed through the transmission shaft. At 540 C test temperature the temperature at the outer

wall of the furnace was 140 C and at the strain gauges was 60 C.

3.3.6 Temperature control and recording arrangement

The modified temperature measuring and control arrangement described before in Section 3.2.3 and shown graphically in Figure 9 was used in the high temperature fretting wear tests. The control thermocouple was located inside the fretting wear furnace with its hot junction as near as possible to the heating element, while the recording thermocouple was located with its hot junction as near as possible to the contact point between the rider and the flat specimen.

4. Experimental results

4.1 Introduction

The effect of fretting on Ti-6Al-4V and Inconel 718 alloys was determined by its influence on the fatigue strength and wear of the surface. Fatigue was studied by applying a fluctuating axial tensile stress while wear was investigated by three means:

1. Measurement of wear volume.
2. Use of the scanning electron microscope as well as the optical microscope which allowed study of fretting surface topography in both the fretting fatigue and the fretting wear specimens.
3. Surface profile measurements using the Talysurf.

Other techniques such as sectioning of the surface, microhardness traverses, TEM, EBMA, X-ray diffractometry, Auger spectroscopy, give some information on the processes occurring in the surface layers of the fretting parts.

4.2 Fatigue and fretting fatigue results

4.2.1 Ti-6Al-4V (IMI 318) alloy

4.2.1.1 Fretting fatigue results

Fretting fatigue tests on the identical Ti-6Al-4V alloy (IMI 318) in the mill annealed condition have previously been conducted by Wharton (8) and repetition of those tests was unnecessary and inadvisable due to shortage of material. Tests were therefore conducted only at 200, 400 and 600 C. All specimens were tested at 247 MN/m^2 tensile mean stress and 32 MN/m^2 clamping pressure following the previously chosen values in the room temperature tests (8). The results obtained are shown graphically in Figure 27. Specimens tested at 600 C crept drastically but no creep was observed in the specimens tested at 400 C. Consequently, it was found impossible to run tests at 600 C for more than 10^6 cycles because of the creep effect. In any case this temperature would be considered too high for this material.

The two specimens which were tested at 200 C with alternating stresses more than 140 MN/m^2 have more cycles to failure than expected. This is due to the gross slippage which occurred in the first few cycles as shown in Plate 10.

The fretting fatigue strengths at 10^7 cycles and the strength reduction factors (based on the fretting fatigue strength of the alloy at room

temperature) are as follows:

Temperature °C	Fretting fatigue strength MN/m^2	Strength reduction factor
R.T.	247 ± 85	1.0
200	247 ± 77	1.1
400	247 ± 77	1.1
600	247 ± 70	1.2

Although the effect of temperature on the fatigue strength in the presence of fretting is not particularly marked, the results reveal a significant decrease in fatigue life at stresses above the fatigue limit as the temperature is raised.

4.2.1.2 Plain fatigue results

Ti-6Al-4V (IMI 318) specimens in the mill annealed condition were tested in the absence of fretting at room temperature, 200, 400 and 600 C. Unfortunately, it was found impossible to obtain plain fatigue curves at any of the temperatures below 600 C at the same mean stress used in the fretting fatigue tests, i.e. 247 MN/m^2. For this reason the mean stress was increased as the test temperature decreased to enable plain fatigue curves to be obtained. The results are shown in the table below.

To compare the fatigue and the fretting fatigue results, an adjustment for the fatigue results was made to determine the fatigue stresses at 247 MN/m^2 mean stress. This adjustment was made using the modified Goodman's law (see Appendix C) and the results are given in the table. At 600 C, the fatigue tests were conducted at 247 MN/m^2 mean stress, so no adjustment was necessary at this test temperature. S-N fatigue curves in the absence of fretting for the adjusted values of the strength at 247 MN/m^2 mean stress were produced as shown in Figure 28.

The plain fatigue strengths at 10^7 cycles and the strength reduction factors (based on the plain fatigue strength of the alloy at room temperature) are as follows:

Temperature °C	Plain fatigue strength MN/m^2	Strength reduction factor
R.T.	247 ± 430	1.0
200	247 ± 380	1.13
400	247 ± 295	1.45
600	247 ± 130	3.3

It seems from the results that there is a significant decrease in the plain fatigue strength as the temperature is raised. It should be pointed out that the specimens tested at 400 C experienced a small amount of creep, while those tested at 600 C crept drastically and for this reason the run out number of cycles was taken as 10^6 cycles for specimens tested at 600 C, otherwise the specimen would be subjected to compressive stress during part of the stress cycle. The high value of the strength reduction factor at 400 and 600 C is due to creep.

4.2.2 Ti-6Al-4V (AMMRC)

4.2.2.1 Fretting fatigue results

Fretting fatigue tests have been conducted on Ti-6Al-4V (AMMRC) in the as received condition at room temperature and 100 C. All specimens were tested at 400 MN/m^2 tensile mean stress and 32 MN/m^2 clamping stress. The obtained results are shown graphically in Figure 29. All the fretting fatigue results were somewhat scattered but appeared to lie on one curve. This leads to the conclusions that in the presence of fretting there is no distinction between the behaviour of this alloy at the two testing temperatures. The fretting fatigue strength at 10^7 cycles is 400 ± 83 MN/m^2. These results agree reasonably closely with those obtained for Ti-6Al-4V (IMI 318), see Section 4.2.1.1.

4.2.2.2 Plain fatigue results

Plain fatigue tests have been conducted on Ti-6Al-4V alloy (AMMRC) in the as received condition at room temperature and 100 C. All specimens were tested at 400 MN/m^2 tensile mean stress. The results obtained are shown graphically in Figure 29. These results reveal that there is no significant effect on the plain fatigue strength of the alloy as the temperature is raised from room temperature to 100 C. The plain fatigue strength at 10^7 cycles at the two testing temperatures is very similar, namely 400 ± 290 MN/m^2 at room temperature and 400 ± 283 MN/m^2 at 100 C. The strength reduction factor at 100 C, based on the plain fatigue strength of the alloy at room temperature is 1.02, which is in comparatively good agreement with the values obtained for IMI 318 alloy, see Section 4.2.1.2.

4.2.3 Inconel alloy 718 (annealed)

4.2.3.1 Fretting fatigue results

A few fretting fatigue tests were carried out on the material in its annealed condition at room temperature and 600 C as exploratory tests. The stressing conditions were a tensile mean stress of 256 MN/m^2 and a clamping stress of 32 MN/m^2. Few tests were conducted because this material is usually used in practice in the aged condition and also there was a shortage of material.

Figure 30 shows the results obtained. These results show an improvement in the fretting fatigue strength as the temperature is raised from room temperature to 600 C, although at higher stresses the fretting fatigue curve at 600 C approaches the room temperature one. The fretting fatigue strength at 10^7 cycles at 600 C seems to be around 256 ± 210 MN/m^2.

4.2.3.2 Plain fatigue results

No plain fatigue tests have been conducted on the material in the annealed condition due to shortage of material and because the material is usually used in practice in the aged condition.

4.2.4 Inconel 718 alloy (aged)

The Inconel 718 alloy was supplied in the annealed condition. It was decided to solution heat treat and age it to develop its maximum tensile and fatigue strength as this is the condition of the alloy in most practical cases. The heat treatment and the resulting properties are given in Section 3.2.5.3.2.

4.2.4.1 Fretting fatigue results

Fretting fatigue tests were carried out on the aged specimens at room temperature, 280, 540 and 700 C under the following stress conditions:

Tensile mean stress = 550 MN/m^2

Clamping stress = 32 MN/m^2

This high mean stress value was chosen so that the fatigue curves in the absence of fretting could be obtained with the same conditions, and consequently, comparison between the plain fatigue and the fretting fatigue results could be made.

One specimen only was tested at 700 C as creep of the specimen rendered determination of a complete curve impossible at this high temperature.

The results obtained are shown graphically in Figure 31. The curves in this figure show that the fatigue limit of aged Inconel 718 alloy in the presence of fretting at 10^7 cycles endurance is 550 ± 120 MN/m^2 at room temperature and 280 C. However, at stresses above this, the life at 280 C is approximately an order of magnitude greater than the life at room temperature. At 540 C, the fretting fatigue strength at 10^7 cycles is improved dramatically as it rises to 550 ± 250 MN/m^2, although at higher stresses the curve approaches the room temperature curve. This behaviour has the same trend previously found in the annealed alloy, see Section 4.2.3.1. The isolated result at 700 C lies between the 280 and 540 C curves.

4.2.4.1 Plain fatigue results

Plain fatigue tests have been carried out on the aged specimens at room temperature, 280, 540 and 700 C, under stress conditions the same as that for fretting fatigue tests, see Section 4.2.4.1. Two tests only were performed at 700 C because the specimens tended to creep at the higher alternating stresses.

The results obtained are shown graphically in Figure 31. These results show that all the plain fatigue results of tests carried out at elevated temperatures were somewhat scattered but appeared to lie on one curve giving a fatigue strength at 10^7 cycles of 550 ± 325 MN/m^2. The room temperature curve shows that the plain fatigue strength at 10^7 cycles is 275 MN/m^2, i.e. somewhat lower than the fatigue strength at the higher temperatures. The elevated temperatures curve shows longer fatigue lives at lower stresses than that of the room temperature one; however, at the higher stresses the fatigue lives of the room temperature specimens are longer.

On comparing the fretting fatigue results with the plain fatigue results, it was found that the fretting fatigue strength at 10^7 at 540 C (250 MN/m^2) approaches the room temperature plain fatigue strength at the same number of cycles (275 MN/m^2).

4.3 Fretting wear results

4.3.1 Preliminary fretting wear tests

As stated before in Section 2.3, preliminary fretting wear tests were conducted at room temperature to find the optimum radius of the spherical surface of the rider tip. The material used in these tests was Ti-6Al-4V alloy (IMI 318) in the annealed condition. The rider and flat specimen used are shown in Figure 14 but with the spherical radius for the rider

tip = 25, 50 and 100 mm. The tests were conducted with slip amplitude (peak to peak) = 35 mm. The normal load was 2.5 N.

After conducting the fretting wear tests, the projected area of the fretting scar was determined using an optical microscope. The results are shown graphically in Figure 32.

The initial pressure at the start of the test, which is the mean pressure calculated as given in Appendix D, has been considered in this diagram as the pressure at 10 cycles instead of at zero number of cycles. A compensation for this has been taken into consideration when the curves were drawn.

The results show that the optimum radius of the spherical surface is 100 mm as it gave the smallest ratio of initial pressure to final pressure. This gave an average value for the pressure throughout the test = 23 MN/m^2. Consequently, it has been decided to increase the normal load from 2.5 N to 2.75 N to get an average value for the pressure closer to the value used in the fretting fatigue tests. Also it was decided to use a rider tip with spherical surface radius = 100 mm in all the following tests. Obviously, larger radii approach the ideal case, i.e. flat on flat contact, but it was found difficult to use a larger radius than 100 mm as this has the following disadvantages:

1. It needs larger normal load to produce the same pressure, which may overload the vibration generator.

2. The location of the contact area is not guaranteed to be at the centre of the spherical surface of the rider tip.

4.3.2. Calculations for fretting wear tests

The effect of fretting on the material has been determined by measuring the volume of material removed from the rider or the flat specimen which was in the form of a spherical segment and assuming the wear scar to be completely flat. This volume was calculated using the formula

$$V = \frac{1}{6} \pi h (h^2 + 3r^2)$$

and $$h = R - \sqrt{R^2 - r^2}$$

where V = wear volume in mm^3

r = the scar radius in mm

R = the radius of the spherical surface of the rider tip = 100 mm.

The scar radius r was measured by means of an optical microscope and taking the mean value of four values of r, i.e.

$$r = \frac{r_1 + r_2 + 2 r_3}{4} \text{ mm}$$

where r_1 = the measured radius of the scar of the rider perpendicular to the slip direction

r_2 = the measured radius of the scar of the flat specimen perpendicular to the slip direction

r_3 = the measured radius of the scar of the rider parallel to the slip direction.

4.3.3 Fretting wear results of Ti-6Al-4V alloy (AMMRC)

This series of tests was conducted on the material in the as received condition at room temperature and 100 C at slip amplitudes of 10 and 40 μm. It has generally been noticed during these tests that the amplitude of slip was fluctuating in the first two minutes of the test. The amplitude value was frequently readjusted to keep it as close as possible to the specified value of the test. After the initial two minutes the slip amplitude became stable, but, during the test, as the number of cycles increased, the amplitude of slip increased. Readjustments were frequently made to keep the amplitude value constant.

The results obtained are shown graphically in Figures 34 and 35 which show the effect of the number of cycles and the amplitude of slip on the fretting damage determined by the volume of material removed. Both of the figures, at room temperature and 100 C, show that as the number of cycles increased, the fretting damage increased. This is true for the two slip amplitudes used in this series of tests. The series of plates (21-29) demonstrate this fact. These plates are optical pictures for the scars found on the flat specimens, the slip direction being parallel to the horizontal.

The small value for the amount of material removed from a specimen tested at 100 C with 10 mm slip amplitude is, for 3.5×10^6 cycles, due to leaving the test running overnight without observation and the next morning the amplitude of slip was found to be zero due to adhesion between the contact surfaces. It was difficult to determine when adhesion occurred. In the specimen tested at room temperature with 10 μm slip amplitude and for test duration of 6 000 cycles there were many tiny points of contact, as shown in Plate 21. This makes it difficult to calculate the volume of material removed, and accordingly, it has not been shown in Figure 34.

The results reveal that the slip amplitude has a significant effect on the fretting damage. As the slip amplitude is increased, the fretting damage increases. This is true for both testing temperatures, although it is more remarkable at room temperature as shown in Plates 21-26.

To demonstrate the effect of temperature on the fretting damage, the results were redrawn as shown in Figures 36 and 37. It can be seen that there is no significant effect on the fretting damage when the testing temperature was raised from 20 C to 100 C. This is true for both of the slip amplitudes used in this series of tests. This is demonstrated by Plates 24-29. The little difference observed at 10 μm slip amplitude, (Figure 36) is within the scatter of results.

4.3.4 Fretting wear results of Inconel 718 (aged)

This series of tests was conducted on the material in the aged condition at room temperature, 280 and 540 C using two slip amplitudes, 10 and 40 μm. It was generally noticed during these tests that the amplitude of slip fluctuated in the first two minutes of the test. The slip amplitude was frequently readjusted to keep it as close as possible to the specified value of the test. After the initial two minutes slip amplitude became stable, but, during the test, it was found, for all the tests conducted at room temperature and those conducted with 10 μm slip amplitude at 280 C, that as the number of cycles increased, the amplitude of slip decreased. Readjustments were frequently made to keep the slip amplitude constant.

The results obtained are shown graphically in Figures 38-40. These results reveal that as the number of cycles increases, the fretting damage

increases. This is true for the fretting results at room temperature with both 10 and 40 μm slip amplitude and for the specimens tested at 280 C with 10 μm slip amplitude. This can be seen in Plates 30-32 for tests conducted at room temperature with 40 μm slip amplitude. At 280 C, as the amplitude of slip was raised from 10 μm to 40 μm, there was a remarkable decrease in the rate of metal removed per cycle, which decreased further at 540 C at both of the slip amplitudes. Plates 33 and 34 show this for the specimens tested at 540 C with 40 μm slip amplitude. It was also found that the fretting damage in the early stages of the fretting tests conducted at room temperature with the two slip amplitudes and those at 280 C with 10 μm slip amplitude was very small compared with the large values found in the case of 280 C with 40 μm slip amplitude and the 540 C ones with the two slip amplitudes.

The results in Figures 38-40 show that the slip amplitude has a considerable effect on the fretting damage. At 540 C (Figure 40) there is a slight increase in the fretting damage as the slip amplitude is increased from 10 to 40 μm, while the rate of metal removal per cycle is the same. At 280 C, as the slip amplitude increased from 10 to 40 μm, there is a marked increase in the fretting damage in the early stages of fretting, but in the long run the fretting damage is the same. It was also found that, at 280 C, the rate of metal removal decreased as the amplitude increased. The behaviour at room temperature is completely different in contrast with that at 280 C. In the early stages of fretting at room temperature, it was found that as the slip amplitude increased the fretting damage increased, becoming more pronounced as the test continued.

The results were redrawn as shown in Figures 41 and 42 to demonstrate the effect of testing temperature on the fretting damage. At 10 μm slip amplitude, (Figure 41) it was found that there is no significant difference between the fretting damage produced at room temperature or 280 C, while there is a marked difference at 540 C where the rate of material removed is much lower than in the other two cases. Also the amount of material removed in the early stage of the fretting test is much higher at 540 C than at 20 and 280 C but approaching each other in the long run. At 40 μm slip amplitude (Figure 42) it was found that, as the temperature increased. the fretting damage in the early stages of the test increased while the rate of material removed decreased. It appears from Figure 42 that the fretting damage at the three test temperatures becomes similar after 10^4 to 10^5 fretting cycles.

4.3.5 Friction measurements

Friction force has frequently been recorded during the fretting wear tests, and typical oscillograph traces are shown in Plates 9a,b at high and low recording speeds respectively. The friction force and the coefficient of friction have been calculated as given in Appendix E.

4.3.6 Friction results for Ti-6Al-4V alloy (AMMRC)

Variation in coefficient of friction with number of cycles in tests performed at room temperature and 100 C is shown graphically in Figures 44 and 45. The friction results at room temperature (Figure 44) indicate no increase in the coefficient of friction in the first 500 cycles and then it increases gradually until it becomes steady at 10^4 cycles, but starts to drop slightly at 10^5 cycles. At 100 C (Figure 45), the coefficient of friction remains approximately constant in the first 400 cycles and then rapidly increases to a maximum value followed by a rapid fall and then rapid increase again to reach another maximum value at 3 000 to 6 000 cycles, after which a gradual fall again occurs which continues throughout

the rest of the test at 40 μm slip amplitude, but starts to increase gradually again at 10^5 cycles at 10 μm slip amplitude.

It seems that the slip amplitude has some effect on the coefficient of friction. In the early stage of the fretting test, the coefficient of friction is higher at 40 μm slip amplitude, with a slight decrease in the coefficient of friction as the number of cycles increases. The 10 μm slip amplitude curves always have the lowest and the highest values for the coefficient of friction. All these observations apply for both the room temperature and 100 C results.

To investigate the effect of temperature on the coefficient of friction the previous results have been redrawn as shown in Figures 46 and 47. At 10 μm slip amplitude (Figure 46) the 100 C curve fluctuates while the room temperature one does not. Furthermore, the room temperature curve has the lowest value for the coefficient of friction in the early stage of the fretting test as well as the highest value throughout the test. In addition, there is a significant difference in the coefficient of friction throughout the test as the temperature increases. These observations also apply in the case of 40 μm slip amplitude (Figure 47) but on a much smaller scale.

4.3.7 Friction results for Inconel 718 alloy (aged)

Variation in coefficient of friction with the number of cycles is shown graphically in Figures 48-50. There is little effect of the number of fretting cycles on the coefficient of friction except, generally speaking, that the coefficient of friction remains approximately constant in the early stage of the fretting test, followed by a stage characterised by an increase, decrease, or fluctuation of the coefficient of friction between maximum and minimum. The onset of the second stage and its duration depends on the slip amplitude and the test temperature. Following the second stage, in the third or final stage the coefficient of friction becomes approximately steady again, except at room temperature with 10 μm slip amplitude where it increases with number of cycles, with a different value from that in the first stage.

One of the effects of the slip amplitude on the coefficient of friction is the existence of the fluctuation in the coefficient of friction in the second stage in the tests carried out at 10 μm, while this fluctuation is absent at 40 μm. Also it was found that the value of the coefficient of friction in the first stage is always lower at 10 μm than at 40 μm. These observations apply at all test temperatures.

The effect of temperature on the coefficient of friction is shown in Figures 51 and 52. It was found that, generally speaking, the mean value of the coefficient of friction in the first stage, the maximum value in the second stage, and the mean value in the third stage, decreased at both slip amplitudes as the temperature was increased. It was also found that the coefficient of friction attained a steady value after about 6 000 cycles in the tests performed at 280 and 540 C at 40 μm and at 540 C at 10 μm (see Figures 50 and 52).

4.4 Optical microscopy in plan

4.4.1 Fretting fatigue specimens

In all the pictures in this section the direction of sliding is approximately parallel to the vertical direction, otherwise the sliding direction is indicated by an arrow.

Fretting scars on the Ti-6Al-4V alloy (IMI 318) showed deep ridges and valleys due to roughening of the surface. They also showed evidence of material transferred between the specimen and the bridge feet. The optical examination revealed that the amount and the size of individual particles of the transferred material increased as the testing temperature was raised. This is shown in Plate 11 for a specimen tested at 400 C at 247 $\pm$ 93 MN/m^2 which failed after 759 000 cycles.

In contrast with the features found on titanium alloy (IMI 318), Ti-6Al-4V alloy (AMMRC) showed mild fretting damage of shallow ridges and valleys uniformly distributed all over the scar surrounded by compacted debris. This is shown in Plate 12 and at higher magnification in Plate 13 for a specimen tested at 100 C at 400 $\pm$ 91 MN/m^2 which failed after 81 000 cycles.

Examination of the Inconel alloy 718 (aged) specimens tested at room temperature at all stress levels and those tested at 280 C tested at alternating stresses below $\pm$ 260 MN/m^2 showed features different from those tested at 280 C at alternating stresses above 260 MN/m^2 and all the 540 C and 700 C specimens. In the former the scars have the same features as the titanium alloys, i.e. transferred material and ridges and valleys surrounded by compacted debris. Plate 14 for a specimen tested at 280 C at 550 $\pm$ 114 MN/m^2 which endured 12.6 x 10^6 cycles revealed at higher magnification exactly the same features as those shown in Plate 13. The latter case did not show the ridges and valleys structure previously observed, but showed large smooth, slightly furrowed, grey areas. These grey areas are moderately light-reflecting and are at a higher elevation than the surrounding areas, which suggests that they were load bearing areas. These areas were observed previously by Stott et al (9) and have been referred to as glazes. Plate 15 shows one of these glaze areas formed on a specimen tested at 540 C at 550 $\pm$ 260 MN/m^2 which failed after 981 000 cycles. It also reveals a set of parallel cracks within the glaze area running at right angles to the fretting direction. It seems that there is no relation between the area covered by this glaze and the level of the alternating stress or the number of fretting cycles.

Generally the fretting scars on the three alloys tested are elliptical in shape as shown in Plate 14 and the fracture always occurred at the boundary between the slip and non-slip regions as shown in Plate 12.

6.4.2 Fretting wear specimens

In all the pictures in this section the direction of sliding is approximately parallel to the horizontal direction, otherwise the sliding direction is indicated by an arrow.

Examination of the scar produced on the rider showed that it is identical in shape and features to that formed on the mating surface, i.e. the flat specimen, as shown in Plates 16 and 23 for rider and flat specimen respectively of Ti-6Al-4V alloy (AMMRC) tested at room temperature with 10 μm slip amplitude for 3.5 x 10^6 fretting cycles. For this reason it was decided to examine the flat specimens in the optical microscope as well as in the scanning electron microscope.

All the flat specimens were examined directly after stopping the

fretting test and before doing any cleaning operation on them, taking care not to disturb any loose debris which may exist in the scar. The observations under the optical microscope revealed generally the production of fine loose debris, black in colour, distributed all over the scar and on the unfretted area surrounding the scar as shown in Plate 17 for an Inconel alloy 718 specimen tested at room temperature at 40 μm slip amplitude for 6 000 fretting cycles. This debris could easily be removed by brushing the specimen with a soft camel-hair brush as shown in Plate 30. Plate 30 is actually of the specimen after ultrasonic cleaning but there was no significant difference after brushing and after ultrasonic cleaning. This suggests that the adherent debris, if any exists, strongly adheres to the surface and is not removed by ultrasonic cleaning.

Examination of the Ti-6Al-4V alloy (AMMRC) showed that the scar has mottled dark grey areas of compacted debris and black areas of uncompacted debris. As the number of fretting cycles increases the area covered by the compacted debris increases. This applies for specimens tested at room temperature and 100 C at both 10 and 40 μm slip amplitudes. This is demonstrated by the series of Plates 21-29. Also it is found that this compacted debris, i.e. the mottled dark grey areas, forms in the early stages of the fretting test at the outer edge of the scar, progressing towards the centre of the scar as the number of fretting cycles is increased, as shown in Plates 24-26. The mottled grey areas are the load bearing areas as they are at higher elevation than the surrounding areas. Generally, the scar size increases as the number of cycles increases, as shown in Plates 21-23 for specimens tested at room temperature and at 10 μm slip amplitude. This also applies at 40 μm slip amplitude as shown in Plates 24-26 and also at 100 C as shown in Plates 27-29. The observations reveal that as the slip amplitude is raised from 10 μm to 40 μm, the scar size increases, as is demonstrated by Plates 21-23 at 10 μm and Plates 24-26 at 40 μm slip amplitudes. There is no significant change in the scar size as the temperature is raised from room temperature, (Plates 24-26) to 100 C (Plates 27-29).

Comparing Plates 18 and 125 for Inconel alloy 718 specimens suggests that the mottled dark grey area is compacted debris and the shiny, highly light-reflecting white area is metallic surface.

Optical observation of Inconel alloy 718 specimens tested at room temperature at 10 and 40 μm slip amplitudes shows that the scar has mottled dark grey areas of compacted debris and black areas of not fully compacted debris as well as some white metallic areas. As the number of fretting cycles increases the area covered by the compacted debris increases. These features are shown in Plates 30-32 for Inconel 718 specimens tested at 40 μm slip amplitude. Plate 19 is a higher magnification of Plate 32 and shows the mottled dark grey area of compacted debris which is raised above the original surface and the breaking up of this compacted layer to reveal the white high light-reflecting metallic area underneath it (see also Plate 131a). This suggests that the mottled grey areas are load bearing areas since they are at a higher elevation than the surrounding areas. Also when this layer breaks up it takes a long time to re-build itself, and this is why the surface underneath it has a metallic appearance.

The Inconel 718 alloy specimens tested at 280 C at 10 μm slip amplitude show the same features and behaviour as those tested at room temperature.

Comparison between Plates 20 and 141 for Inconel alloy 718 specimens tested at 280 C at 40 μm slip amplitude leads to the suggestion that the slightly furrowed smooth grey area is the glaze while the black areas are the surface after removal of the glaze. This grey glaze area is quite different in appearance from the mottled grey area mentioned above and

shown in Plate 19. This suggests that they have different properties. Also the areas revealed after removal of the glaze are black in colour instead of being white and metallic as found at room temperature. This is probably due to the surface oxidising rapidly in contact with the atmosphere. It should be mentioned here that the specimens tested at 280 C at 10 μm slip amplitude show these black areas but no grey glaze areas.

The specimens tested at 540 C at both 10 and 40 μm slip amplitude show the same features as those tested at 280 C at 40 μm slip amplitude. The area covered with the glaze increases as the number of cycles increases (see Plates 33 and 34). It is also concentrated at the centre of the scar which may be due to the fact that the high pressure at the centre of the scar facilitates the formation of the compacted layer more rapidly than at the outer edge of the scar.

4.5 Scanning electron microscopy

All the specimens were examined in the Cambridge Stereoscan 600 scanning electron microscope to study the surface morphology of the scars. The procedure for preparing the specimens consisted of washing them carefully ultrasonically with trichloroethylene and then drying in hot air. Each pair of bridges, having two feet, when clamped onto the specimen produced four separate fretting damage areas, two on each side of the specimen gauge length. Failure of the specimens in every case was found to occur at one of these fretted areas.

In all the pictures of the fretting fatigue specimens and bridges the direction of sliding is approximately parallel to the vertical direction of while for the fretting wear tests it is parallel to the horizontal direction; otherwise the sliding direction is indicated by an arrow. Also the tilt angle was approximately 45° from the normal to the surface unless specified.

4.5.1 Examination of fretting fatigue damage to Ti-6Al-4V alloy (IMI 318)

The general impression obtained of the damaged surfaces was of transfer of material from one surface to the other, this becoming much greater in volume as the temperature was raised. Plates 35-37 show the mating areas on a specimen and bridge foot from a test conducted at 600 C with 247 ± 62 MN/m^2 which survived 10^6 cycles without failure. Plate 35 shows material transferred to the specimen from the bridge foot. This is visible in Plate 36 at the bottom right hand corner. Previously developed cracks are found in the vicinity, which in places are covered by the transferred material. Plate 37 is a picture of the bridge foot and shows the region from which transference occurred to the specimen surface.

It was found from the scanning electron microscope observations that the material had been removed and transferred from one of the surfaces to the other by one or more of the following processes:

1. Formation of ridges which may be caused by the ploughing action of the asperities or welding and breaking of the welds. For example at 200 C the process begins by the formation of ridges on the specimen surface as shown in Plate 38 for a specimen tested at 247 ± 139 MN/m^2 which failed after 210 000 cycles. As the temperature was raised, the ridge formation was enhanced. This can be seen in smeared material on the specimen tested at 400 C at 247 ± 93 MN/m^2 which failed after 750 000 cycles, Plate 39, and on a bridge foot fretted against a specimen tested at 600 C at 247 ± 124 MN/m^2 which failed after 119 000 cycles, Plate 40.

2. Removal of large thick particles caused by surface fatigue or welding and breaking of welds. Plate 41 shows a large particle which has been pushed backwards and forwards in the transferred material and will eventually become detached, on a specimen tested at 400 C at 247 ± 108 MN/m^2 which failed after 222 000 cycles. Plate 42, of a specimen tested at 247 ± 154 MN/m^2 which failed after 137 000 cycles, shows a deep depression made by the reciprocating motion of a large particle which has eventually become detached (see also Plate 41). The removal of material by adhesion might result in severe cracking of the underlying surface. Plate 43, of a specimen tested at 400 C at 247 ± 170 MN/m^2 which failed after 118 000 cycles, reveals a large crack in material transferred from the bridge foot to the specimen, which was running perpendicular to the fretting direction and propagated out of the fretting scar. The bottom of Plate 44 reveals a crack in the underlying surface due to material removal in a specimen tested at 400 C at 247 ± 124 MN/m^2 which failed after 183 000 cycles.

3. Delamination. Plates 45-47 demonstrate the removal of material by delamination. Plates 45 and 46 for a bridge foot fretted against a specimen tested at 600 C at 247 ± 154 MN/m^2 which failed after 97 000 cycles showing in the first plate delamination of smeared, transferred material, and in the second plate the progress of delamination process and how a plate-like particle will eventually become detached by delamination. The complete break-up and detachment of this plate-like particle from the surface resulted in that form of surface damage shown in Plate 47 for a specimen tested at 400 C at 247 ± 77 which failed after 11 x 10^6 cycles.

It seems that the relative frequency of the above three processes depends on the testing conditions. Further reciprocating motion between the fretting surfaces causes:

1. in the first process, i.e. formation of ridges, smearing of those ridges as demonstrated in Plate 39. This could lead to the development of a layered structure as shown in Plate 48, for a specimen tested at 200 C at 247 ± 93 MN/m^2 and failed after 940 000 cycles, which reveals the layer structure in the vicinity of the site of fatigue fracture;

2. in the second process reattachment of the large separated particles again to the surface as shown in Plate 35, and occasionally acting as a barrier to the movement of transferred material, especially the delaminated platelets;

3. in the third process the delaminated sheets or platelets to be:

   a) reattached again to the surface as shown in Plate 49 for a specimen tested at 400 C at 247 ± 93 MN/m^2, which failed after 8 814 000 cycles. Repetition of this process in the same site resulted in the piling-up of platelets and led to the layered structure as shown in Plate 48. As the temperature was raised to 400 C, these piles of platelets became more marked (Plates 50 and 51). Plate 50 is an oblique view of transferred material, found on a surface of specimen tested at 400 C at 247 ± 109 MN/m^2 which failed after 222 000 cycles, revealing its layered structure and the piled-up platelets. Plate 51 shows a later stage with the development of a large protuberance on the surface of a specimen tested also at 400 C at 247 ± 93 MN/m^2 which failed after 749 000 cycles. Further increase in the temperature to 600 C encouraged this behaviour. In some cases, where there was a large particle actin

as a barrier for the movement of the transferred platelets, these piles of platelets grew to large proportions, sometimes having the appearance of an elephant's trunk. This is shown in Plates 52-55 which are for material transferred to the bridge foot from a specimen tested at 600 C at 247 ± 170 MN/m2 which failed after 24 000 cycles. Plate 52 shows elephant's trunk growths at sites A and B. Plate 53 shows the formation at site A. This is shown at higher magnification in Plate 54, where it can be seen that the individual platelets have a very reproducible shape. Plate 55 shows a less organised build-up of platelets in the neighbourhood of the elephant's trunk.

b) Occasionally, at the highest temperature where these platelets were plastic enough to be rolled up by the action of the fretting movement, lath or rod-like particles were formed, as shown in Plate 56 for a specimen tested at 600 C at 247 ± 139 MN/m^2 which failed after 45 000 cycles. This is shown at higher magnification in Plate 57, which reveals that they show signs of being transparent to electrons and are thought to be largely oxide. The specimen has been ultrasonically cleaned and so the rods are not loose debris. The underlying material shows regular striations in directions at right angles to each other which are not thought to be scratches.

4.5.2 Examination of fretting fatigue damage to Ti-6Al-4V alloy (AMMRC)

Plate 58 is a general view of the impression made by one of the bridge feet on a specimen tested at room temperature at 400 ± 84 MN/m^2 which was unbroken after 20×10^6 cycles. A region of compacted debris is visible around the major part of the edge of the scar, with a rougher area in the centre. Plate 59 is a close up of the former and Plate 60 of the latter. This applies for both the scars on the specimen or the bridge foot, at room temperature or 100 C and at low alternating stresses as well as higher ones, except that at higher alternating stress the damage is more severe as shown in Plate 61 for a specimen tested at room temperature at 400 ± 176 MN/m^2 which failed after 81 000 cycles. Although the damage is more severe in this plate than in Plate 58, the same areas are still distinguishable.

Plate 62 is of a specimen tested at 100 C at 400 ± 83 MN/m^2 which did not fail after 12×10^6 cycles. Comparison between it and Plate 58 gives an indication that there is no difference between the damage produced at room temperature and that at 100 C.

It seems that the material was removed in one or more of the following ways:

1. largely by welding and breaking of welds from all over the scar area, resulting in the production of loose debris as shown in Plate 60;

2. occasionally by break-up of the compacted debris into small flakes as shown in Plate 63 which is a close-up of the compacted debris at the bottom left corner of Plate 61. Another example at higher magnification is shown in Plate 64 for a specimen tested at 100 C at 400 ± 151 MN/m^2 which failed after 141 000 cycles. This is shown at a higher magnification in Plate 66, where it appears that the underlying material reveals the microstructure of the alloy. Although there were a few isolated cases of delamination, this series of specimens showed no evidence of the piled-up platelets and the layered structures which were seen in the Ti-6Al-4V alloy (IMI 318).

Once the material was detached, it was pushed out of the scar area due to the relative movement between the fretting surfaces, to accumulate with some wrinkling at the edges, as shown in the series of Plates 67-70, for a specimen tested at 100 C at 400 ± 152 MN/m^2 which failed after 122 000 cycles. Plate 67 shows that the fatigue fracture lies at the edge of the scar, while the other plates at larger magnification show the debris found at the top left corner.

4.5.3 Examination of fretting fatigue damage to Inconel 718 alloy (aged)

Examination of specimens tested at room temperature revealed that removal of material by disruption of the surface due to adhesion was the damaging feature on short life specimens, i.e. at high stresses. Plate 71, for a specimen tested at room temperature at 550 ± 260 MN/m^2 which failed after 131 000 cycles shows a large particle which has been pulled out of the surface by adhesion forces which is likely to become detached leaving a deep depression similar to the one alongside it. Plate 72, for a specimen tested also at room temperature at 550 ± 300 MN/m^2 which failed after 83 000 cycles, shows how the removal of metal by adhesion progresses. Plate 73, for the same specimen, shows areas of roughening and a fatigue crack.

As the stress is decreased, i.e. long life specimens, the disruption of the surface is caused by adhesion and delamination. Plate 74, at the fracture site of a specimen tested at room temperature at 550 ± 120 MN/m^2 with a life of 10^7 cycles, shows a large particle of material about to be pulled from the surface by adhesion, resulting in a secondary fatigue crack running perpendicular to the fretting direction. The rest of the area shows evidence of delamination with the material that is about to be removed riddled with fine parallel cracks at right angles to the direction of movement, Plate 75. Only one case of piled-up platelets has been found as shown in Plate 76 for a specimen tested at room temperature at 550 ± 132 MN/m^2 which failed after 566 000 cycles.

At 280 C, there is already evidence of the formation of a glaze on the specimens tested at stresses of 550 ± 260 MN/m^2 or greater. Such a glaze is characterised, according to Stott et al (10), by many distinct, well-formed, small abrasion grooves, parallel to the direction of sliding. Plates 77 and 78, for a specimen tested at 550 ± 350 MN/m^2 which failed after 212 000 cycles, show such glaze formation, although this is breaking down by delamination. Also, a layered structure has been found in this specimen as shown in Plate 79.

At 280 C, with intermediate stress, i.e. 550 ± 260 MN/m^2, which failed after 1 780 000 cycles, the glaze has also been found as in Plates 80 and 81, which broke down by delamination, sometimes resulting in the initiation of fatigue cracks perpendicular to the direction of movement. Also there is evidence of adhesion resulting in plastic deformation as shown in Plate 82. This is shown in higher magnification in Plate 83, which reveals signs of plastic deformation by rotating blocks in a particular crystal with evidence of mechanical twinning below the glaze. Plate 84, for the same specimen, shows smaller regular accretions of transferred material. The similarity between this transferred material and the structure of Plate 83 suggests that the former may be individually transferred blocks of rotated material.

The low-stress, long-life specimens tested at 280 C showed no sign of glaze formation, but only adhesion. The general appearance of a specimen tested at 550 ± 114 MN/m^2 which endured 12×10^7 cycles is shown in Plate 85. Plates 86 and 87 at the site of the fatigue fracture of a specimen tested at 550 ± 143 MN/m^2 which failed after 4 600 000 cycles, show

secondary cracks perpendicular to the direction of fretting and roughened areas due to surface disruption by adhesion with some particles just about to be detached from the surface.

At 540 C, at all stress levels, the general features were the formation of glaze disrupted by delamination or adhesion, the damage being more severe at higher stresses. This severe damage to the glaze by adhesion or creep of underlying material is shown in Plates 88 and 89 for a specimen tested at 550 ± 350 MN/m^2 which failed after 56 000 cycles, while Plate 90, for a bridge foot fretted against this specimen, shows how the glaze was disrupted by delamination, resulting in fine debris shown at the top of the picture or in the formation of platelets as shown in Plate 91. Further fretting results in piling up of these platelets (Plates 92 and 93) to form such structures as the elephant's trunk one described before. This is shown at higher magnification in Plates 94 and 95. At low stress levels, the damage to the glaze layer is less severe, mainly caused by delamination, although there is some damage caused by adhesion. Plate 96 shows one of the large areas of glaze oxide found on a specimen tested at 550 ± 240 MN/m^2 and endured 2 650 000 cycles, while Plate 97 shows how this glaze oxide was disrupted by delamination. Plate 98 is a higher magnification of the previous one revealing the multi-layer nature of the surface film, each layer about 5 μm thick. Plate 99, for a bridge foot fretted against the previous specimen, shows large areas of glaze oxide, while Plate 100 shows how the delaminated platelets can pile up, growing to large proportions and having the appearance of a goose's neck. This is shown at higher magnification in Plate 101, where it can be seen that the individual platelets are glaze oxide having a very reproducible shape.

A large glaze area has been found on a specimen tested at 700 C at 550 ± 228 MN/m^2 and failed after 4 180 000 cycles (Plate 102). Also some smooth areas were found but these contained systems of parallel cracks at right angles to the direction of movement (Plate 103). In other areas severe surface breakdown had occurred (Plate 104). This is shown at higher magnification in Plate 105, which reveals cleavage facets.

4.5.4 Examination of fretting fatigue damage to Inconel 718 alloy (annealed)

Examination of the annealed specimens showed that at room temperature there was no glaze formation and the surface was disrupted by delamination or adhesion; Plate 106 shows a specimen tested at 256 ± 170 MN/m^2 which failed after 673 000 cycles.

At 600 C, there is evidence of glaze formation which was disrupted mainly by delamination and sometimes by adhesion; Plates 107 and 108 show a specimen tested at 256 ± 170 MN/m^2 which endured 249 000 cycles and broke at the grips.

4.5.5 Examination of the fretting wear damage to Ti-6Al-4V alloy (AMMRC)

The general feature observed in the fretting scar produced at room temperature at 40 μm slip amplitude is the production of fine loose debris in the early stage of fretting, i.e. after 6 000 fretting cycles (Plate 109). This fine loose debris might be produced by the action of abrasion or adhesion, leaving roughened areas full of this loose debris (Plate 110), while some of it was pushed out around the scar, (Plate 109). Plate 111 shows the configuration of that debris found outside the scar and it seems that it has irregular shape with particle size ranges between 1 and 7 μm. Plates 109-111 show the fretting scar before cleaning. After cleaning it ultrasonically, although the loose debris outside and inside the scar has been removed (Plates 112 and 113), there is still some fine adherent debris.

Further fretting, i.e. after 10^5 cycles, produces a layer of compacted debris due to sintering of the fresh loose debris, as shown in Plate 114, which is breaking down at some places. As fretting continued, the processes of building up and breaking down of the compacted debris are repeated, as shown in Plates 115 and 116 for the flat specimen tested at room temperature at 40 μm slip amplitude for 3×10^6 cycles. The light areas indicate that these compacted layers are charging up either because they are becoming detached from the surface or because they are composed of particles of metal covered with a thin oxide film.

At room temperature, if the slip amplitude was decreased from 40 to 10 μm, the same type of damage was still observed but not as severe as in the first case. This can be seen by comparing Plates 112 and 113 with Plates 117-119 for a flat specimen tested at room temperature at 10 μm slip amplitude for 6 000 cycles. This series of plates shows very light damage to the surface and demonstrates how the fretting damage started by the production of fine debris from pits on the surface. The charging up of this adherent debris indicates that it is composed of either fully oxidised particles or metallic particles covered with a thin oxide film.

Raising the temperature to 100 C produced few changes except for the feature shown in Plates 120 and 121, which is similar in appearance to the glaze oxide film previously observed in the Inconel 718 alloy. These are of a flat specimen tested at 100 C at 40 μm slip amplitude which fretted for 3.5×10^6 cycles. Distinct, well-formed, parallel tracks can be observed on the compacted layer which has a thickness of about 5 μm. Another example is shown in Plate 122 for a specimen tested at 100 C at 10 μm slip amplitude for 10^5 cycles. It should be mentioned that these glaze-like layers have only been observed on those specimens tested at 100 C for more than 6 000 cycles at both 10 and 40 μm slip amplitudes.

4.5.6 Examination of the fretting wear damage to Inconel 718 alloy (aged)

Examination of the fretting scars produced at room temperature on flat specimens tested at 10 μm slip amplitude reveals that the process starts with the production of fine debris which rapidly becomes compacted to cover the whole scar with a thin compacted layer as shown in Plates 123 and 124. This compacted layer starts to break up, mainly, by delamination. Continued fretting causes further removal of the compacted layer, leaving areas of the scar free from it as shown in Plates 125 and 126 for 8×10^4 fretting cycles. The areas free from this layer start again to produce debris, as can be seen in the centre of the scar in Plate 125. Further fretting produces more debris, reforming the compacted layer, followed by removal, the process continually repeating itself. Plates 127 and 128, after 10^6 cycles, show the process in the stage of break-up and reconstitution of compacted debris into small flakes. The thickness of the compacted debris appears to be 1-2 μm.

The same processes occur in the same sequence when the amplitude of slip is increased from 10 to 40 μm but they proceed faster. Comparison between Plate 123 and Plate 129 of specimens tested at 10 and 40 μm slip amplitudes respectively for 6 000 cycles reveals in the latter the early formation of compacted debris with large areas of it removed, while the former is approximately completely undamaged. This is also confirmed by Plate 130, of a specimen tested at room temperature at 40 μm slip amplitude and fretted for 8×10^4 cycles. Comparison between this plate and the corresponding plate (Plate 125) shows that in the former the compacted layer has been reformed, while the latter has not yet started. Plate 131, of a specimen tested at room temperature at 40 μm slip amplitude for 10^6 cycles, shows the same feature as the corresponding one tested at 10 μm

slip amplitude (see Plate 128). It has also been found that the compacted layer thickness is somewhat larger with the 40 μm slip amplitude than with the 10 μm, ranging between 2-4 μm. In general, the glaze film has not been observed in the specimens tested at room temperature whether at low or high amplitude of slip, or at short or long test duration. The fine debris produced was spheroidal in shape with particle size ranging between 1-2 μm as shown in Plate 132 of a specimen tested at 40 μm slip amplitude for 8×10^4 cycles.

At 280 C, the specimens tested at 10 μm slip amplitude show that the same processes as at room temperature were involved but they proceeded faster at 280 C, resulting in thicker compacted layer or occasionally in the accumulation of compacted layers one above the other. Plate 133 of a specimen fretted 6 000 cycles shows the formation of the compacted layer most of which has been disrupted, while Plate 134 shows an intermediate stage, after 8×10^4 cycles, where the compacted debris has reformed again. This is shown at higher magnification in Plate 135 to demonstrate the multi-compact layers stacked one over the other. Plate 136 shows a later fretting stage, i.e. after 10^6 fretting cycles. It has been noticed that removal of material occurred both by delamination, as shown in Plates 135 and 136, and by adhesion, as shown in Plate 136, which is shown at larger magnifications in Plates 137 and 138. The glaze film is absent on this group of specimens.

Examination of the specimens tested at 280 C with 40 μm amplitude of slip reveals the following facts:

1. the process starts with the production of fine debris, followed by sintering of this debris to form a compacted layer, break-up of this layer, rebuilding-up of a new layer and the repetition of this process as the fretting continues. This is demonstrated by Plates 139-141 after 6 000, 8×10^4 and 10^6 fretting cycles respectively;

2. the compacted debris always has the glaze characteristics of distinct, well-formed, small abrasion grooves, parallel to the direction of sliding. This is shown in Plates 142-144 after 6 000, 8×10^4 and 10^6 cycles respectively. The latter is shown at higher magnification in Plate 145;

3. the fine debris produced is spheroidal and has a particle size of 1 to 2 μm;

4. this compacted glaze layer breaks up and is removed by delamination as is clear in Plate 143, and results in the formation of plate-like fragments, see Plates 139-142;

5. the glaze film has a thickness of about 5 μm and is composed of fine compacted debris of 1-2 μm grain size. This is shown clearly in Plate 142, where one of the delaminated fragments of the glaze layer has been turned over by the fretting action;

6. in the long run, the glaze layers may be accumulated one over the other as shown in Plate 146 after 10^6 fretting cycles, which reveals the stacked layers;

7. it seems that the glaze layer has formed in less than 6 000 fretting cycles.

These features on the 280 C specimens tested at 40 μm slip amplitude have also been observed in tests at 540 C with 10 and 40 μm slip amplitudes. Plate 147 of a specimen tested at 10 μm slip amplitude for 6 000 fretting

cycles, confirms that the glaze has formed in less than 6 000 cycles, that it is being removed by delamination and that its thickness is about 5 μm. Plates 148 and 149, of a specimen tested at 10 μm slip amplitude for 10^6 fretting cycles, show the glaze layer together with some adherent turned-over delaminated fragment revealing the nature of this layer. This fragment at the right of Plate 149 shows that it has been passed over by the mating fretting surface, revealing that the parallel abrasion grooves on the substrate are extended over the fragment. Plates 150-152, of a specimen tested at 40 μm slip amplitude for 8×10^4 cycles, show the glaze layer and how it has been removed by delamination. Its thickness is about 5 μm.

5. Discussion of results

5.1 Introduction

The fretting fatigue strength was determined on specimens which were continuously fretted by the bridges clamped on the specimen for the whole duration of the test. This procedure allows full play for any conjoint action that there may be between fretting and the fatigue process itself and can be likened to a corrosion fatigue test. It has the advantage of more closely resembling the condition in which fretting-fatigue occurs in practice but has the disadvantage that as the alternating stress is varied, so is the alternating strain, which causes variation of the amplitude of movement at each stress level.

5.2 Ti-6Al-4V (IMI 318) results

5.2.1 Discussion of the plain fatigue results

From the results obtained in this investigation and shown in Figure 28, it can be stated that as the temperature increases, the plain fatigue strength decreases. This is shown graphically in Figure 53 for the fatigue strengths at 10^7 cycles.

The present results have been calculated from the actual results obtained using the modified Goodman relationship (see Appendix C). Frost et al (11) gave a general equation:

$$\pm \sigma = \sigma \sigma_o \{1 - \left(\frac{\sigma_m}{\sigma_t}\right)^n\} \qquad (1)$$

where $\pm \sigma$ is the fatigue limit (or strength at a given endurance) when a tensile mean stress σ_m is present,

$\pm \sigma_o$ is the fatigue limit (or strength at the same endurance) at zero mean stress,

σ_t is the tensile strength

n is constant

It seems from this relationship that n depends on the material, test temperature and maybe many other factors. When n equals 1 this equation tends to the modified Goodman relationship, and when n equals 2 it gives the Gerber relationship.

In the present investigation n was considered to be 1 but for more accurate results the value of n would have to be determined, which would

need a large number of specimens. As there was a shortage of material available for this series of tests, n was considered as 1. Nevertheless, it was found that the present results were in good agreement with many other published data.

Wood and Favor (12) have reported a value of 247 ± 400 MN/m^2 at room temperature for Ti-6Al-4V alloy having tensile strength of 980 MN/m^2.

Syers (13) has reported a value of 350 ± 350 MN/m^2 at room temperature which was reduced to 270 ± 270 MN/m^2 as the temperature was increased to 350 C. These values were for sheet specimens 1.5 mm thick tested in a repeated tensile mode (R = 0). Using the modified Goodman relationship these values corresponded to 247 ± 409 MN/m^2 and 247 ± 279 MN/m^2 at room temperature and 350 C respectively. The Ti-6Al-4V alloy possessed the following mechanical properties:

0.2% proof stress	865 MN/m^2
Tensile strength	970 MN/m^2
Elongation	8%

Although the above quoted values differ slightly to the present results (see Figure 53) it was found that the latter were in good agreement with those of Hoeppner and Goss (14). They found that the fatigue strength of annealed Ti-6Al-4V, 1.25 mm thick at room temperature, in direct stress tests, is 417 ± 341 MN/m^2 which corresponds to 247 ± 434 MN/m^2 after adjustment using the modified Goodman relationship.

Partlo (15) found a value of 570 MN/m^2 at room temperature in rotating bending tests for specimens annealed at 925 C followed by air cooling and having an ultimate tensile strength of 1010 MN/m^2, yield strength of 880 MN/m^2 and 17% elongation. This was a specimen of 6.9 mm diameter. His value corresponds to 247 ± 434 MN/m^2 which is approximately the same as the present results.

Also Persimo (16) found in rotating bending tests on a specimen of 13 mm gauge diameter that the fatigue strength was 538 MN/m^2 at room temperature, reduced to 490 at 204 C. This means that his results at 247 MN/m^2 mean stress are 409 and 373 at room temperature and 204 C respectively. These values are very close to the present results, see Figure 53.

Although the present results and the quoted ones are in good agreement the slight difference between them may be attributed to (11):

1. the effect of using specimens of different shape and size;
2. surface finish effect;
3. the effect of using different types of tests, i.e. rotating bending and direct stress fatigue tests;
4. the effect of using different batches with different mechanical properties;
5. the error arising from calculating the adjusted fatigue strength in the present investigation and in the quoted one by taking n equals 1 in equation (1).

5.2.2 Discussion of fretting fatigue results

The results shown in Figures 27 and 28 show a dramatic reduction in the fatigue strength at room temperature due to fretting. The strength

reduction factor is about 5 based on the plain fatigue strength at room temperature. The already low fretting-fatigue strength at room temperature decreases further, but not dramatically, as the temperature is successively raised to 200, 400 and 600 C. The similarity between the values of the strength reduction factor at different temperatures in the case of plain fatigue, see Section 4.2.1.2, and the corresponding values in the case of fretting fatigue, see Section 4.2.1.1, suggests that this further deterioration is due to the reduction in fatigue properties rather than any specific aggravation of the fretting damage. The big difference between the values obtained at 600 C is attributed to the very low value of the plain fatigue strength at 600 C. However, it was pointed out that this temperature would be considered too high for this material.

Although the effect of temperature on the fatigue strength in the presence of fretting is not particularly marked, there is a significant decrease in fatigue life at stresses above the fatigue limit as the temperature is raised. This is no doubt due to the dramatic decrease in the plain fatigue life at higher temperatures as shown in Figure 28.

Syers (13) reported a fretting fatigue strength value of 115 ± 115 MN/m^2 at room temperature corresponding to a reduction of 67% based on the plain fatigue strength. As the temperature was raised to 350 C the fretting fatigue strength reduced to 95 ± 95 MN/m^2, corresponding to a reduction of 65%. The reduction in fretting fatigue strength due to a temperature rise from room temperature to 350 C was 17%. His tests were conducted on 1.5 mm thick sheet material with 93 MN/m^2 clamping pressure. When the clamping pressure decreased to 46 MN/m^2, the fretting fatigue strength at room temperature was 80 ± 80 MN/m^2.

Hoeppner and Gross (14) have found that the fretting fatigue strength of 1.5 mm thick sheet of annealed Ti-6Al-4V alloy when tested at room temperature with a clamping pressure of 21 MN/m^2 in direct stress tests is 133 ± 109 MN/m^2 (extrapolated). Although there is a slight difference between the quoted results and the present results, they are generally in good agreement as shown in Figure 53.

5.2.3 Examination of fretting fatigue damage and the mechanism of fretting fatigue failure.

Fretting damage on titanium alloys at room temperature has previously been studied by Wharton (8). He found that the mechanism of fretting fatigue failure involves the formation of adhesive welds at the early stages of fretting which are then subjected to a high strain fatigue action. As a result cracks can be initiated in the welds and may propagate away from the surface under the influence of combined stresses and will eventually cause failure. In later stages surface damage and debris production may be the result of a delamination process.

Syers (13) also reported that fretting fatigue damage is essentially of the delamination type.

Although the nature of the surface damage caused by fretting at elevated temperatures does, however, display features which are not seen at room temperature, it seems that there is not much difference between the mechanism of fretting fatigue at room temperature and that at elevated temperatures.

The present observations of the fretting damage suggest that welding may occur in the very early stage of fretting. As the temperature is increased, the probability of occurrence of these welds decreases. In the later stages material removal may be by surface fatigue, see Plates 41 and 42, or by delamination (Plates 45, 46, 47 and 49). These results are in

agreement with those at room temperature (8,13).

The present observations suggest that the layered structure or the piled-up platelets are always associated with delamination and that delamination is observed even at the shortest life, i.e. at the highest alternating stress level (see Plates 44-48, 56 and 57).

One of the main differences in the surfaces fretted at higher temperatures has been the comparative absence of cracks and the evidence of greater plasticity. This is maybe due, as mentioned above, to the welding mechanism being less active as the temperature is increased, and the shorter the fretting stage associated with this mechanism. The cracks shown in Plates 43 and 44 may have been produced in that early stage and propagated as the test continued. This is based on the well-established fact that a fatigue crack is initiated at about the same moment that maximum adhesion is developed between the fretting surfaces (17). Also Waterhouse (17) pointed out that there is no evidence that the subsurface cracks which result in plate-like particles lifting from the surface subsequently develop into fatigue cracks propagating into the body of the material. So, the proposed mechanism of fretting fatigue at high temperatures involves:

1. a very short stage of fretting associated with the formation and breaking up welds and results in the production of loose particles and crack initiation. The duration of this stage decreases as the temperature increases. It also depends on the nature of the material and the environment, and the reactivity of the material to the environment and the loading conditions;

2. the continuous reciprocating movement causing a rise in the temperature of the surface and the loose particles of several hundred degrees, which means that plasticity is increased. The deformation caused by the fretting action is so great that the material is welded back on to the original surface;

3. further fretting action causing the removal of material by delamination, as suggested by Suh (18, 19), resulting in the formation of loose platelets. The delamination process is enhanced in the transferred material as the isolated oxide particles entrapped in the interface act as the dislocation obstacles postulated in Suh's delamination theory of wear. This is also the reason why it is more marked as the temperature increases;

4. the previously initiated cracks, if any exist, propagating due to the stresses.

Due to the nature of this series of tests it was difficult to determine the duration of the first stage and if delamination process is effective also in this stage or not.

5.3 Ti-6Al-4V (AMMRC)

5.3.1 Plain fatigue results

Although the strength reduction factor is approximately the same for this alloy and IMI 318 as the temperature was raised from room temperature to 100 C (see Sections 4.2.1.2 and 4.2.2.2) there is a significant difference between the fatigue strengths at 10^7 cycles, as shown in Figure 53. This may be attributed to two main reasons:

1. the effect of using two different batches with different

mechanical properties and different microstructures;

2. as discussed in Section 5.2.1, the error arising from calculating the adjusted fatigue strength due to considering n = 1 in equation (1),

However, it seems that the results obtained comparatively agree with those quoted in Figure 53.

The suggestion which can be put forward from these results is that there is no significant difference between the fatigue strength at room temperature and at 100 C. Also there is no significant difference in the fatigue life at all alternating stress levels in both cases.

5.3.2 Fretting fatigue results

Although the results obtained were for tests conducted at a mean stress much larger than that used for IMI 318, they agree together as shown in Figure 53. This leads to the conclusion that the mean stress has a very slight effect, if any, on the fretting fatigue strength. This agrees with the findings of Wharton (8). Also the results agree reasonably well with the quoted ones mentioed before in Section 5.2.2.

The final conclusion is that there is no distinction between the fatigue behaviour of this alloy at the two testing temperatures in the presence of fretting. This confirms the previously mentioned suggestion, see Section 5.2.2, that any deterioration in the fretting fatigue properties is attributed to the reduction in fatigue properties rather than any specific aggravation of the fretting damage, as there is no significant difference between the plain fatigue strengths at the two testing temperatures. This also leads to the suggestion that the operating fretting fatigue mechanism may be the same at both temperatures.

5.3.3 Examination of fretting fatigue damage and the mechanism of fretting fatigue failures

Although the fretting fatigue strength of this alloy is approximately the same as that of IMI 318, it seems that their fretting fatigue mechanisms are somewhat different, which leads to a difference in appearance of the fretting damage.

In contrast with the observations on IMI 318, adhesion is the most predominant cause for metal removal rather than delamination. Also it seems that it is effective throughout the test as it was found in the short life specimens as well as the long life ones.

Bethune and Waterhouse (20) found that the adhesion developed between metal surfaces in fretting initially increases linearly with amplitude of slip, passing through maximum at 40 μm. As the resultant slip amplitudes in the present series of tests are always less than 40 μm, and as adhesion is the predominant mechanism, so, raising the alternating stress should result in increasing the adhesion. This was true from the observations of the fretting damage at low stress, Plate 58, and at high stress, Plate 61.

The suggestion, which has previously been put forward in Section 5.3.2, that the fretting fatigue mechanism involved may be the same at both testing temperatures, has been confirmed by the observations of the fretting fatigue damage, see Plates 58 and 62.

The fretting fatigue mechanism which can be deduced is as follows:

1. formation of local welds at isolated areas and breaking of these welds resulting in the production of loose debris and in roughening of the surface. This process seems to be effective from the start of the fretting action until the end of the test;

2. sintering of the loose debris to produce a compacted layer;

3. breaking of the compacted layer to produce interconnected cracks, Plate 64, of crazy paving and resulting in the removal of this layer;

4. material may occasionally be removed by delamination process especially from transferred material and compacted layers. Due to the nature of this series of tests it was difficult to determine when the delamination process started to be effective. However, from the observations it was found to occur in the present range of test durations;

5. the fine debris produced by processes 1, 3 and 4 may be pushed out of the fretting area due to the relative reciprocating motion between the fretting surfaces to accumulate with some wrinkling at the edges of the scar.

5.3.4 Fretting wear results

The results shown in Figures 34 and 35 reveal the linear relationship between the volume of material removed and the number of fretting cycles at both testing temperatures and slip amplitudes. Uhlig (21) proposed a quantitative expression for fretting damage which predicts that the fretting damage, measured as weight loss, is linear with number of cycles. The present results seem to verify his equation. His equation also predicts a linear relationship between fretting damage and amplitude of slip. Although the present results cannot show whether this linear relationship exists or not because only two slip amplitudes have been used in this series of tests, the general trend is verified, i.e. as the slip amplitude increases the fretting damage increases. There is agreement between this finding and that of the fretting fatigue results, see Section 5.3.3, in that the fretting fatigue damage increases as the alternating stress increases. Also it was found that raising the test temperature from room temperature to 100°C had no significant effect on the fretting damage as shown in Figures 36 and 37. Again this agrees with the previous finding in Section 5.3.2 for the fretting fatigue strength and in Section 5.3.3 for the fretting fatigue damage. These findings lead to the conclusion that:

1. the fretting wear mechanism is the same at both testing temperatures;

2. the fretting wear mechanism seems to be similar to that of the fretting fatigue mechanism proposed earlier in Section 5.3.3.

5.3.5 Friction measurement results

The frictional force between fretting surfaces is one of the non-controllable parameters which has been considered in fretting wear studies. Studying the variation in frictional force during fretting tests is a useful means of studying the mechanism of fretting and fretting-induced damage. For example, the formation of glaze layer is associated with a drop in the coefficient of friction (9). Also, Milestone (22) attributed the initial increase in the coefficient of friction to removal of the original surface oxide film, and the further increase was due to welding of the asperities and interlocking of the roughened surfaces. For this reason, it was decided to study the frictional force variations during the fretting wear test.

The present results shown in Figures 44 and 45 give the general form for the coefficient of friction versus number of fretting cycle curves. The coefficient of friction, generally, starts with low value which increases suddenly after a certain number of fretting cycles to reach an approximately steady state. Further fretting causes a slight fluctuation of the coefficient of friction below and above the steady state value. The starting value of the coefficient of friction was about 0.2-0.4 while the final value after 3.5×10^6 cycles was about 0.7-0.9. Milestone (22) found corresponding values of 0.2-0.3 and 1.1-1.2 respectively in tests conducted on the same material, which are in reasonable agreement with the present results.

From the shape of the curve can be suggested a general idea of the mechanism involved during fretting:

1. the first stage: the relative reciprocating motion results in smearing the asperities present on the surface, resulting in smoothing of the surface and consequently a slight reduction in the coefficient of friction. This process is more effective and more noticeable at higher amplitudes rather than at lower; notice the slight decrease in the coefficient of friction between the start of the test and 400 fretting cycles at 40 μm slip amplitude, Figures 44 and 45. During this stage also the fretting action results in breaking of the original surface-oxide film and causes its removal from the surface and the production of loose debris, leaving clean metal surfaces in contact. As this process is more severe in the case of 40 μm slip amplitude, a higher coefficient of friction is to be expected.

2. the second stage: once there are two clean metal surfaces in contact after stage 1, welding of the asperities on the fretting surfaces will occur, followed by breaking of these welds, resulting in roughening of the surfaces and interlocking of the roughened surfaces. These events result in the production of debris and in the sudden and dramatic increase in the coefficient of friction. It seems that this stage starts after about 500 to 1 000 fretting cycles depending on the fretting conditions. As the processes involved in stage 1 are more effective at the higher amplitude, the number of cycles required to remove the original oxide layer, and consequently to start the second stage, will be smaller. This is true at the two testing temperatures as shown in Figures 44 and 45. This is also the reason for the earlier start of stage 2 at 100 C rather than at room temperature as shown in Figures 46 and 47 for both slip amplitudes.

3. third stage: which is the steady stage and starts by debris produced from the previous stages being compacted by the combined effects of pressure and fretting action and results in the formation of a smooth dense layer. Further fretting causes the disruption and removal of this layer with the production of fine debris. The process of formation and removal of this compacted layer is repeated as fretting continues. The presence of the smooth compacted layer lowers the coefficient of friction which rises when it is removed. This is why the coefficient of friction fluctuates around a steady state value during this stage. As the amplitude of slip increases, the fretting damage increaseses, see Section 5.3.4, and more debris is produced. Consequently, the thicker the compacted layer the thicker will be the layer of loose debris. As both of these layers increase in thickness, the coefficient of friction decreases. This is why the coefficient of friction at 40 μm slip amplitude is lower than that at 10 μm at this stage, see Figures 60 and 61, and why this stage starts earlier in the 40 μm tests. Also, this is the

reason for the lower coefficient of friction at 100 C, see Figures 46 and 47.

It is obvious from the analysis given above that study of the variations in the frictional force during the fretting tests provides information which cannot be obtained by, for example, study of the volume of metal removal or scanning electron microscope observations. The following facts emerge:

1. the adhesion starts as early as 500 fretting cycles;

2. the compacted layer forms as early as 3 000 cycles;

3. from the number of fluctuations of the coefficient of friction in the early stage, can be determined how often the compacted layer is reformed.

However, the study of the frictional force alone cannot provide information such as how in the third stage the compacted layer is removed. This question can be answered by examination of the fretting damage in the scanning electron microscope.

5.3.6 Examination of fretting wear damage and the mechanism of fretting wear

The three-stage fretting mechanism mentioned above, see Section 5.3.5, has been confirmed by observations of the fretting damage in the scanning electron microscope. Although the first stage usually ends before 6 000 cycles, it was possible, by chance, to get a unique and clear example of it at room temperature at 10 μm slip amplitude at 6 000 fretting cycles as shown in Plates 117-119. The different processes mentioned in this mechanism can be seen clearly in Plates 109-122. A clear example of adhesion and production of debris is shown in Plates 118 and 119. An example of the large quantity of fine loose debris which will later be compacted is shown in Plates 109 and 110 before cleaning the specimen; this should be compared with Plates 112 and 113 after cleaning. An example of the compacted layer is shown in Plate 114, partially removed, revealing that the underlying material is rough and possibly composed of the compacted debris. The process of formation and removal of the compacted debris is demonstrated by Plates 112, 114 and 115 for specimens tested at room temperature at 40 μm after 6 000, 10^5 and 3×10^6 cycles respectively.

The debris produced has irregular shape with particle size ranging between 1 and 7 μm, as shown in Plates 110 and 111. The charging up of this debris indicates that it is either wholly oxide particles or metallic particles covered with a thin oxide film. However, Plate 119, which shows fine debris partially detached from the surface, and its bottom part uncharged, leads to the suggestion that they are more likely to be metallic particles covered with a thin oxide film.

5.4 Inconel 718 alloy (aged)

5.4.1 Plain fatigue results

Although the fatigue results at elevated temperatures in the absence of fretting show considerable scatter it appears that they belong to one population giving a fatigue strength at 10^7 cycles of 550 ± 325 MN/m^2 reduced to 550 ± 275 MN/m^2 at room temperature.

The results of rotating beam tests (23) on bar specimens given the same heat treatment are as follows:

Test temperature °C	Fatigue strength at 10^7 cycles (σ_m = 0) MN/m^2	Adjusted fatigue strength at 10^7 cycles (σ_m = 550 MN/m^2) MN/m^2
20	634	389
316	758	452
538	655	382
649	606	321

Although there is some difference between the present results and the quoted ones for the reasons mentioned before in Section 5.2.1, they are still comparable. For example, Brown et al (24) found that the grain size has a pronounced effect on the fatigue properties of the alloy when they conducted fatigue tests at 454 C. It should be pointed out that the average grain size of their alloy was 20 μm while that the present investigation was 11 μm.

Only two specimens have been tested at 700 C due to interference from creep at the higher alternating stresses. This temperature in any case would be considered too high for this material.

The elevated temperature curve shows longer fatigue lives at lower stresses than that of the room temperature one, which may be attributed to the ageing effect at such elevated temperatures and long tests. At higher stresses the fatigue lives of the elevated temperature specimens are shorter due to the creep of the material at that level of stress.

5.4.2 Fretting fatigue results

In contrast with the fretting fatigue behaviour of Ti-6Al-4V alloy at elevated temperatures, it seems that the Inconel 718 alloy behaves differently. Figure 54 shows the effect of raising the temperature on the fretting fatigue strength at constant number of cycles. The following observations require explanation:

1. the improved fretting fatigue strength at 10^7 cycles at 540 C;
2. the improved fretting fatigue strength at 10^5 cycles at 280 C;
3. the longer fatigue life at higher stresses at 280 C compared with 20 C;
4. the longer fatigue life at stresses above 260 MN/m^2 at 280 C compared with 540 C.

The observations of the fretting damage in the scanning electron microscope, see Sections 4.4.3 and 4.4.6, reveal the formation of a protective thermally softened oxide layer (termed a glaze). Such glazes have been observed in the sliding wear of nickel-based alloys of the Nimonic and Incoloy types in the temperature region 150 to 800 C by Stott et al (10) and also in nickel-chromium alloys (9). Its appearance in the scanning electron microscope is described as showing"many distinct, well-formed, small abrasion grooves, parallel to the direction of sliding". The formation of this glaze oxide film is characterised by a reduction in coefficient of friction and a corresponding reduction in the wear rate.

In the present investigation the observations revealed that no glaze

formed at any of the specimens tested at room temperature. As the temperature was raised to 280 and 540 C the glaze formed. This is in good agreement with the results of Stott et al (9,10) who found a transition temperature above which the glaze formed. This conclusion from the present results is that the observations of Stott et al are not only applicable to the case of sliding wear, but also to fretting wear. The more important additional finding in the case of fretting is that there is a transition slip amplitude, as well as a transition temperature, above which the glaze forms. It seems that the value of the transition slip amplitude depends on the material and the testing conditions, but this needs more investigation and should be the subject of future work.

The present results reveal that at 280 C the specimens tested at stresses $>550 \pm 260$ MN/m^2, corresponding to 24 μm slip amplitude, have evidence of glaze formation, while those tested at stresses $<550 \pm 215$ MN/m^2, corresponding to 20 μm slip amplitude, have no evidence of glaze formation. All the specimens tested at 540 and 700 C have evidence of glaze formation. The above observations were confirmed by results obtained from the fretting wear tests. From the above mentioned observation it is possible to explain the four observations mentioned above in this section, as follows:

1. it is apparent from the present study that not only is the glaze oxide capable of reducing friction and wear but also of preventing the type of surface damage which leads to the initiation of fatigue cracks in the presence of fretting;
2. for the glaze to give effective protection it must:
   a) form rapidly with the onset of fretting since it is known that fatigue cracks are initiated in the early stages of the process (17, 25);
   b) be stable and not break down easily or if it does,
   c) be capable of repairing itself rapidly.

At room temperature these conditions are not met, although Plates 74 and 75 show that smooth areas, which have undoubtedly been load bearing, are formed but they are full of fine cracks which lead to their breakdown, possibly by a delamination process, and the reformation process, if occurring at all, is not rapid enough to maintain the smooth layer. It is doubtful whether this smooth layer has the same properties as the true glaze layer since it does not show the parallel abrasion marks of the latter. As there is no glaze formed at room temperature, it is expected that the fretting fatigue strength, as well as the fretting fatigue lives, is dramatically reduced.

At 280 C the glaze layer is formed above the transition slip amplitude, but below it there is an oxide layer which is not a glaze. This is why the fretting fatigue strength at 10^5 cycles is improved. This is also the reason for the longer fatigue life at higher stresses at 280 C compared with 20 C.

At 540 C the glaze layer is formed at all stress levels. This is why the fretting fatigue strength at 10^7 cycles is improved. At high stresses creep of the bulk material led to cracking of the surface layers, see Plate 89, and this is possibly the reason for the shorter fatigue lives at high stresses at 540 C compared with 280 C.

At 700 C the glaze layer is also formed, but the effect of the fatigue action and the increased shear stresses in the fretting region has caused creep of the bulk material leading to cracking of the surface layer. This is why the point at 700 C lies between 280 and 540 C curves.

5.4.3 Observations of the fretting fatigue damage and the fretting fatigue mechanism

It is clear from the observations mentioned in Section 4.4.3 that there are many mechanisms involved in the fretting fatigue of this alloy depending not only on the test temperature but also on the slip amplitude.

At room temperature, there is no glaze formed, and the classical mechanism of metal removal by adhesion is involved in the early stages of the fretting fatigue combined with delamination in the later stages. It seems that this mechanism is also involved at 280 C below a certain slip amplitude, the transition amplitude of about 22 μm, where there was no evidence of glaze formation.

Where glaze is formed, as in the case of 280 C above the transition slip amplitude, and at 540 and 700 C, the metal was removed mainly by delamination with few isolated, if any, cases by adhesion, but at the high temperatures and stresses, i.e. 540 and 700 C, it seems that the effect of the fatigue action and the increased shear stresses in the fretting region have caused creep of the bulk material leading to cracking of the glaze layer.

5.4.4 Fretting wear results

The results shown in Figures 38-40 reveal the linear relationship between the volume of material removed and the number of fretting cycles at all test conditions. This agrees with the proposed equation of Uhlig (21). His equation also predicts a linear relationship between fretting damage and amplitude of slip. Although the present results cannot say whether the linear relationship exists or not because only two slip amplitudes have been used in this series of tests, the general trend is verified, i.e. as the slip amplitude increases the volume of material removed increases.

At room temperature and 280 C at 10 μm slip amplitude, the rate of material removed is larger compared with that of 280 C at 40 μm slip amplitude and 540 C. This is because in the latter case a protective adherent glaze oxide layer has been formed which did not exist in the former case. The fact that at 280 C at 40 μm slip amplitude the rate of material removal is large compared with that at 540 C is because when the glaze formed at 280 C breaks down by delamination it is unable to reform rapidly enough to keep pace with the fretting action.

The similarity in the behaviour at room temperature and 280 C with low slip amplitude, see Figure 41, and also the same behaviour at 280 C with 40 μm slip amplitude and 540 C, see Figure 42, support the proposed fretting mechanisms given in Section 5.4.3. Also it is confirmed by the fact that, during the tests conducted at room temperature and 280 C at 10 μm slip amplitude, as the number of cycles increases the amplitude of slip decreases (due to roughening of the surface), and readjustments have frequently been made to keep the slip amplitude constant.

The big difference in the rate of material removal at 10 μm and 40 μm slip amplitudes in the 280 C tests confirms the existence of a transition slip amplitude above which glaze forms and below which it does not. Although the value of this transition slip amplitude could not be determined accurately as only two test amplitudes have been used, it appears to be around 22 μm from the fretting fatigue results.

One of the features revealed from Figures 41 and 42 is that in the early stages of the fretting tests as the temperature was raised, the volume

of material removed increased. This is attributed to the fact that the higher the temperature the greater the thickness of the oxide film, and consequently the larger the amount of material removed when this oxide layer is disrupted.

Bill (26) conducted fretting tests on a nickel base alloy (Ni-20 Cr-2Al) at temperatures up to 816 C. He found that fretting wear was reduced with increase in temperature up to 540 C. At higher temperatures an increase in the volume of material removed was observed, as shown in Figure 55. These results are in good agreement with the present results at 40 μm slip amplitudes after about 550 000 cycles, corresponding to 44 m total path length.

Hurricks (6,27,27) in his fretting studies of mild steel at elevated temperatures found that a thick oxide layer formed at temperatures above 140 C which had a protective and lubricant effect thereby reducing the fretting damage.

Stott et al (9) found from their sliding wear tests on nickelchromium alloys at temperatures from 20 to 800 C that above a certain transition temperature relatively low wear was observed after a time but below which it remained relatively high throughout. They attributed this behaviour to the formation of the glaze layer above the transition temperature. They stated also that once the glaze is formed, very little further wear occurred for the high chromium content alloys. Their results are in good agreement with the present ones.

5.4.5. Frictional force measurement results

It appears from the study of the friction results shown in Figures 48-52 that there are principally two different mechanisms involved in the fretting wear of this alloy, one at room temperature and the other at elevated temperatures.

At room temperature, see Figure 48, the coefficient of friction starts in the first stage with a moderate value of about 0.6 which increases suddenly in the second stage after a certain number of fretting cycles to reach approximately a steady value of about 0.9. Further fretting causes a slight fluctuation of the coefficient of friction around the steady value. These values are comparable with those of Stott et al (9) on a nickel-chromium alloy having 20% chromium. The room temperature fretting wear mechanism consists of three stages. The first stage is characterised by smearing of the asperities present on the surface resulting in smoothing of the surface and consequently the coefficient of friction is reduced slightly. This process is more effective and more noticeable at the higher amplitude rather than at the lower one. The slight decrease in the coefficient of friction in the first stage at 40 μm slip amplitude in Figure 48 should be noted.

Also in this stage the fretting action results in breaking up of the original surface oxide film and causes its removal from the surface and the production of loose debris, leaving clean metal surfaces in contact. As this process is more active at 40 μm slip amplitude, it is expected to result in a higher coefficient of friction in this stage at this amplitude, see Figure 48.

In the second stage, once there are two clean metal surfaces in contact together from stage 1, welding of the asperities on the fretting surface occurs followed by breaking of these welds resulting in roughening of the surfaces and interlocking of the roughened surfaces. These events are

associated with a sudden and dramatic increase in the coefficient of friction as well as the production of debris. The start of this stage depends on the fretting conditions.

The third stage, the steady stage, starts by compacting the debris produced from the previous stage under the combined effects of pressure and the fretting action and results in the formation of a smooth compacted layer. Further fretting causes the disruption and removal of this layer with the production of fine debris. The process of formation and removal of this compacted layer is repeated as the fretting continues. The presence of the smooth compacted layer results in a decrease in the coefficient of friction while its absence results in an increase. This is why the coefficient of friction fluctuates around a particular value during this stage. The high temperature mechanism at 540 C also comprises three stages. It seems that the first stage is the same as that described above for the room temperature mechanism. In this stage the coefficient of friction is about 0.3, rather lower than that found by Stott et al (9) which is about 1.5. This may be attributed to the large difference in the starting surface finish in the present work, i.e. 0.1 μm c.l.a., and their work, i.e. 25 μm c.l.a. and also the much higher amplitude. The only difference in this stage between the room temperature and the high temperature mechanism is that clean metal is never exposed as new oxide layers form rapidly on the surfaces at this high temperature.

In the second stage the glaze starts to form at some isolated areas of the fretting surfaces by one of the mechanisms proposed by Stott et al (9,10). These isolated areas grow with further fretting until they cover the majority of the fretting surfaces. As these areas grow, the coefficient of friction decreases.

The third stage is the same at both room temperature and high temperature except that the compacted debris in the latter is of the glaze type which is associated with a drop in the coefficient of friction, i.e. about 0.9 at room temperature while at 540 C it is about 0.15.

At intermediate temperatures, i.e. 280 C, the alloy exhibited two completely different behaviours at the two testing amplitudes, i.e. 10 and 40 μm. At the lower amplitude the alloy behaves as at room temperature, which suggests that the room temperature mechanism is involved in this case. At the higher amplitude the alloy behaves as at 540 C which suggests that the high temperature mechanism is involved in this case. The scanning electron microscope observations, see Section 4.4.6, confirm this idea.

One of the clear observations when studying the effect of temperature on the frictional behaviour of the alloy is as the temperature is raised the coefficient of friction decreases, see Figures 51 and 52. This is true for the two amplitudes and for all the stages. This is because as the temperature increases the thickness of the compacted layer as well as the thickness of the layer of loose debris increases. Consequently, the coefficient of friction decreases.

Another important observation is that as the temperature increases, see Figure 52, or as the slip amplitude increases, see Figure 50, the transition from a high coefficient of friction to a low value, i.e. the second stage of the high temperature mechanism, begins and ends earlier. This observation reveals the role of slip amplitude as well as temperature in glaze formation. Also the role of temperature is consistent with the observations of Stott et al (9) who suggest that the transition from a high coefficient of friction to a low value occurs within the period when glaze is first observed. Their data showed that as the temperature increased the time at which the glaze was first observed decreased. This

shows the similarity between sliding wear and the fretting wear in this respect.

5.4.6 Observation of the fretting wear damage and the fretting wear mechanisms

It is clear from the observations mentioned in Section 4.4.6 that there are two mechanisms involved in the fretting wear of this alloy, i.e. the low temperature mechanism and the high temperature. Details of these mechanisms are given in Section 5.4.5 which are confirmed by the fretting wear damage study and the friction measurement study, Sections 5.4.4 and 5.4.5. respectively. It was also found that the fretting wear and the fretting fatigue mechanisms are consistent. Although the fretting wear results could not give a value for the transition slip amplitude at 280 C, the fretting fatigue results were able to. The fretting wear results revealed when the second stage of the high temperature mechanism which is associated with the formation of the glaze occurred, whereas the fretting fatigue results could not, showing how these two types of tests are complementary to each other.

One of the important pieces of evidence which cannot be obtained from the wear or friction studies is how the material is removed. The scanning electron microscope observations show that it is mainly removed by delamination in the high temperature mechanisms, i.e. delamination of the glaze layers, while in the low temperature mechanism it occurs by delamination and crazing of the compacted layer.

One of the most interesting features observed also is that shown in Plates 142, 148 and 149, which supports the previous suggestion (9,10) that the glaze is actually a layer of compacted debris.

5.5 Inconel 718 alloy (annealed)

Since it is not usual to use this alloy in practice in the annealed condition, only an exploratory test has been conducted to study the effect of the microstructure on the fretting fatigue behaviour of this alloy. Although there are not enough results, it seems that the alloy has the same behaviour under fretting fatigue condition as in the aged and the annealed condition, except that in the former it exhibited higher fretting fatigue strengths, see Figures 30 and 31. The dramatic increase in the fretting fatigue strength as the temperature was raised was also found in the annealed as well as in the aged condition.

The similarity in behaviour between the annealed and the aged condition suggests that the fretting fatigue mechanisms involved in the former are the same as that of the latter. The scanning electron microscope observations confirm this fact, Plates 106-108. This also leads to the conclusion that glaze formation is independent of the heat treatment condition or the microstructure. More information is needed to clarify this point and requires further study.

References

1. Waterhouse, R.B. and Taylor, D.E., "The effect of heat treatment and decarburization on the fretting fatigue behaviour of a 0.7 per cent carbon steel", Proc. Instn. Mech. Engrs., Vol. 185, 1970-71, pp. 691-695.

2. Waterhouse, R.B. and Wharton, M.H.,"The behaviour of three high-strength titanium alloys in fretting fatigue in a corrosive environment", Lubrication Engng., Vol. 32, No. 6, June 1976, pp. 294-298.

3. Waterhouse, R.B., "Fretting in hostile environments", Wear, Vol. 34, No. 3, Oct. 1975, pp. 301-309.

4. Hurricks, P.L., and Ashford, K.S., "The effect of temperature on the fretting wear of mild steel", Proc. Instn. Mech. Engrs., Vol. 184 (3L), 1969-70, pp. 165-175.

5. Hurricks, P.L., "The fretting wear of mild steel from room temperature to 200 C", Wear, Vol. 19, 1972, pp. 207-219.

6. Hurricks, P.L., "The fretting wear of mild steel from 200 C to 500 C", Wear, Vol. 30, 1974, pp. 189-212.

7. Overs, M.P., "Fretting wear and fatigue of sprayed molybdenum coatings", M.Phil. thesis, 1978, The University of Nottingham.

8. Wharton, M.H., "Environmental effects in the fretting of titanium alloys", Ph.D. thesis, 1977, The University of Nottingham.

9. Stott, F.H., Lin, D.S., Wood, G.C. and Stevenson, C.W., "The tribological behaviour of nickel and nickel chromium alloys at temperatures from 20 to 800 C", Wear, Vol. 36, 1976, pp. 147-174.

10. Stott, F.H., Lin, D.S., and Wood, G.C., "The structure and mechanism of formation of the 'glaze' oxide layer produced on nickel-based alloys during wear at high temperatures", Corr. Sc., Vol. 13, 1973, pp. 449-469.

11. Frost, N.E., Marsh, K.J., and Pook, L.P., Metal Fatigue, Oxford, Clarendon Press, 1974.

12. Wood, R.A., and Favor, R.J., Titanium Alloys Handbook, MCIC-HB-02, Metals and Ceramics Information Center, Battelle, Ohio, U.S.A., (December 1972).

13. Syers, G., "The evaluation of certain anti-fret media on the titanium alloy 6Al-4V and 2.5 Cu with some observations on the mechanism of fretting", Research Report No. LLR 10245/55/75, Materials Laboratory, Rolls-Royce (1971) Ltd., Small Engine Division, Leavesden, Watford WD2 7BZ (July 1975).

14. Hoeppner, D.W.,and Goss, G.L., Corrosion Fatigue: Chemistry, Mechanics and Microstructure, NACE-2 (1972), p. 617.

15. Partlo, L.J., ASTM STP 459 (1969), p. 144.

16. Persino, R.V., "An investigation on the effectiveness of anodized surface preparations as inhibitors of fretting-fatigue at elevated

temperatures in Ti-Ti joints", M.Sc. thesis, 1966, The Ohio State University.

17. Waterhouse, R.B., "The role of adhesion and delamination in the fretting wear of metallic materials", Wear, Vol. 45, No. 3 (December 1977), pp. 355-364.

18. Suh, N.P., Jahanmir, S., and Abrahamson, E.P., "The delamination theory of wear", Materials Processing Laboratory, Dept. of Mech. Engineering, Massachusetts Institute of Technology (Sept. 1975).

19. Suh, N.P., "The delamination theory of wear", Wear, Vol. 25, 1973, pp. 111-124.

20. Bethune, B., and Waterhouse, R.B., "Adhesion of metal surfaces under fretting conditions, I. like metals in contact", Wear, Vol. 12, 1968, pp. 289-296.

21. Uhlig, H.H., J. Appl. Mechanics, Vol. 21, 1954, p. 401.

22. Milestone, W.D., "A new apparatus for investigating friction and metal to metal contact in fretting joints", ASTM STP 462, Amer. Soc. Testing and Materials, 1970, pp. 318-328.

23. Inconel Alloy 718 Catalogue, Huntington Alloy Products Division, The International Nickel Co. Inc., Huntington, West Virginia (1973).

24. Brown, E.E., Boettner, R.C., and Ruckle, D.L., MCIC-72-10, Metals and Ceramics Information Center (Sept. 1972).

25. Waterhouse, R.B., and Taylor, D.E., "The initiation of fatigue cracks in a 0.7% carbon steel by fretting", Wear, Vol. 17, 1971, pp. 139-147.

26. Bill, R.C., NASA TN-D-7570 (March 1974).

27. Hurricks, P.L., Industrial Lub. and Tribology, (Jan/Feb 1976) 9.

28. Hurricks, P.L., ibid., (Nov/Dec 1975) 209.

29. Rabinowicz, E., "Lubrication of metal surfaces by oxide films", ASLE Trans., Vol. 10, 1967, pp. 400-407.

30. Dove, R.C., and Adams, P.H., Experimental stress analysis and motion measurement, Charles E. Mirrill Books, Inc., Colombus, Ohio (1964), p. 76.

31. Timoshenko, S., and Goodier, A.N., Theory of elasticity, McGraw-Hill, 2nd Ed., 1951.

32. Bowden, F.P., and Tabor, D., The friction and lubrication of solids, Pt. II, Clarendon Press, Oxford, 1964.

CONCLUSION

The major findings in this research project are given in the summary at the beginning of the report and will not be repeated here. The most significant piece of information to come out of this work is that the glaze oxide, which had been observed in reciprocating sliding experiments by Wood and his colleagues on nickel based alloys, is also formed during fretting where the amplitude of movement is much smaller. The formation of the glaze in fretting is, however, a function of the amplitude of slip at lower temperatures. This is illustrated by the observation that at 280 C the glaze only forms at amplitudes above 22 μm, whereas at 540 C the glaze forms at all amplitudes. Where the glaze forms there is a marked improvement in both fretting-fatigue and fretting wear performance. Glaze formation does not occur on the titanium alloy and consequently no improvement in properties occurs on raising the temperature.

In the original proposal it was hoped to prepare thin sections from fretted areas for examination in the transmission electron microscope. Although some progress was being made in this direction the work was unfortunately far from complete at the end of the contract. It is nevertheless hoped that this aspect will be continued in the department since it has implications for other high temperature fretting work which is at present under investigation. However, the conclusions reported above suggest that surface reactions under the influence of sliding contribute much more to the fretting fatigue behaviour than sub-surface interactions between dislocations and second phase particles.

APPENDIX A

Strain Gauges Arrangement

It was decided to use a normal contact load of 2.75 N. Assuming that the coefficient of friction ranges between 0.2 and 1.2 (22, 29), then the expected friction force will be between 0.55 and 3.3 N.

Let the normal force = Y
the friction force = X

The arrangement is that of a simple cantilever, i.e. the transmission shaft, fixed at one end by being rigidly connected to the driving spindle of the electromagnetic vibration generator, which is subjected to two perpendicular forces X and Y acting at the other end of the shaft, i.e. the point of contact of the rider with the flat specimen as illustrated in Figure 16.

Eight strain gauges were attached to the outer cylindrical surface of the shaft at the part which has a reduced cross-sectional area as shown in Figures 15 and 16.

The measurement of X and Y simultaneously and independently is based on the well established following rule (30).

When four strain gauges R_1, R_2, R_3 and R_4 individually measure a strain value ε_1, ε_2, ε_3 and ε_4 respectively connected together in a circuit as shown in Figure 18, then the net strain value, ε_{net}, measured by this circuit is given by

$$\varepsilon_{net} = -\varepsilon_1 + \varepsilon_2 - \varepsilon_3 + \varepsilon_4$$

Suppose that the force X causes a longitudinal strain = ε_X and a lateral strain = $-\nu\varepsilon_X$ while the force Y causes a longitudinal strain ε_Y and a lateral strain = $-\nu\varepsilon_Y$ where ν is the Poisson's ratio, then Table 3 gives the strains experienced by each strain gauge separately according to its position on the transmission shaft as shown in Figure 16.

So, using the previous rule and the data in Table 3 and connecting the strain gauges to the strain gauge measuring instrument as shown in Figure 17, two separate circuits were obtained, one for measuring X and the other for measuring Y independently of each other.

This arrangement of strain gauges increases the sensitivity of the circuits as well as compensates for any variation in results due to a change in temperature.

The strain gauges used were foil strain gauges type N11-FA-5 manufactured by Showa Measuring Instruments Co. Ltd., Tokyo, Japan, with gauge length = 5 mm, resistance = 120 Ω, and gauge factor = 2.1.

The strain gauge circuits were connected to a universal multi-channel amplifier system, type SE 4000 manufactured by S.E. Laboratories (Engineering) Ltd., North Feltham Trading Estate, Feltham, Middlesex.

APPENDIX B

Normal and friction forces arrangement calibrations and studies

1. Introduction

The calibrations were carried out using a simple pulley and string arrangement for lifting the rider off the flat specimen and for pulling the rider to introduce an axial force in the direction of the transmission shaft axis. This was done with the aid of dead weights. Figure 19 shows the arrangement.

Before starting the calibrations both the normal force and the frictional force measuring arrangements were set at predetermined settings as given below in Sections 2 and 3.

2. Normal load setting

All the adjustments in this section have been conducted under the transmission shaft's own weight with the cooling water running. Channel No. 2 in the 4 000-system, channel No. 1 in the amplifier, and channel No. 4 in the recorder with galvanometer model MM 400-120 input were used for the normal load measuring arrangement.

The first step is to balance the bridge circuit with the shaft under its own weight, i.e. Y = weight of shaft, X = 0.

The calibration knob was adjusted to give the following readings:

Meter deflection in 4 000-system = 90 divisions
Light spot displacement in the U.V. recorder = 90 mm

3. Frictional force setting

All the adjustments in this section have been conducted with Y = 275 N and with the cooling water running. Channel No. 4 in the 4 000-system, channel No. 1 in the amplifier, and channel No. 4 in the recorder with galvanometer model MM 400-120 input were used for the frictional force measuring arrangement.

The first step is to balance the bridge circuit with Y = 275 N and X = 0.

The calibration knob was adjusted to give the following readings:

Meter deflection in 4 000-system = 80 divisions
Light spot displacement in the U.V. recorder = 120 mm

4. The relationship between the normal contact force and the light spot displacement in the U.V. recorder

The calibration was carried out by changing the dead weight Y (representing the normal load) keeping X constant, as shown in Figure 19, and recording the corresponding light spot displacement in the U.V. recorder. The results of the calibration are shown graphically in Figure 20 for three different values of X (representing the frictional force). These tests indicate that:

1. the sensitivity at X = 0 is 0.0340715 N/mm

the sensitivity at X = 1 N is 0.034632 N/mm
the sensitivity at X = 2.5 N is 0.035555 N/mm

2. there is about 4% variation in the sensitivity when the friction force changes from 0 to 2.5 N which is acceptable;

3. since the adjustment of the normal contact force in the actual fretting wear tests would be with zero frictional force, calibration results with X = 0 should be used;

4. for normal contact load = 2.75 N, the corresponding light spot displacement = 80 mm.

5. The relationship between the frictional force and the light spot displacement in the U.V. recorder

The calibration was carried out by changing the dead weight X (representing the frictional force) as shown in Figure 19, and recording the corresponding light spot displacement in the U.V. recorder. The results of the calibration are shown graphically in Figure 21 for two different values of Y (representing the normal contact load). These results show that:

1. the sensitivity at Y = 1.5 N is 0.080314 N/mm
the sensitivity at Y = 2.5 N is 0.0686270 N/mm

2. variation in sensitivity due to change of normal contact load by 40% is about 18%. This means that for a change in the normal load of 10%, the corresponding change in the sensitivity will be about 4.5%, which is acceptable;

3. the final conclusion is the acceptance of the calibration results of the frictional force at Y = 2.5 N.

6. The effect of testing temperature on the recorded normal force

When a normal force = 2.75 N is applied to the transmission shaft at the point of contact between the rider and the flat specimen, the resultant light spot displacement in the U.V. recorder is 80 mm. This is according to the previously mentioned settings and calibrations, see Sections 2 and 4. Accordingly, a normal force Y was applied to the shaft using a simple pulley and string arrangement at a point outside the furnace, as shown in Figure 22 with X = 0. The value of Y was chosen to give 80 mm light spot displacement in the U.V. recorder when the furnace was at room temperature. Then the furnace temperature was increased and the light spot displacement was recorded. The results are shown in Table 4. It can be concluded from these results that there is no significant effect of the testing temperature on the recorded normal force value represented by the light spot displacement. The scatter in the readings was within the accuracy of the arrangement.

7. Effect of temperature on the recorded friction force

The arrangement used in this study is shown in Figure 22. After setting the normal load and friction force measuring arrangements to the required setting as given in Sections 2 and 3, a normal force Y and a frictional force X were applied to the transmission shaft using a simple pulley and string arrangement. The values of Y and X were chosen to give 80 and 44 mm light spot displacements in the recorder respectively. The chosen values correspond to a normal force and a friction force at the

rider-flat specimen interface of 2.5 and 3.1 N respectively. The furnace was heated and the frictional force was recorded. The results are given in Table 5. It can be concluded from these results that there is no significant effect of temperature on the recorded friction force.

8. Effect of the inertia force on the recorded normal and friction forces

Since the fretting wear tests were conducted at a test frequency of 50 Hz, the inertia force has to be taken into consideration. To study the effect of inertia force on the recorded normal load and frictional force the arrangement shown in Figure 19 was used with Y = 2.5 N and X = 0, after setting the normal load and the frictional force measuring arrangements to the specified settings, see Sections 2 and 3. Then by operating the rig to oscillate the transmission shaft at 25, 50, 75 and 100 Hz and recording the light spot displacement in the U.V. recorder, the effects of the inertia force were obtained. The results are shown graphically in Figures 23-25, 40 and 41. From these results it can be concluded that:

1. at 40 μm amplitude and 50 Hz the inertia force caused a fluctuation in the normal load of $\pm$ 0.1 N which is less than 4% of the normal load used in the actual tests, i.e. the effect of the inertia force on the normal force is negligible;

2. for a frequency of 50 Hz, a normal load of 2.5 N, and amplitude of oscillation of 40 μm, the resultant noise + inertia curve (representing the recorded friction force) showed maximum amplitude (peak to peak) of 16 mm and minimum one of 9.7 mm. When the amplitude was decreased to 10 μm these values changed to 9 mm and 4.5 mm respectively. These values are too high to be neglected. So the effect of the inertia force on the recorded friction force has to be taken into consideration when calculating the friction force. The actual curve obtained for the frictional force during a fretting wear test is in fact a resultant of the interference between two curves, the noise inertia curve, and the pure frictional force curve. The resultant curve is obtained by the principle of superposition by simply adding the displacements caused by the individual curves at every point. Thus, to obtain the actual amplitude of the frictional force the noise + inertia curve amplitude should be subtracted from the amplitude of the recorded friction force curve.

APPENDIX C

Adjustment of plain fatigue strengths

The plain fatigue strengths obtained from the results were at mean stresses different from the mean stress at which the fretting fatigue tests were conducted, i.e. 247 MN/m^2. To compare the fatigue results with the fretting fatigue results, an adjustment was made to the plain fatigue results to get the plain fatigue strength at 247 MN/m^2 mean stress. This adjustment was done using the modified Goodman law:

$$S_a = S\left(1 - \frac{Sm}{Su}\right) \tag{1}$$

where

Sa = the alternating stress associated with mean stress Sm for endurance N.

S = the alternating fatigue strength (with zero mean stress) for endurance N.

Su = the ultimate tensile strength.

It was impossible to carry out alternating fatigue tests at zero mean stress with the type of specimen used in the present investigation because the compressive load would cause buckling, so an experimental value of S is not available. To solve this problem a series of tests in plain fatigue was conducted at each test temperature with different mean stress levels. If at Sm_1 mean stress and Sa_1 alternating fatigue stress the life is N cycles, then at Sm_2 mean stress the life will be N cycles, at an alternating fatigue stress Sa_2 which is calculated as follows:

Substituting in equation (1)

$$Sa_1 = S\left(1 - \frac{Sm_1}{Su}\right) \tag{2}$$

$$Sa_2 = S\left(1 - \frac{Sm_2}{Su}\right) \tag{3}$$

$$\therefore \quad \frac{Sa_1}{Sa_2} = \frac{Su - Sm_1}{Su - Sm_2}$$

$$\text{or} \quad Sa_2 = Sa_1\left[\frac{Su - Sm_2}{Su - Sm_1}\right] \tag{4}$$

APPENDIX D

Calculation of maximum and mean contact pressures between the spherical surface rider tip and flat specimen (31)

When two spheres are held in contact together by a force W as shown in Figure 33, there is a local deformation near the point of contact which produces a small circular contact region. If the radii of curvature R_1 and R_2 of the two spheres are large in comparison with a, the radius of the circular contact region, then the results for semi-infinite bodies may be applied. The value of the maximum pressure, P_o, can be obtained by equating the sum of the pressures over the contact area to the compressive force, W. For a hemispherical pressure distribution this gives (32):

$$\frac{P_o}{a} \times \frac{2\pi a^3}{3} = = W$$

$$\therefore \quad P_o = \frac{3W}{2\pi a^2}$$

For two spheres having identical elastic properties

$$a = 1.109 \left[\frac{WR_1R_2}{E(R_1 + R_2)}\right]^{1/3}$$

where E is the modulus of elasticity of the materials in contact. The maximum pressure P_o is given by:

$$P_o = \frac{3W}{2\pi a^2} = 0.388 \left[\frac{WE^2(R_1 + R_2)^2}{R_1^2 \cdot R_2^2}\right]^{1/3}$$

For the present case of a spherical surface of rider tip pressed into a plane surface having $R_1 = \infty$, the maximum contact pressure is given by:

$$P_o = 0.388 \left(\frac{WE^2}{R_2^2}\right)^{1/3}$$

$$\text{and} \quad a = 1.109 \left(\frac{WR_2}{E}\right)^{1/3}$$

The mean contact pressure, P_m, is given by:

$$P_m = \frac{W}{\pi a^2}$$

In the present investigation $R_2 = 100$ mm

$W = 2.75$ N

This gives the values shown in Table 7.

APPENDIX E

Calculation of the frictional force

As mentioned in Appendix B the noise and the inertia force have a significant effect on the recorded values of the frictional force. The pure frictional force curve has the shape shown in Figure 43a with constant amplitude = A_f. Figure 43b shows the noise + inertia force curve with variable amplitude A_i varying between $A_{i(max)}$ and $A_{i(min)}$. The recorded frictional force curve is actually the resultant of the interference between curves a and b. The recorded curve is obtained from the principle of superposition by simply adding the displacements caused by the individual curves at every point to get the resultant curve shown in Figure 43c, and in Plates 9a,b which has a variable amplitude A from $A_f + A_{i(max)}$ to $A_f + A_{i(min)}$. By measuring the maximum and the minimum values of A on the recorded chart such as that shown in Plate 9b, the frictional force can be calculated as follows:

$$A_{max} = A_f + A_{i(max)}$$

$$A_{min} = A_f + A_{i(min)}$$

or $$A_f = A_{max} - A_{i(max)} \quad (1)$$

$$A_f = A_{min} - A_{i(min)} \quad (2)$$

adding (1) and (2)

$$\therefore A_f = \frac{A_{max} + A_{min} - A_{i(max)} - A_{i(min)}}{2} \text{ mm}$$

where A_f is the amplitude of the frictional force curve (peak to peak). Since the maximum frictional force corresponds to half the value of A_f

$$\therefore \text{The frictional force} = \frac{A_{max} + A_{min} - A_{i(max)} - A_{i(min)}}{4} \times S \text{ N}$$

where S is the sensitivity in N/mm.

Table 1

Testing conditions for fatigue and fretting fatigue tests

Material	Heat treatment condition	Type of test	Test temperature °C	Mean tensile stress MN/m^2
Ti-6Al-4V	IMI 318* as received	Fatigue	20	371 - 468
			200	324 - 497
			400	401 - 463
			600	247
		Fretting fatigue	200	247
			400	
			600	
	AMMRC** as received	Fatigue	20	400
			100	
		Fretting fatigue	20	400
			100	
Inconel 718 alloy	Annealed	Fretting fatigue	20	256
			600	
	Aged	Fatigue	20	550
			280	
			540	
			700	
		Fretting fatigue	20	550
			280	
			540	
			700	

Notes: * Ti-6Al-4V supplied by Imperial Metal Industries

** Ti-6Al-4V supplied by Army Materials and Mechanics Research Center

The clamping pressure for all the fretting fatigue tests was 32 MN/m^2.

Table 2

Calculations for the slip amplitude in the fretting fatigue tests

Material	Nomenclature	Temperature ^{o}K	Modulus of elasticity E MN/m^2	Alternating stress (A) MN/m^2	Slip amplitude μm
Ti-6Al-4V alloy (AMMRC)	Minimum	293	106×10^3	84	13.9
	Maximum	373	102×10^3	174	29.9
Inconel 718 alloy (aged)	Minimum	293	200×10^3	120	10.5
	Maximum	813	171×10^3	350	35.8

Slip amplitude (peak to peak) = $\frac{17.5\ A}{E} \times 1000\ \mu m$

Notes: 1. The above formula is for 19 mm bridge length with 1.5 mm foot length

2. E values were obtained from manufacturers' data.

Table 3

The strains experienced by each strain gauge separately

Strain gauge No.	Strains
1	$-\varepsilon_X$, $-\varepsilon_Y$
2	$-\varepsilon_X$, ε_Y
3	$-\varepsilon_X$
4	$-\varepsilon_X$
5	$\nu\varepsilon_X$
6	$\nu\varepsilon_X$
7	$\nu\varepsilon_X$, $\nu\varepsilon_Y$
8	$\nu\varepsilon_X$, $-\nu\varepsilon_Y$

Table 4

Effect of temperature on the recorded normal force

Testing temperature ^oC	Light spot displacement mm
21	82
96	78
188	83
339	82
465	78
593	78.5
532	80.5
494	80.5

Table 5

Effect of temperature on the recorded frictional force

Testing temperature ^oC	Light spot displacement mm
22	44
143	48
288	46
457	46
523	41

Table 6

The plain fatigue results of Ti-6Al-4V (IMI 318) at room temperature, 200 and 400 C before adjustment (obtained from S-N curves before adjustment) and after adjustment obtained by calculating method given in Appendix C

Note: The calculation adjusted for Sm_1 = 247.1 MN/m^2

Temperature °C	Number of cycles N	Sa_2 MN/m^2	Sm_2 MN/m^2	Su MN/m^2	Sa_1 MN/m^2	Remarks
Room temperature	12 333 800	339.77	370.66	1037	402.8	
	5 900	443.16	467.88		615.1	
	21 900	417	463.33		574.2	
	60 700	386.11	417		491.9	
	148 900	355.22	417		452.6	
	11 370 400	339.77	417		432.9	
200 C	12 487 000	293.44	324.33	833	338	Unbroken
	16 000	370.66	401.55		503.3	
	22 900	339.77	370.66		430.6	
	11 279 000	293.44	370.66		371.8	Unbroken
	32 100	308.89	370.66		391.4	
	41 800	324.33	370.66		411	
	3 468 500	308.89	370.66		391.4	
	14 300	296.34	496.69		516.3	
400 C	12 047 100	123.55	463.32	726	225.2	Unbroken
	13 900	247.1	463.32		450.5	
	11 587 200	185.33	463.32		337.9	Unbroken
	35 000	231.86	463.32		422.3	
	17 600	211.99	401.55		312.9	
	41 300	200.78	401.55		296.4	
	12 487 300	169.89	401.55		250.8	Unbroken
	11 702 700	185.33	401.55		273.5	Unbroken
	13 602 000	193.05			284.9	Unbroken

Table 7

The initial values of the radius of the contact area, the maximum pressure and the mean pressure before starting the fretting wear tests

Material	Temperature °C	Modulus of elasticity MN/m^2	a mm	P_o MN/m^2	P_m MN/m^2
Ti-6Al-4V	20	106 000	0.152	56.55	37.70
	100	102 000	0.154	55.11	36.74
Inconel 718	20	200 000	0.123	86.34	57.56
	280	186 000	0.126	82.26	54.84
	540	171 000	0.130	77.78	51.85

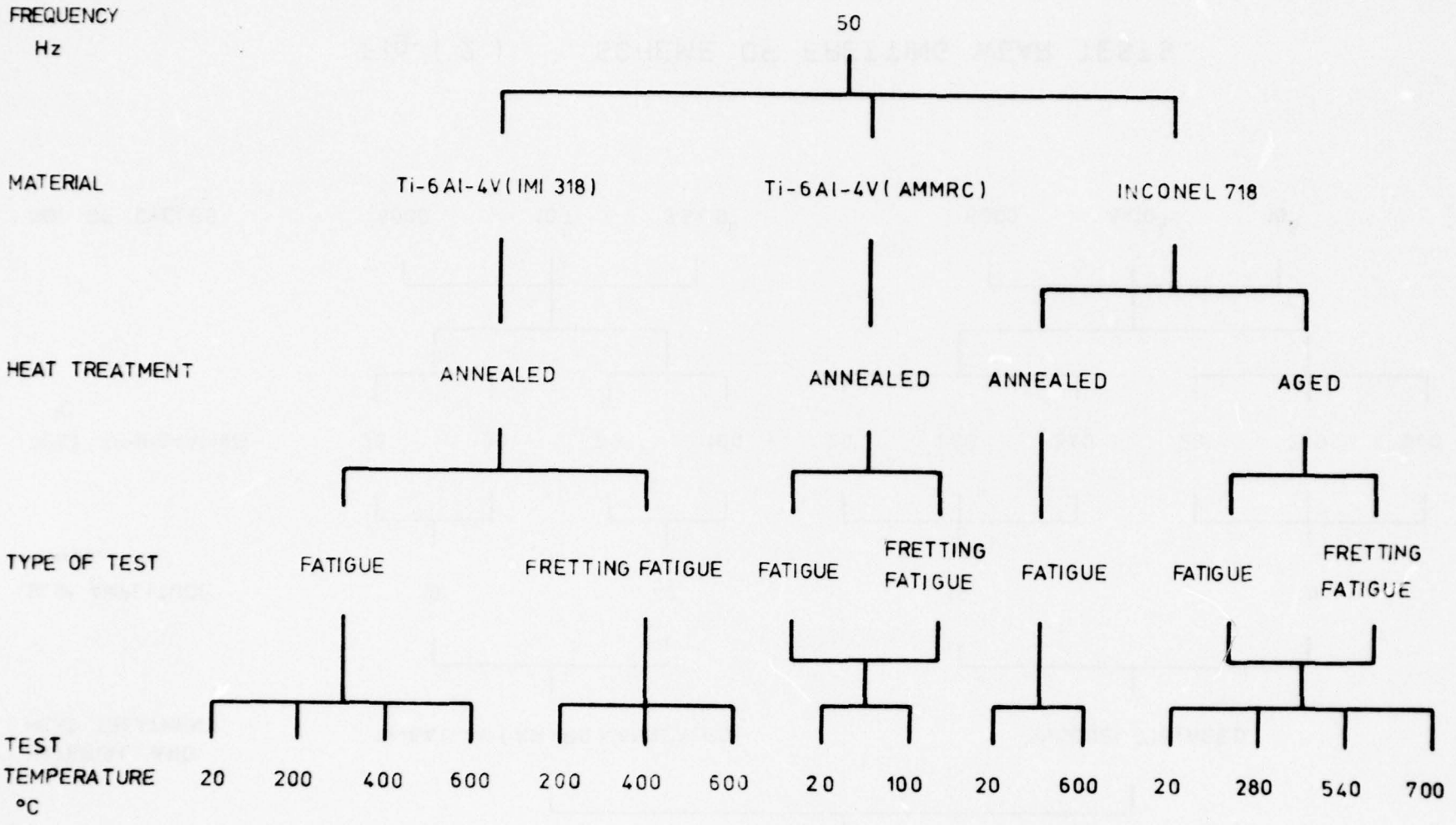

Fig. (1) FATIGUE AND FRETTING FATIGUE TESTS SCHEME.

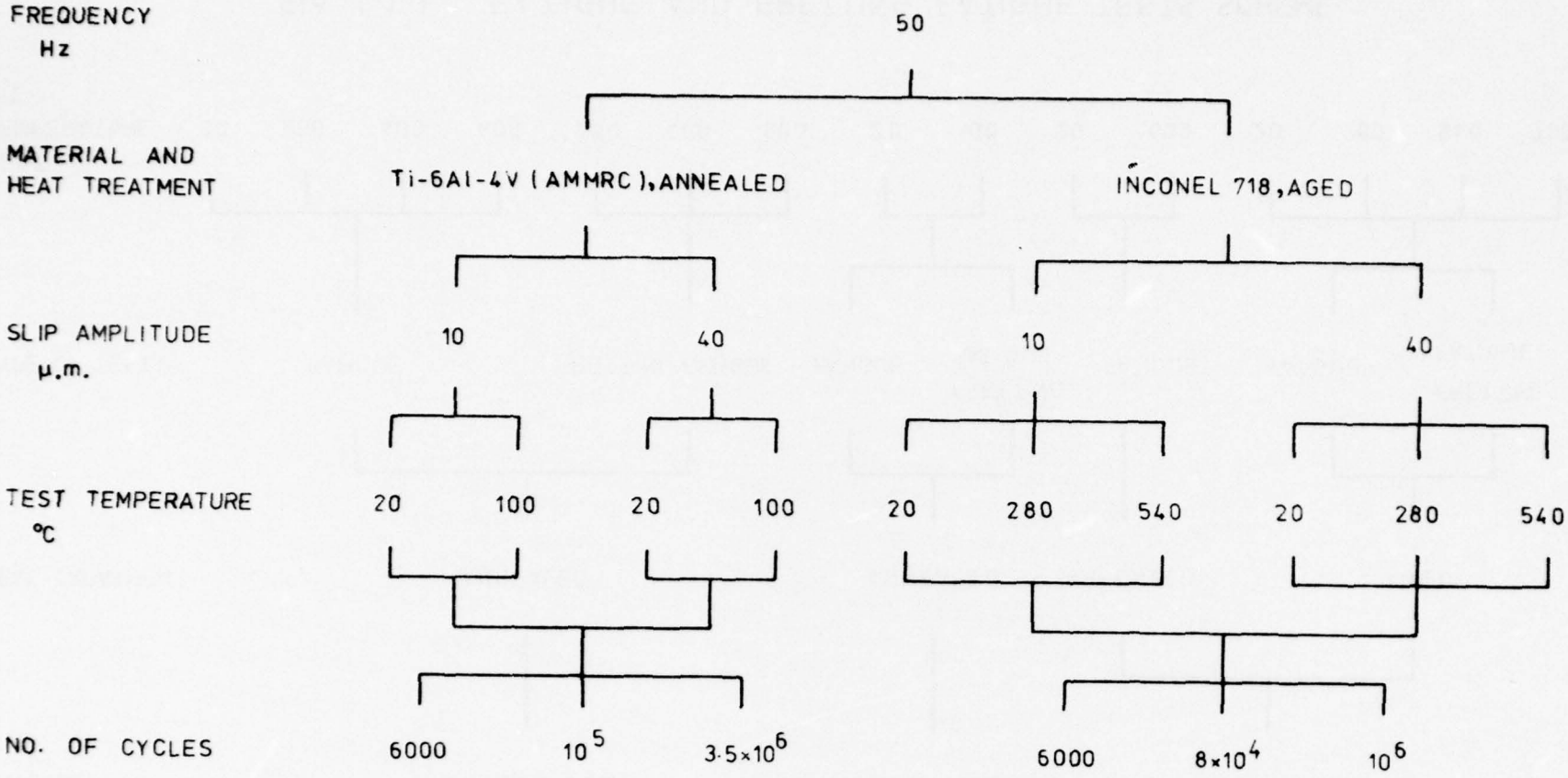

Fig. (2) SCHEME OF FRETTING WEAR TESTS.

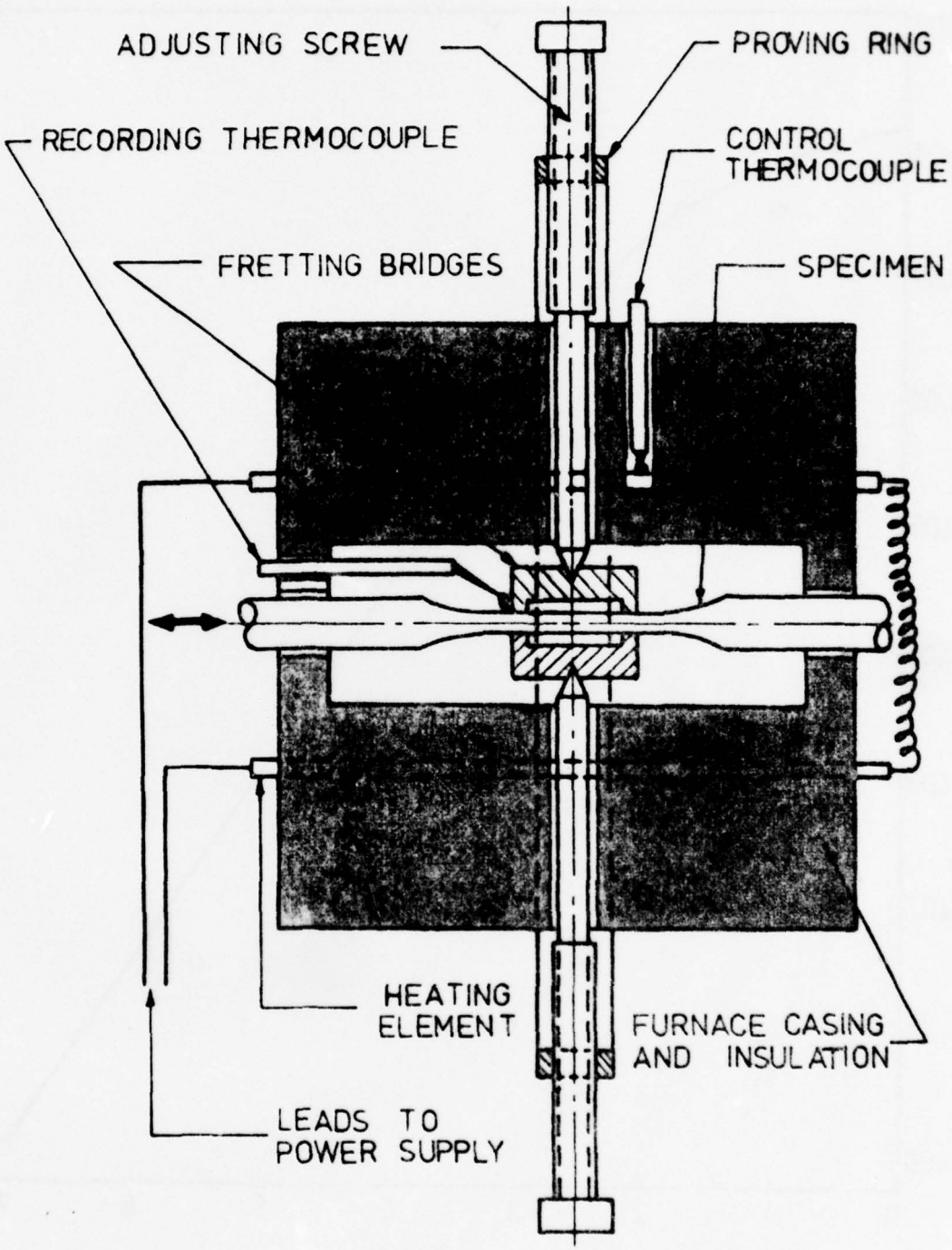

Fig. (3) PLAN VIEW OF FURNACE AND SPECIMEN WITH FRETTING BRIDGES CLAMPED ON TO IT.

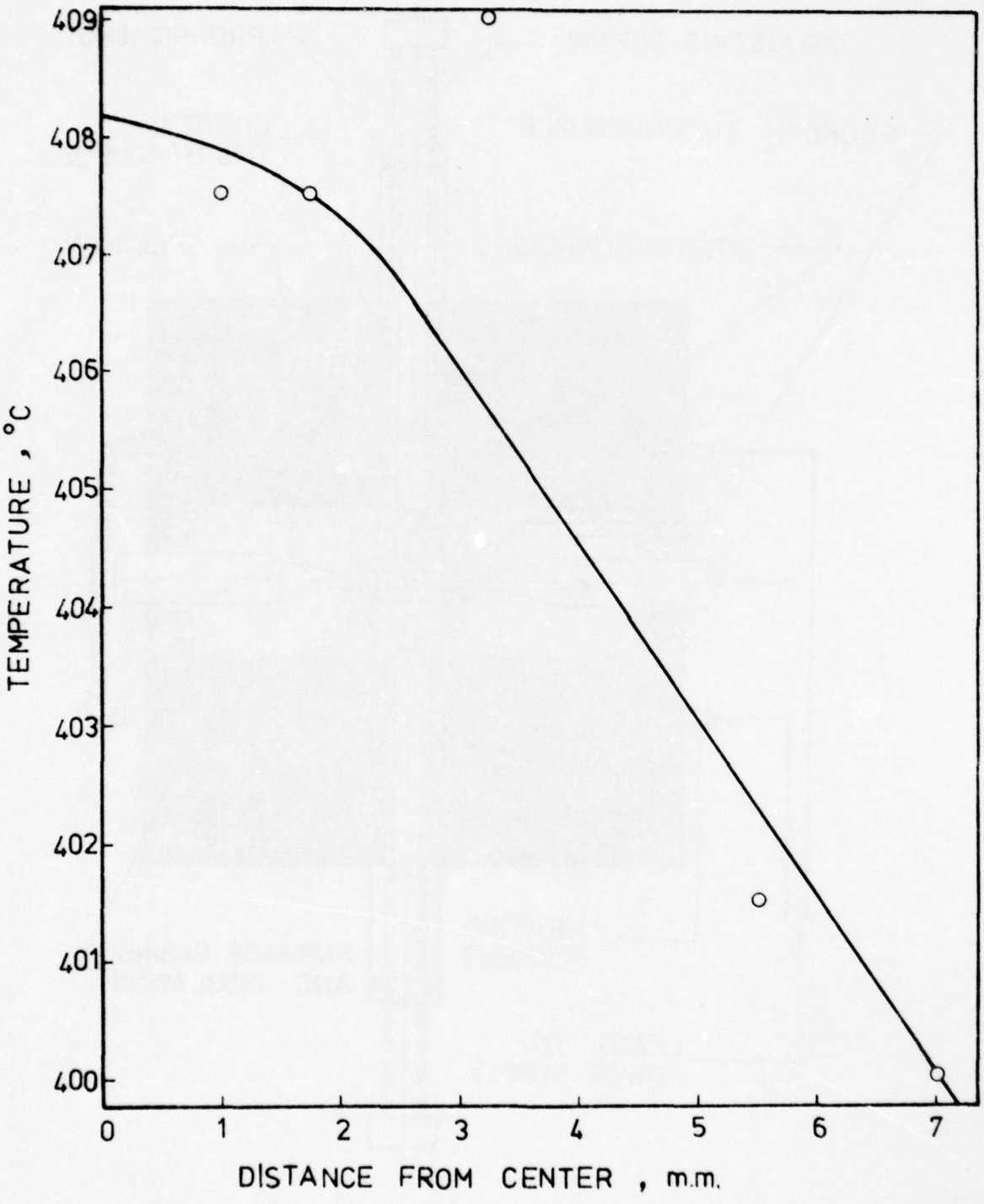

FIG.(4) TEMPERATURE DISTRIBUTION IN THE RADIAL DIRECTION.

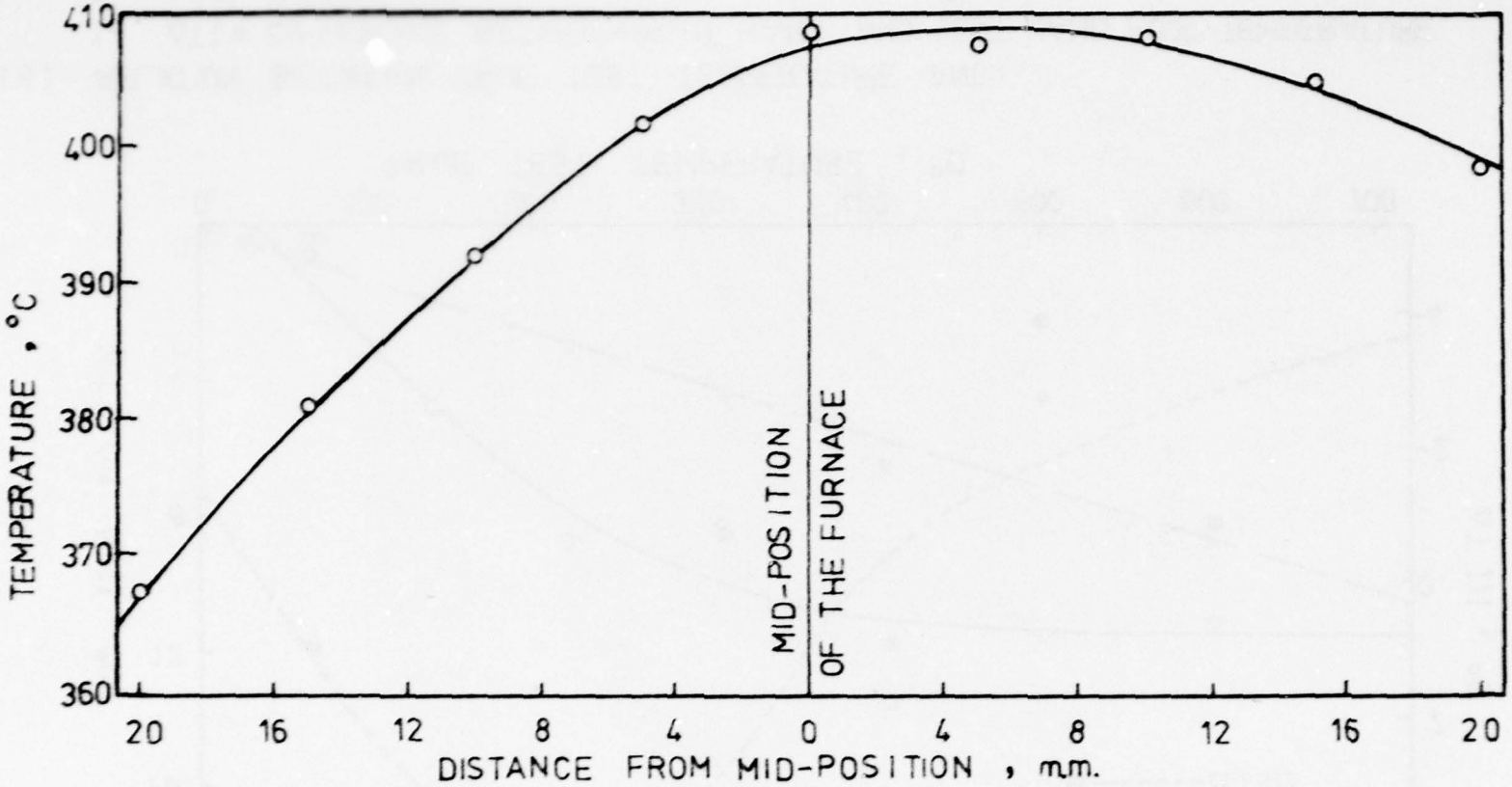

FIG.(5) TEMPERATURE DISTRIBUTION IN THE LONGITUDINAL DIRECTION.

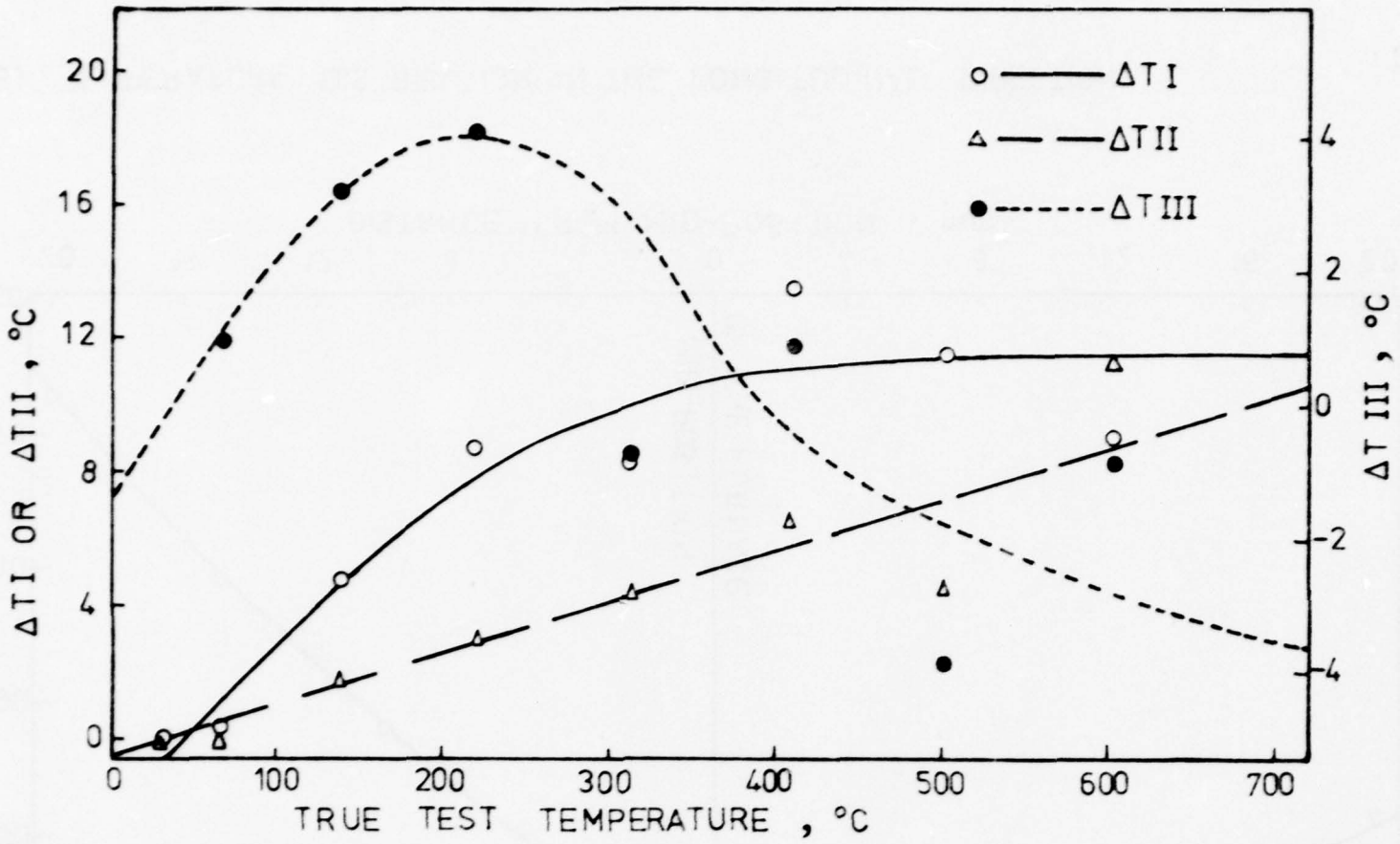

FIG.(6) RELATION BETWEEN TRUE TEST TEMPERATURE AND:

1- ΔT I ≡ DIFFERENCE BETWEENRIGHT HAND AND LEFT HAND FOOT TEMPERATURE.

2- ΔT II ≡ TEMPERATURE VARIATION IN RADIAL DIRECTION.

3- ΔTIII ≡ DIFFERENCE BETWEEN RADIAL AND LONGITUDINAL TEMPERATURE.

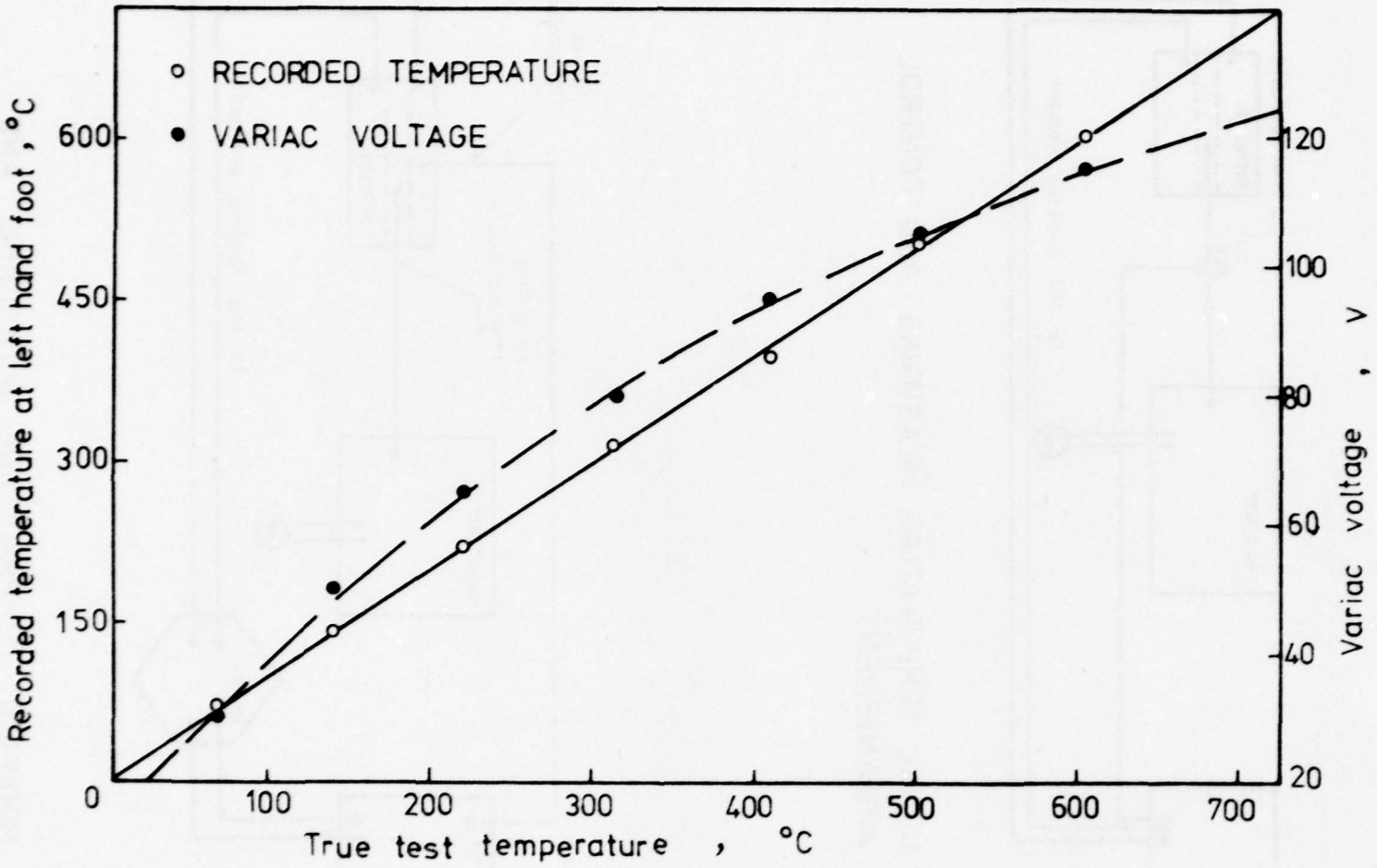

FIG.(7) Relation between true test temperature and recorded temperature at left hand foot of the bridge and the suitable variac voltage.

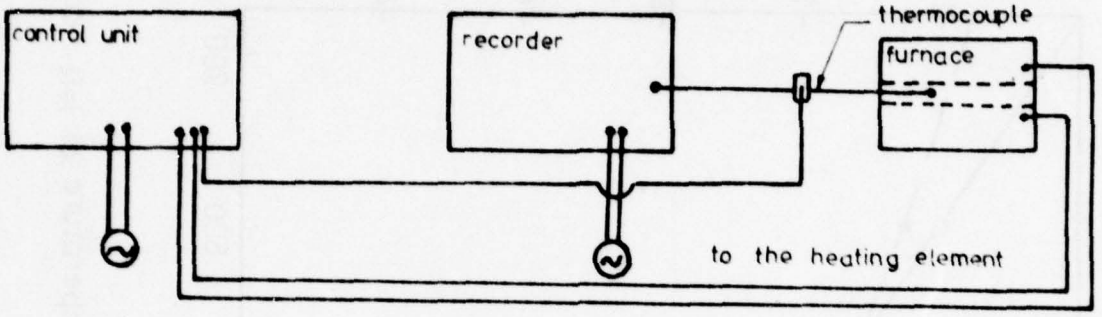

FIG.(8) INITIAL TEMPERATURE MEASURING AND CONTROL ARRANGEMENT.

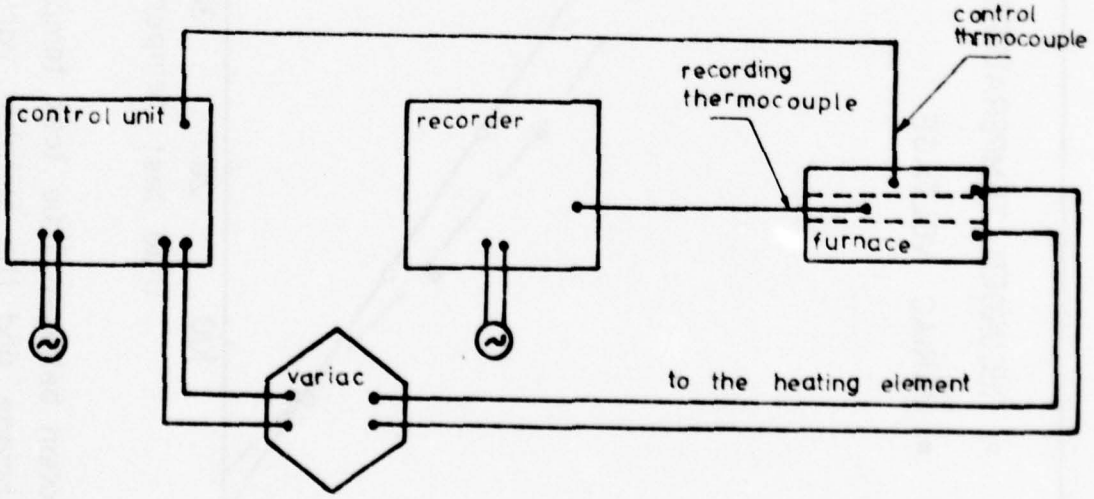

FIG.(9) MODIFIED TEMPERATURE MEASURING AND CONTROL ARRANGEMENT.

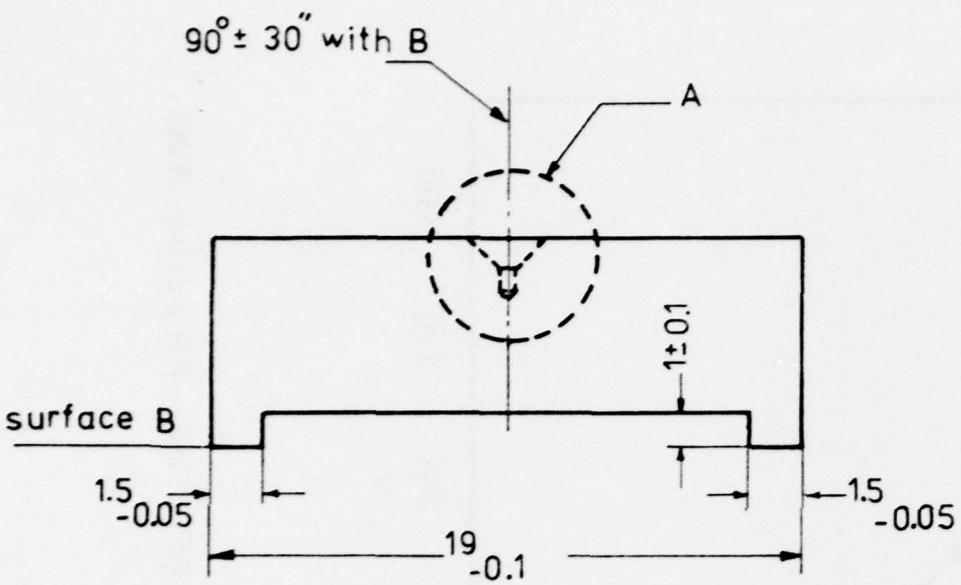

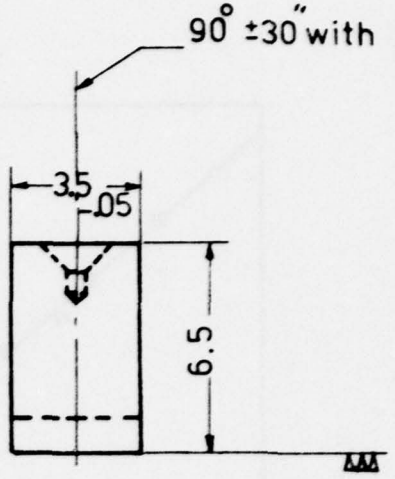

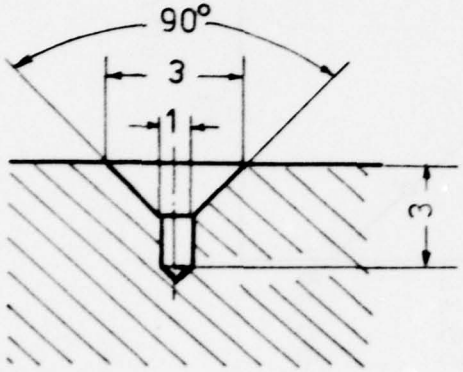

Details of A (Scale 10:1)

Scale 5:1 (10:1)
Dimensions in millemeters

FIG.10 FRETTING FATIGUE BRIDGE.

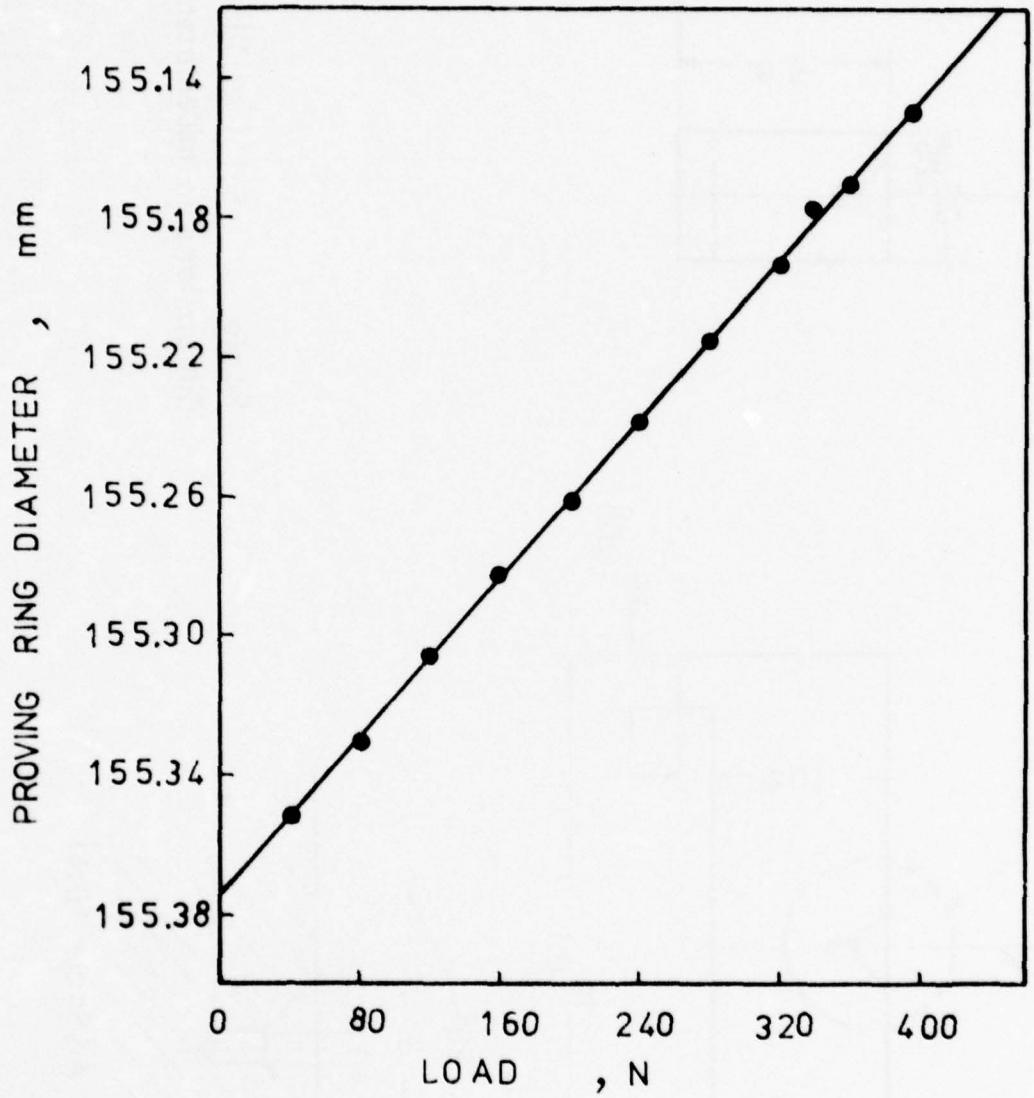

FIG. 11 CALIBRATION OF THE PROVING RING.

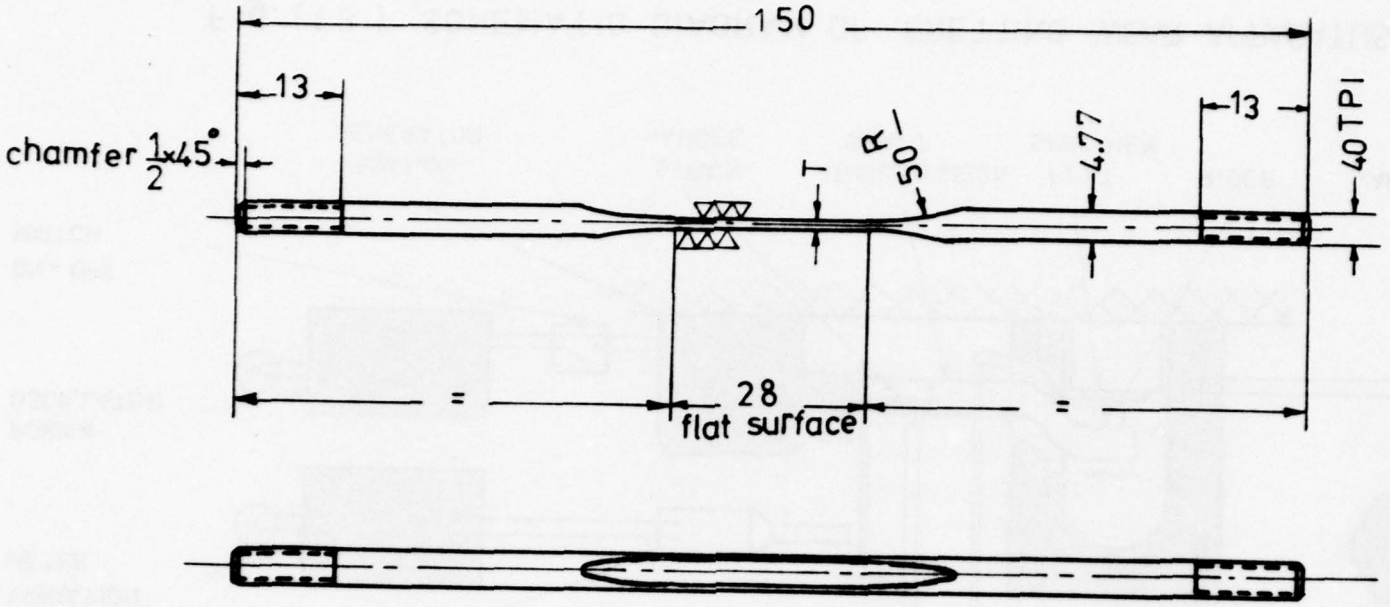

Scale : 1:1
Dimensions : in millemeters

FIG. 12 FATIGUE AND FRETTING FATIGUE SPECIMENS.

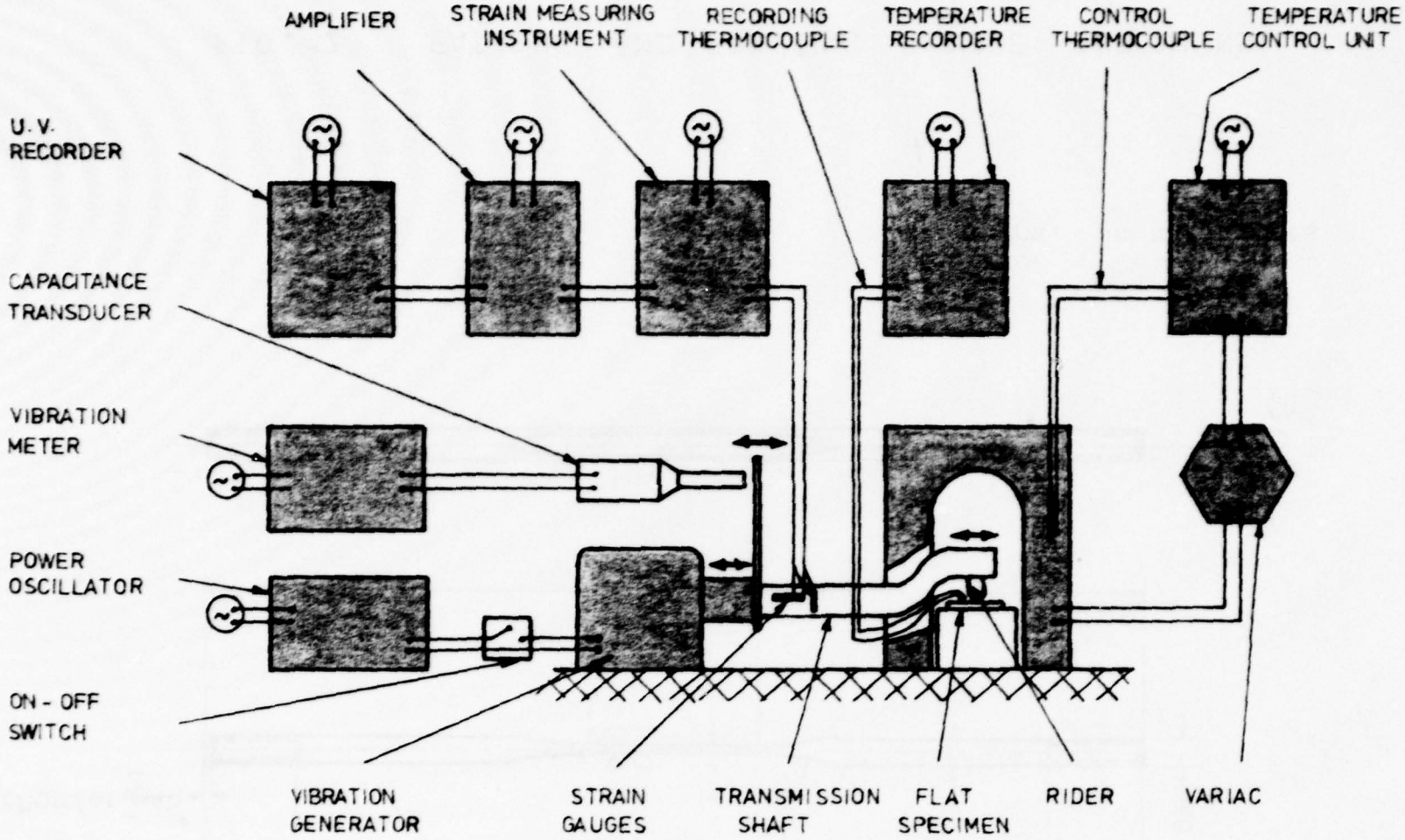

Fig. (13) SCHEMATIC DIAGRAM OF FRETTING WEAR APPARATUS.

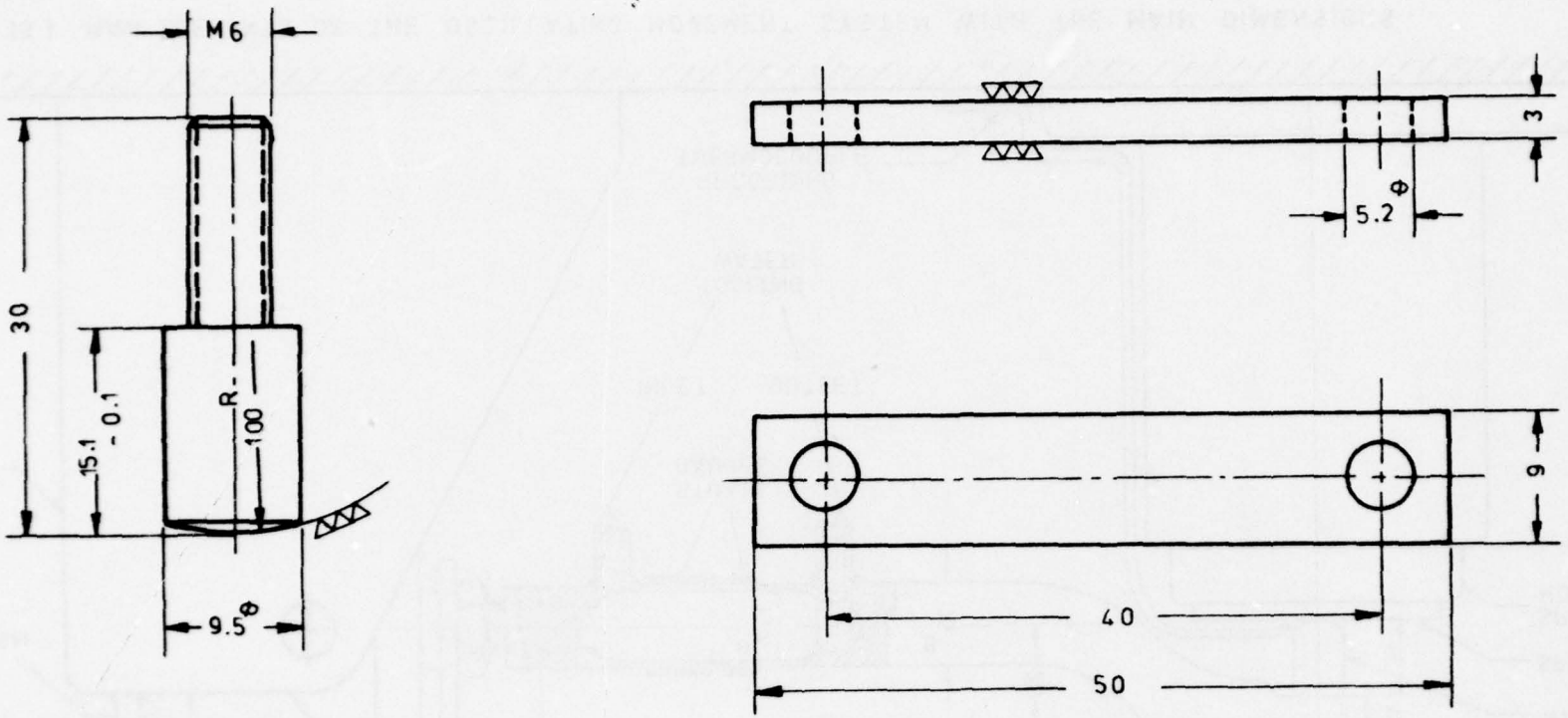

BREAK SHARP CORNERS
DIMENSIONS IN MILLIMETERS
SCALE: 2 : 1

Fig.(14) RIDER AND FLAT SPECIMEN.

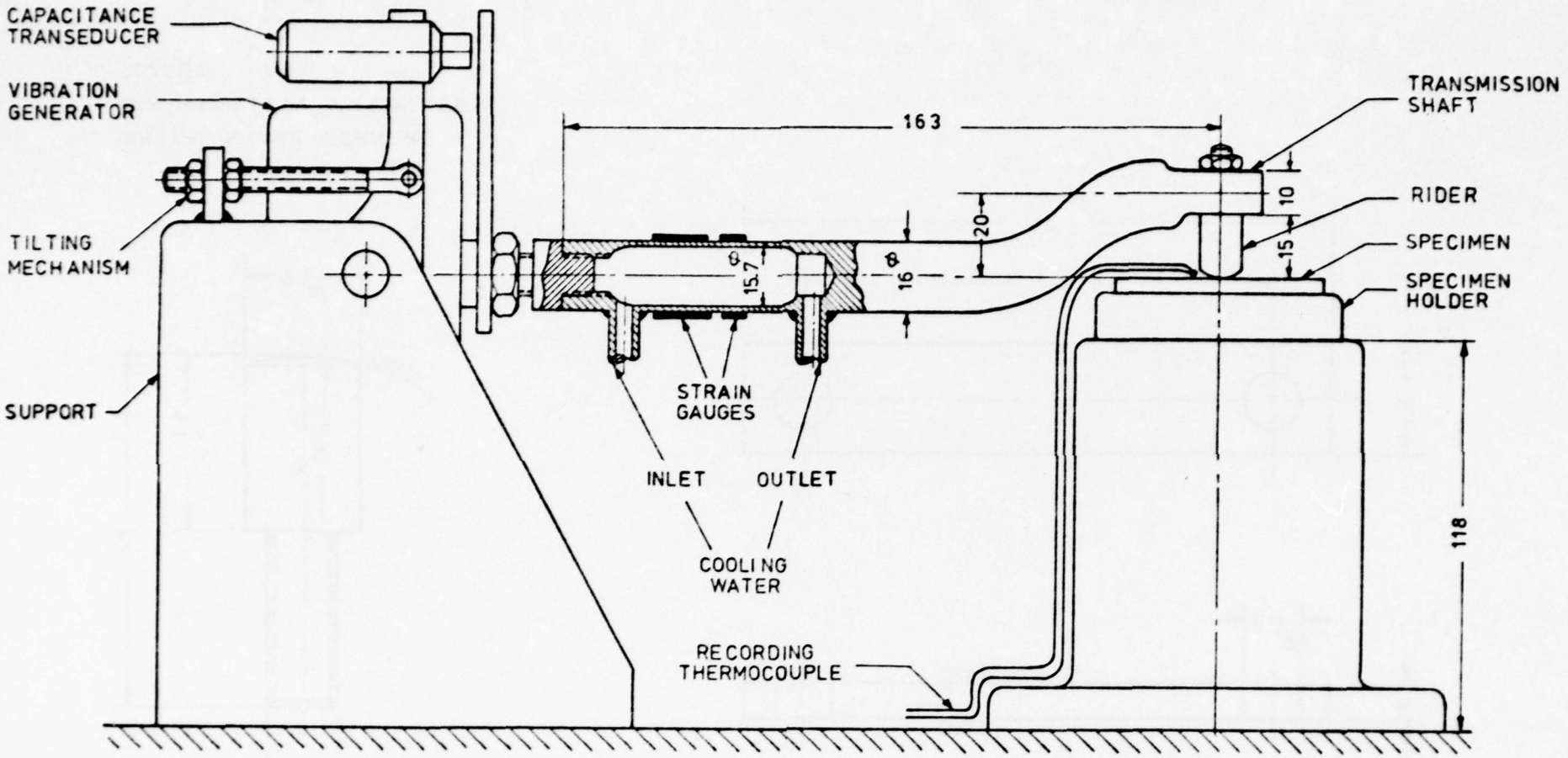

Fig. (15) MAIN ELEMENTS OF THE OSCILLATING MOVEMENT SYSTEM WITH THE MAIN DIMENSIONS.

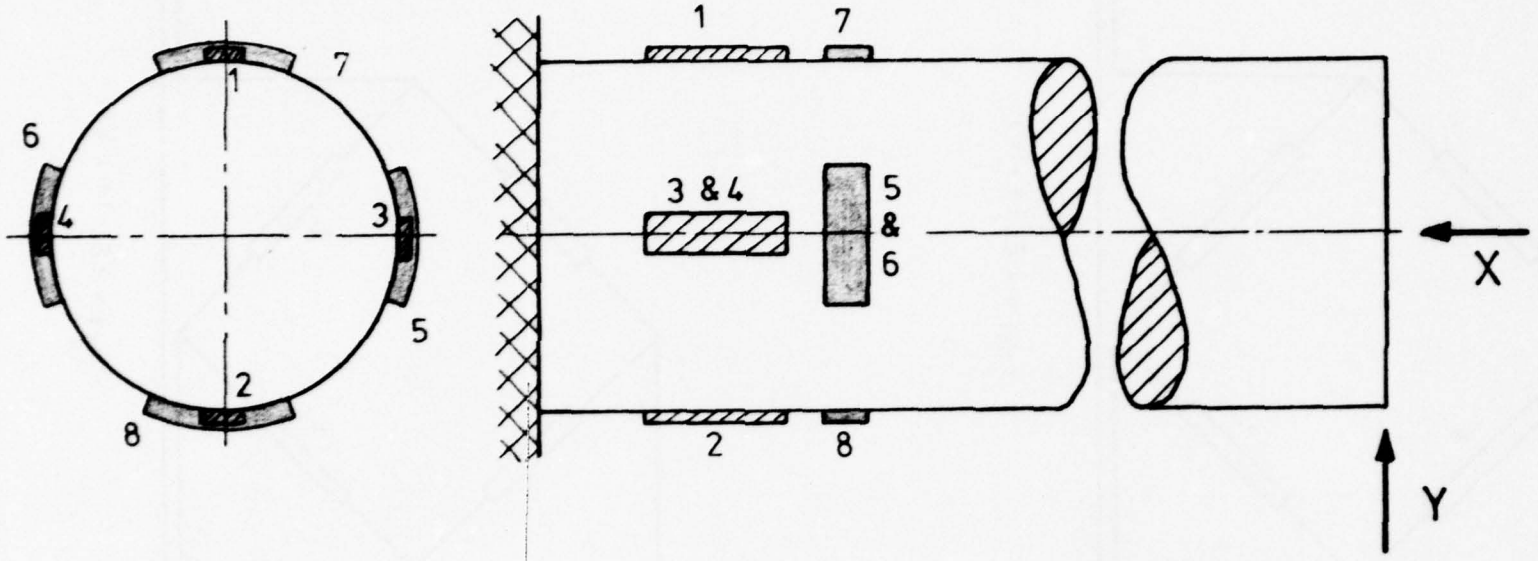

Fig. (16) RELATIVE POSITIONS OF STRAIN GAUGES ON THE SHAFT.

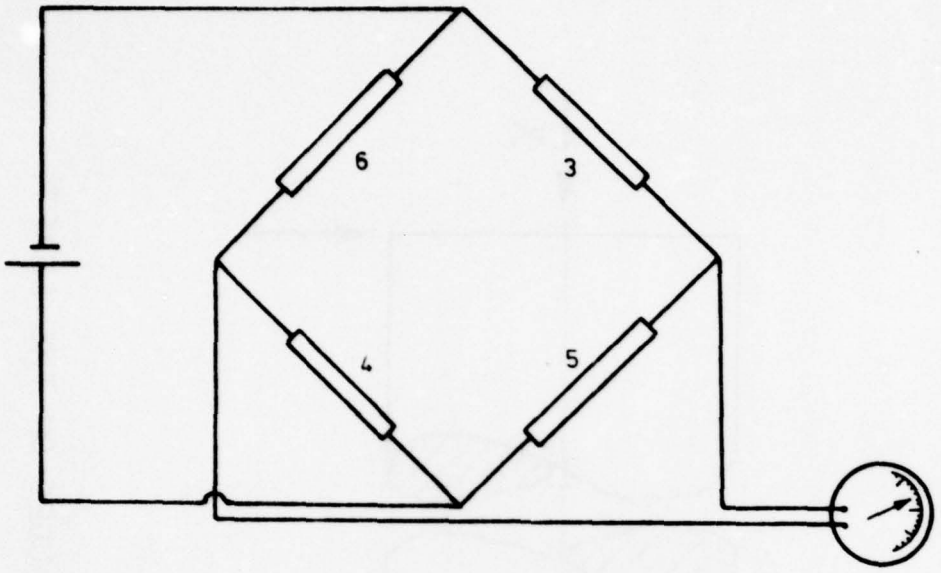

A $E_{net} = 2 E_x (1 + \nu)$

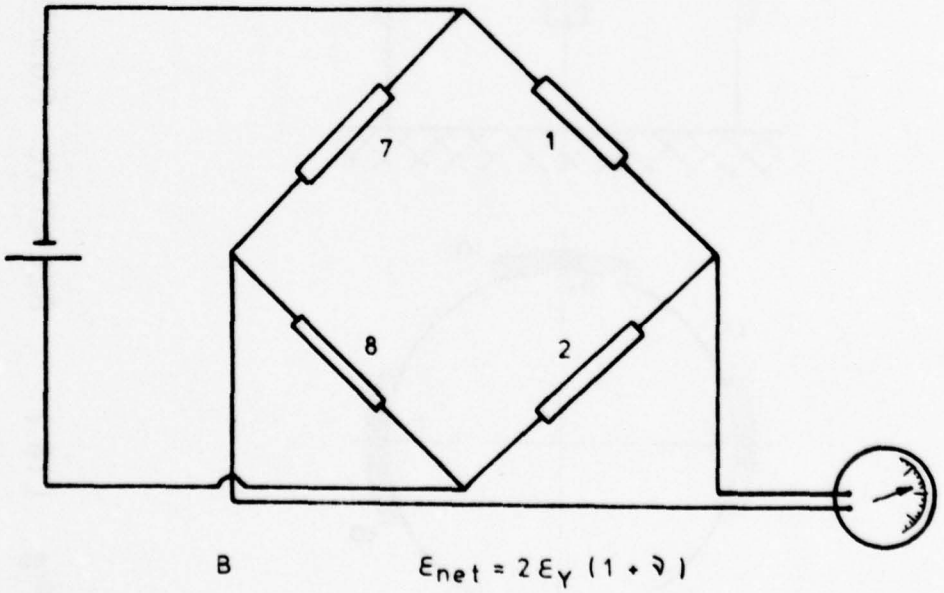

B $E_{net} = 2 E_Y (1 + \nu)$

Fig. (17) STRAIN GAUGES CIRCUITS FOR MEASURING: A-FRICTION FORCE, B-NORMAL FORCE.

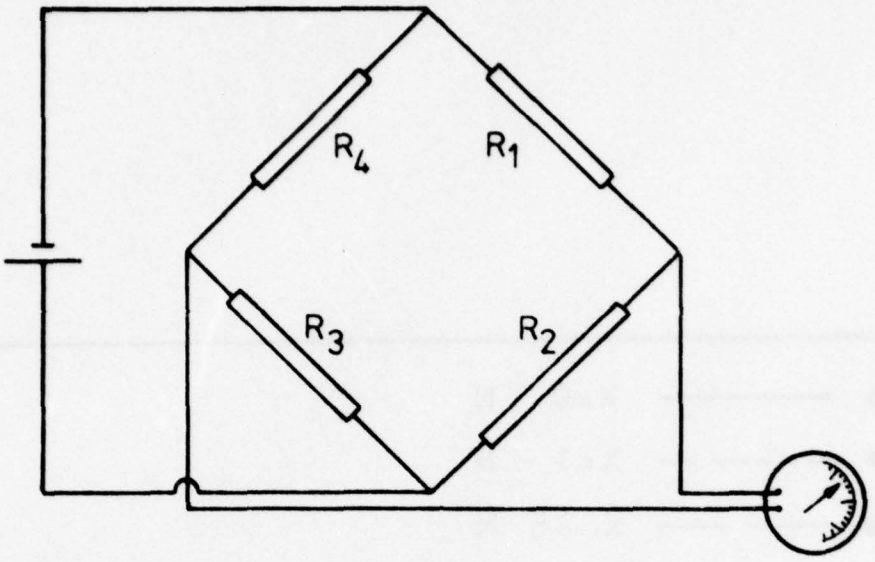

Fig.(18) FULL BRIDGE STRAIN GAUGES CIRCUIT.

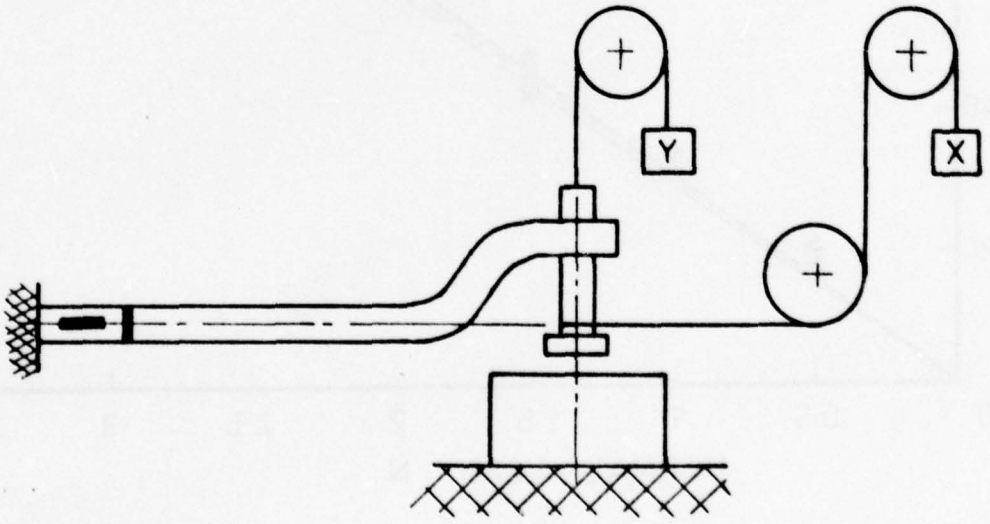

Fig. (19) ARRANGEMENT FOR CALIBRATING THE NORMAL AND FRICTION FORCES.

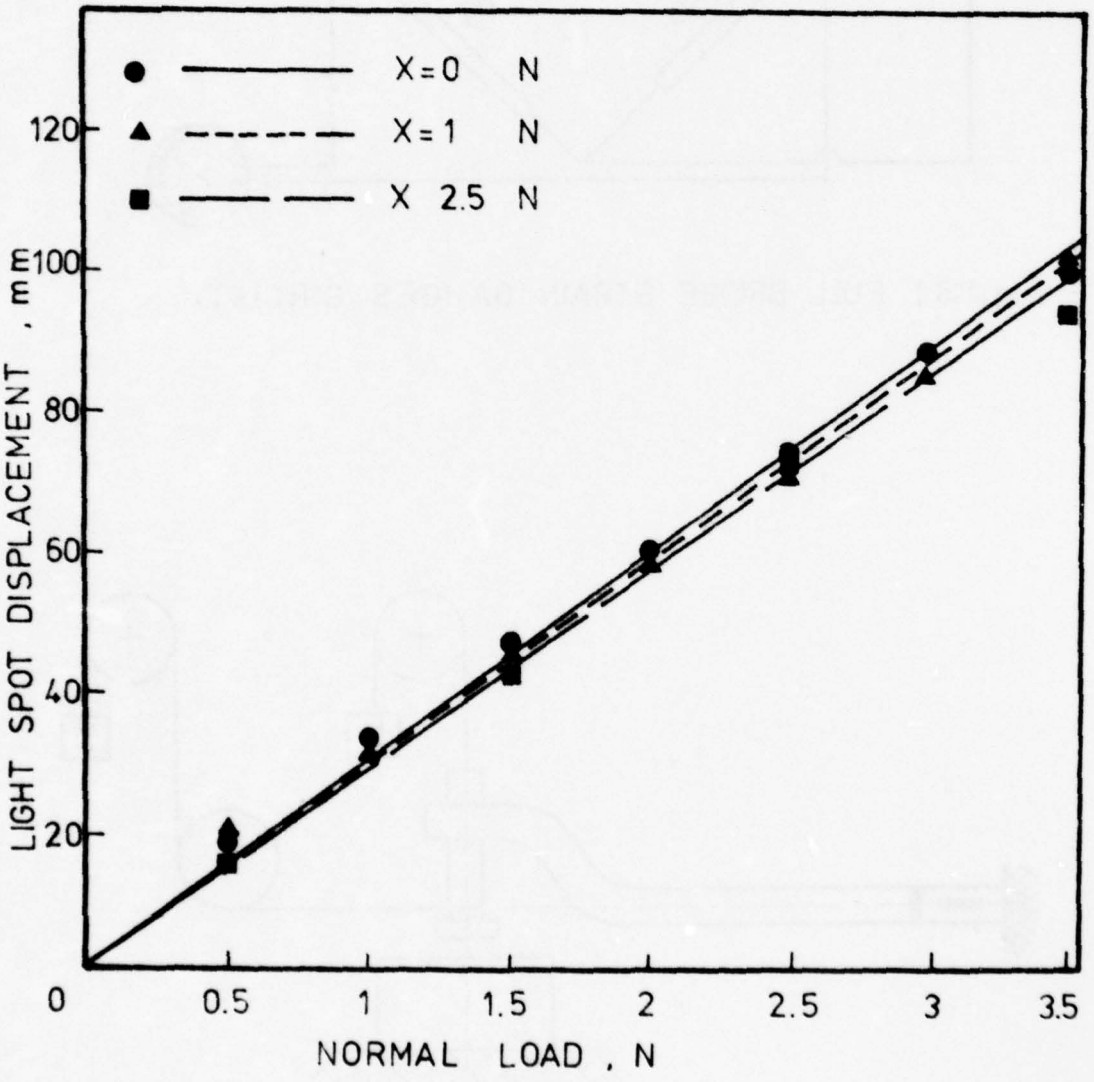

Fig. (20) CALIBRATION RESULTS OF NORMAL FORCE.

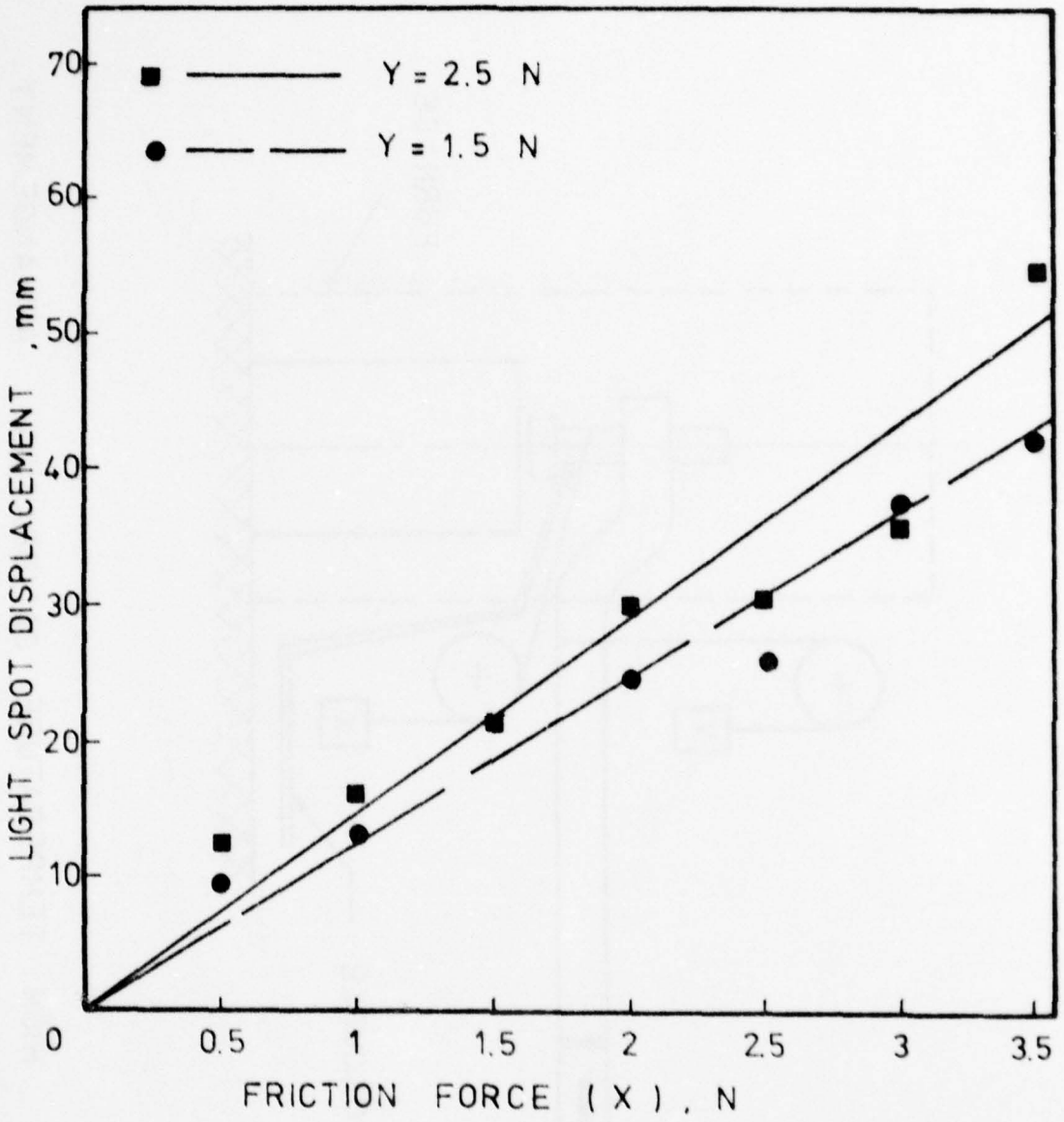

Fig. (21) CALIBRATION RESULTS OF THE FRICTION FORCE.

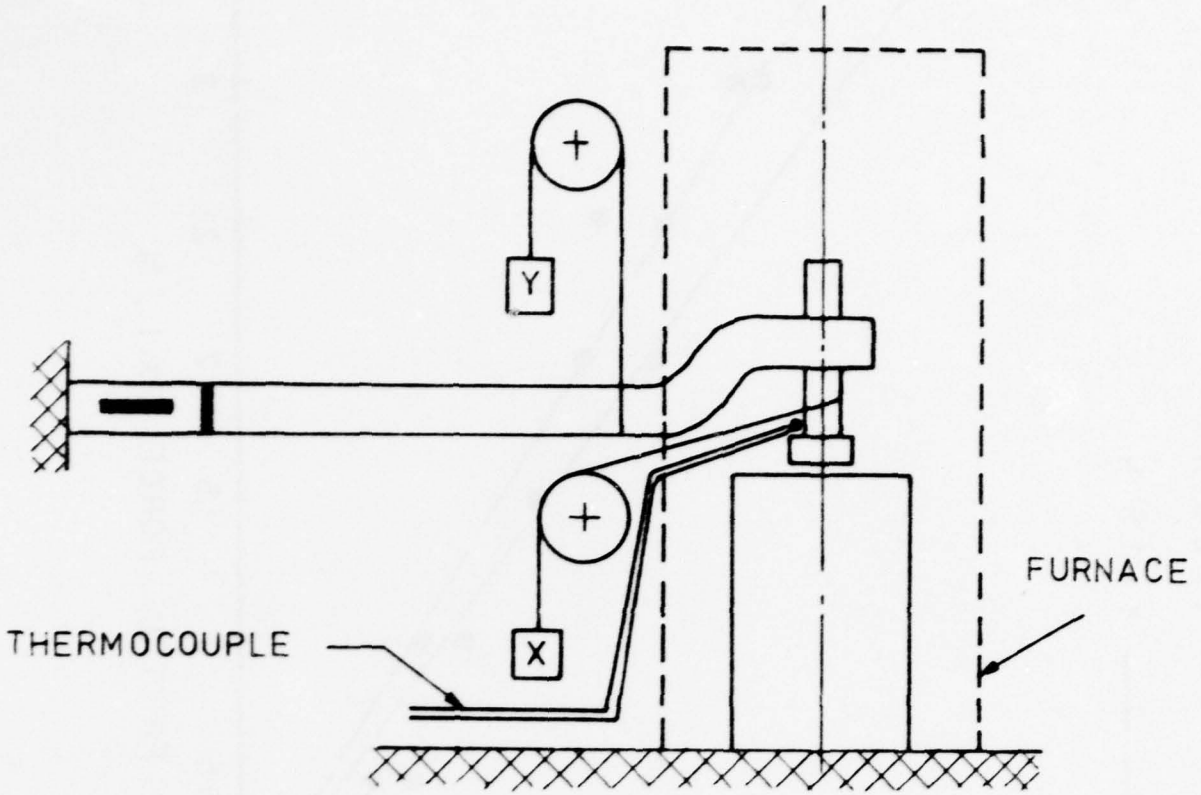

Fig. (22) HIGH TEMPERATURE CALIBRATION ARRANGEMENT.

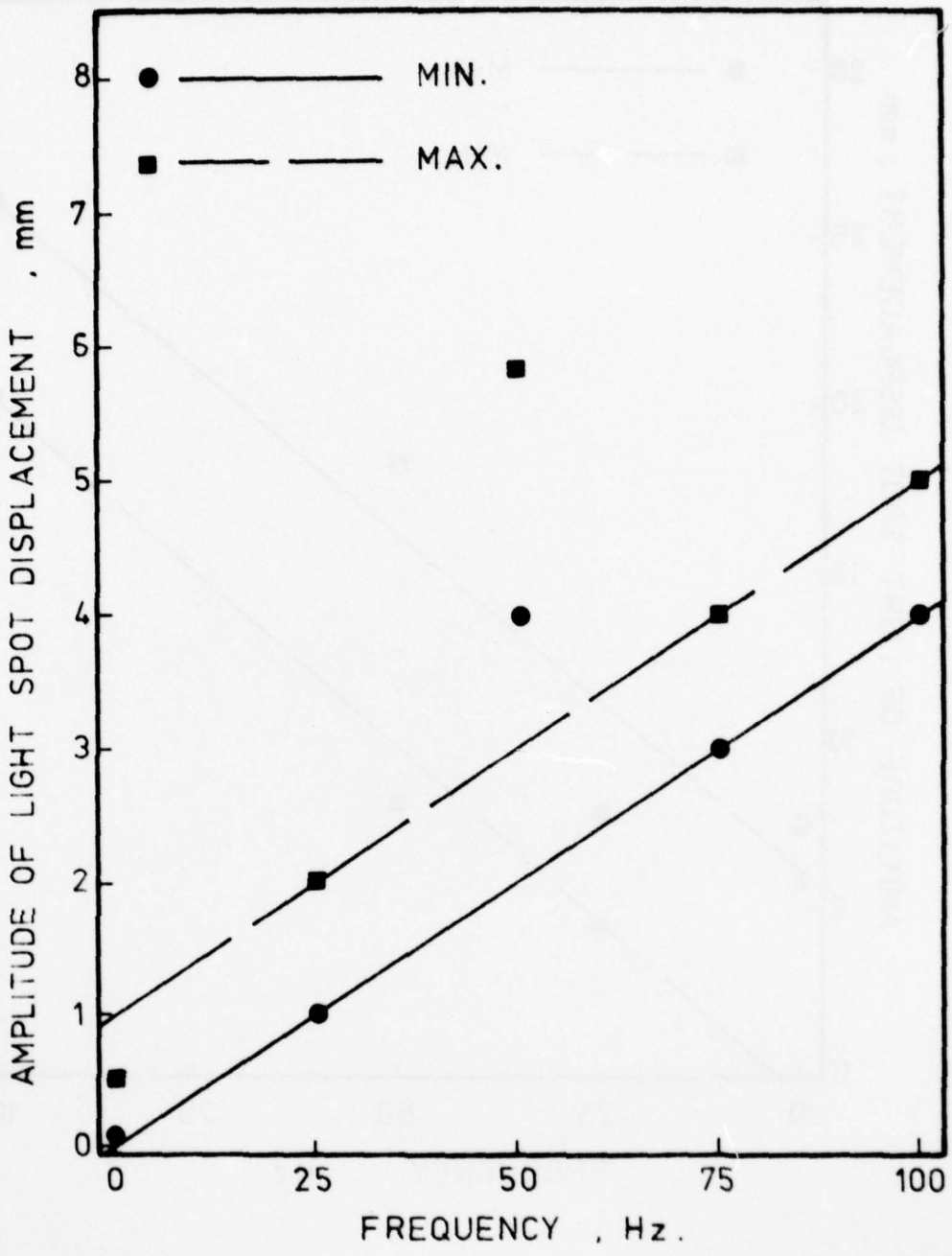

Fig. (23) THE RECORDED SIGNAL PRODUCED BY THE INERTIA FORCE IN THE NORMAL FORCE MEASURING ARRANGEMENT AT 40 μm SLIP.

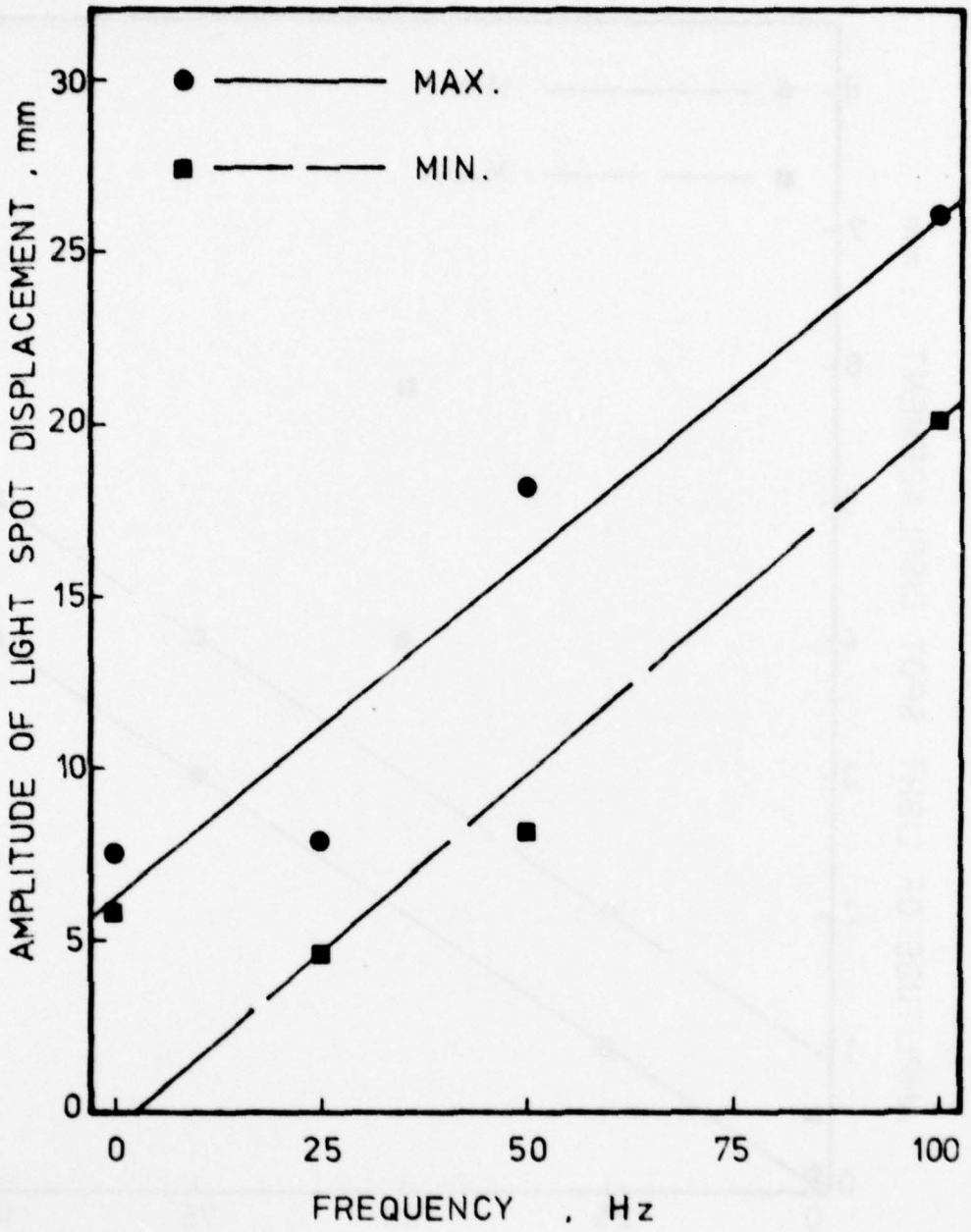

Fig. (24) THE RECORDED SIGNAL PRODUCED BY THE INERTIA FORCE IN THE FRICTION FORCE MEASURING ARRANGEMENT AT 2.5 N NORMAL FORCE AND 40 μm SLIP.

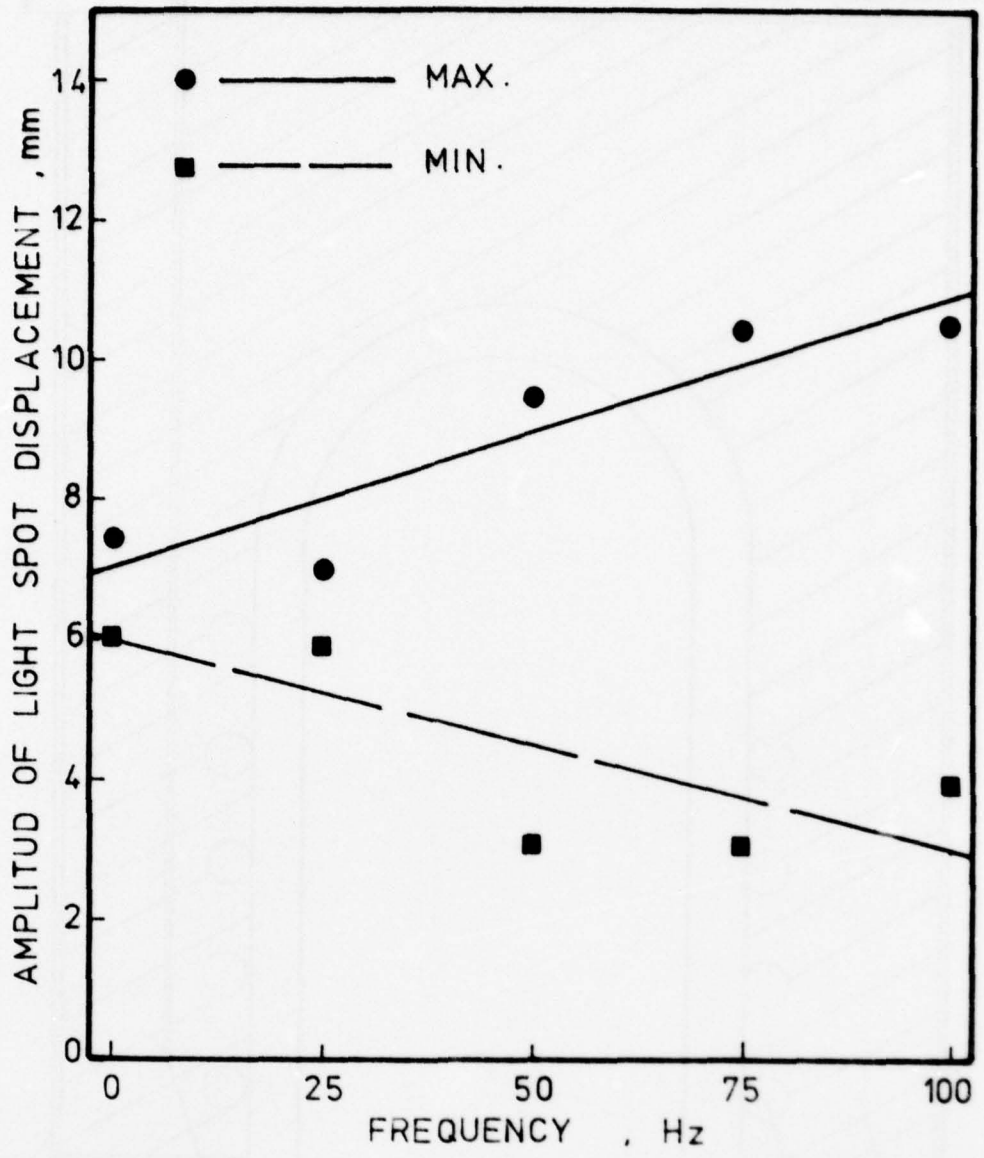

Fig. (25) THE RECORDED SIGNAL PRODUCED BY THE INERTIA FORCE IN THE FRICTION FORCE MEASURING ARRANGEMENT AT 2.5 N NORMAL FORCE AND 10 μm SLIP .

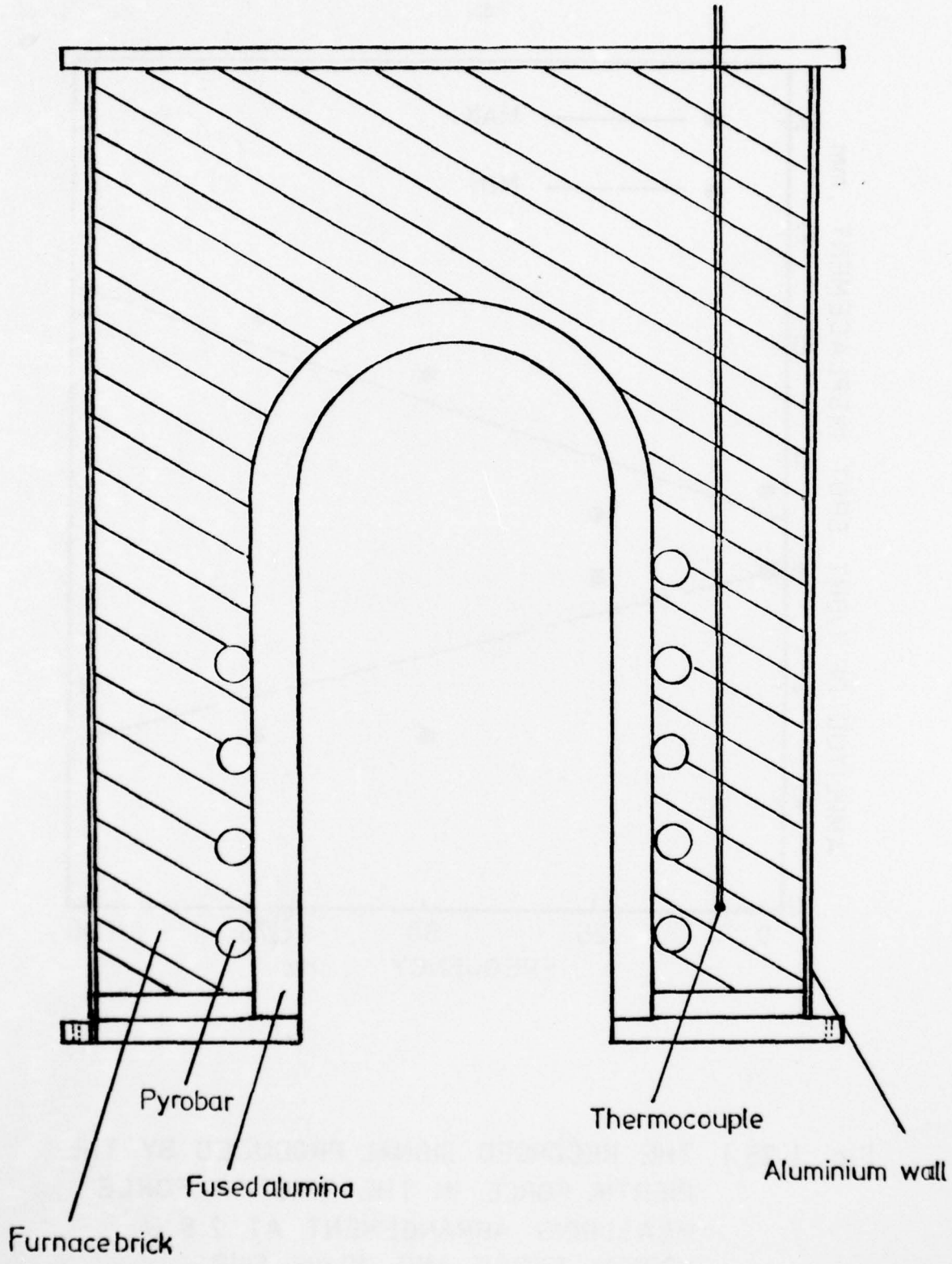

Fig. (26) THE FRETTING WEAR FURNACE .

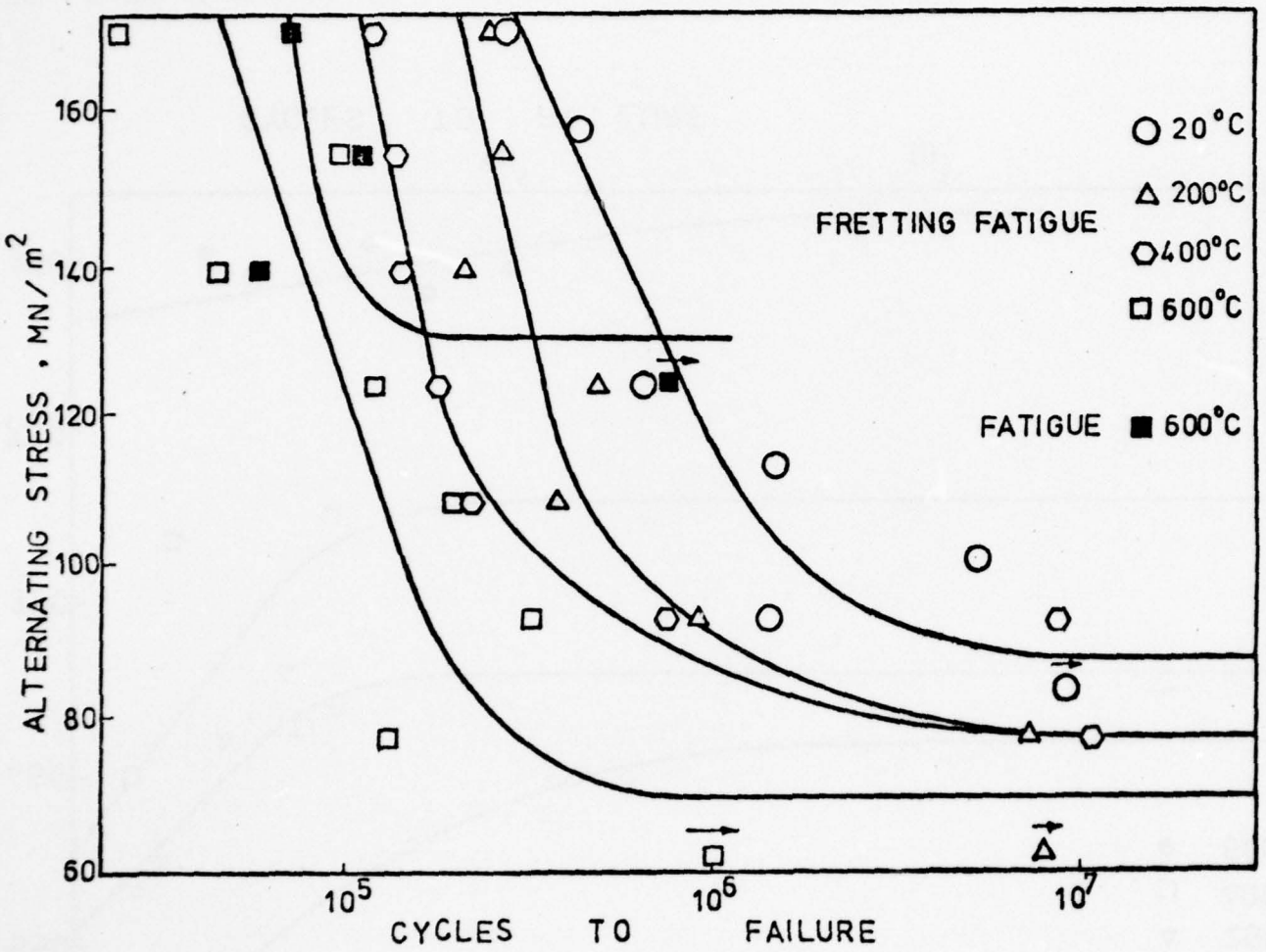

Fig. (27) FRETTING FATIGUE CURVES FOR Ti-ALLOY (IMI 318)

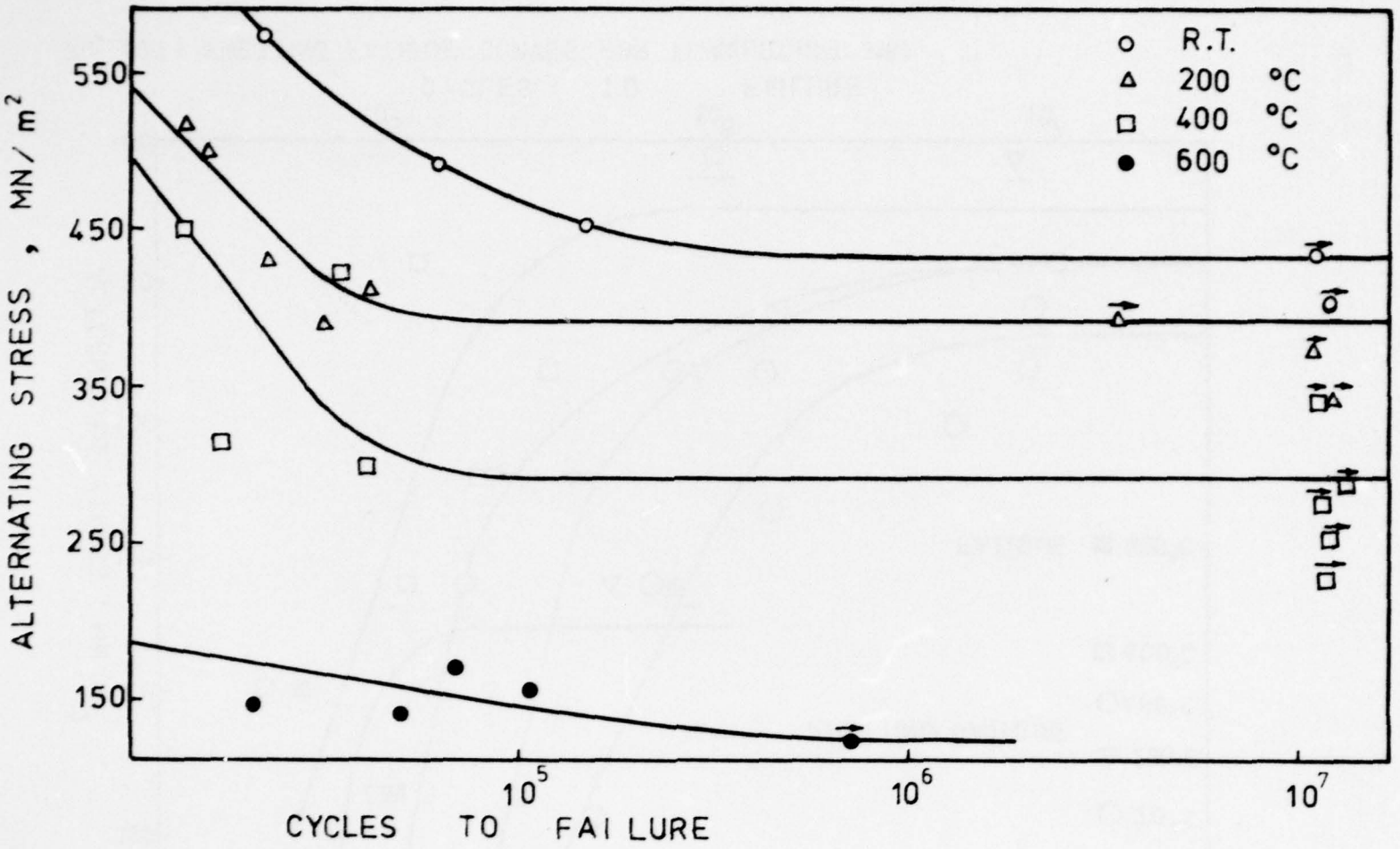

FIG. 28 FATIGUE CURVES OF ANNEALED TI-6AL-4V(IMI 318).MEAN STRESS=247 MN/ m^2.

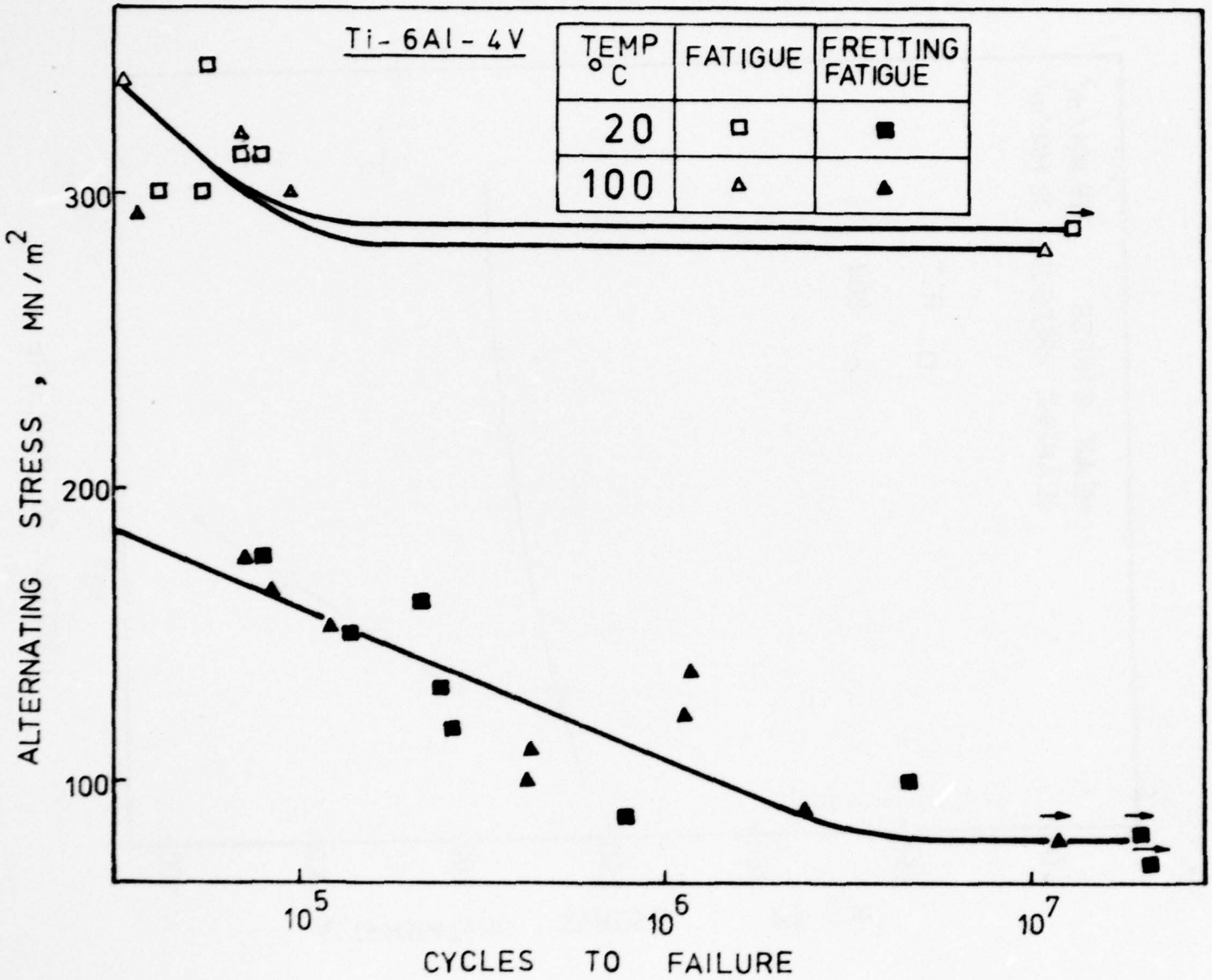

Fig. (29) FATIGUE AND FRETTING FATIGUE CURVES FOR Ti-ALLOY (AMMRC)

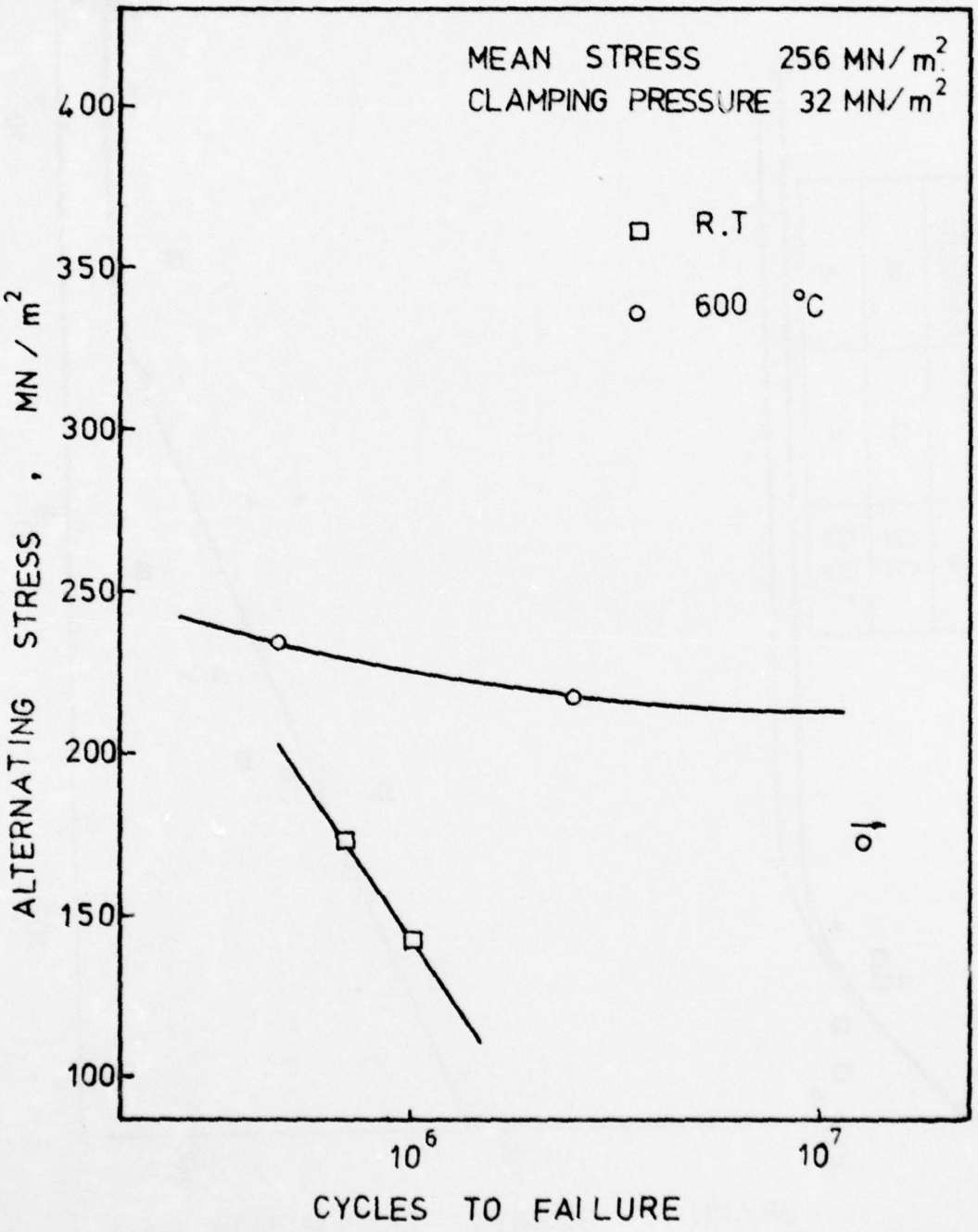

FIG.30 FRETTING FATIGUE CURVES OF ANNEALED INCONEL ALLOY 718 .

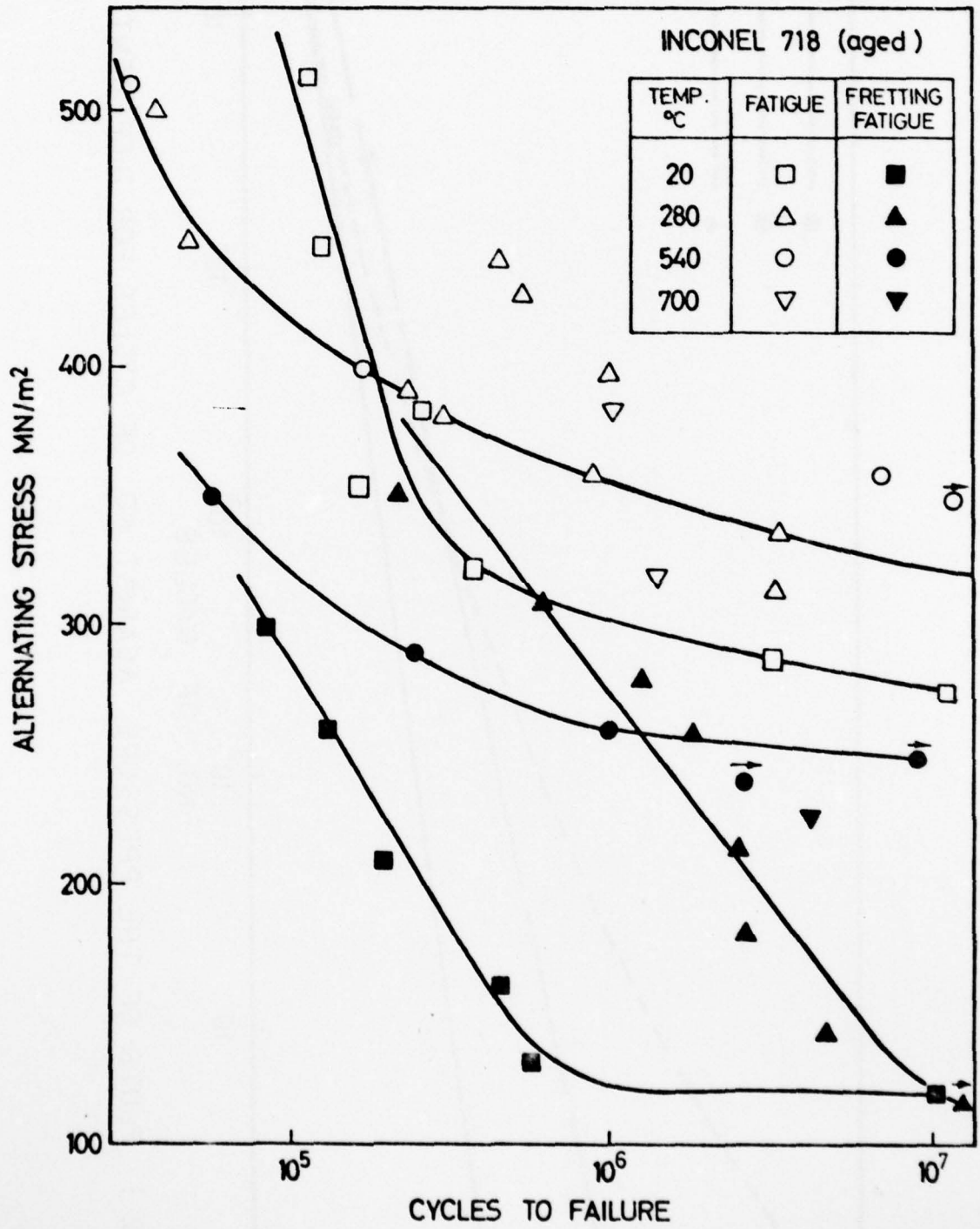

Fig.(31) FATIGUE AND FRETTING FATIGUE CURVES FOR INCONEL 718(AGED)

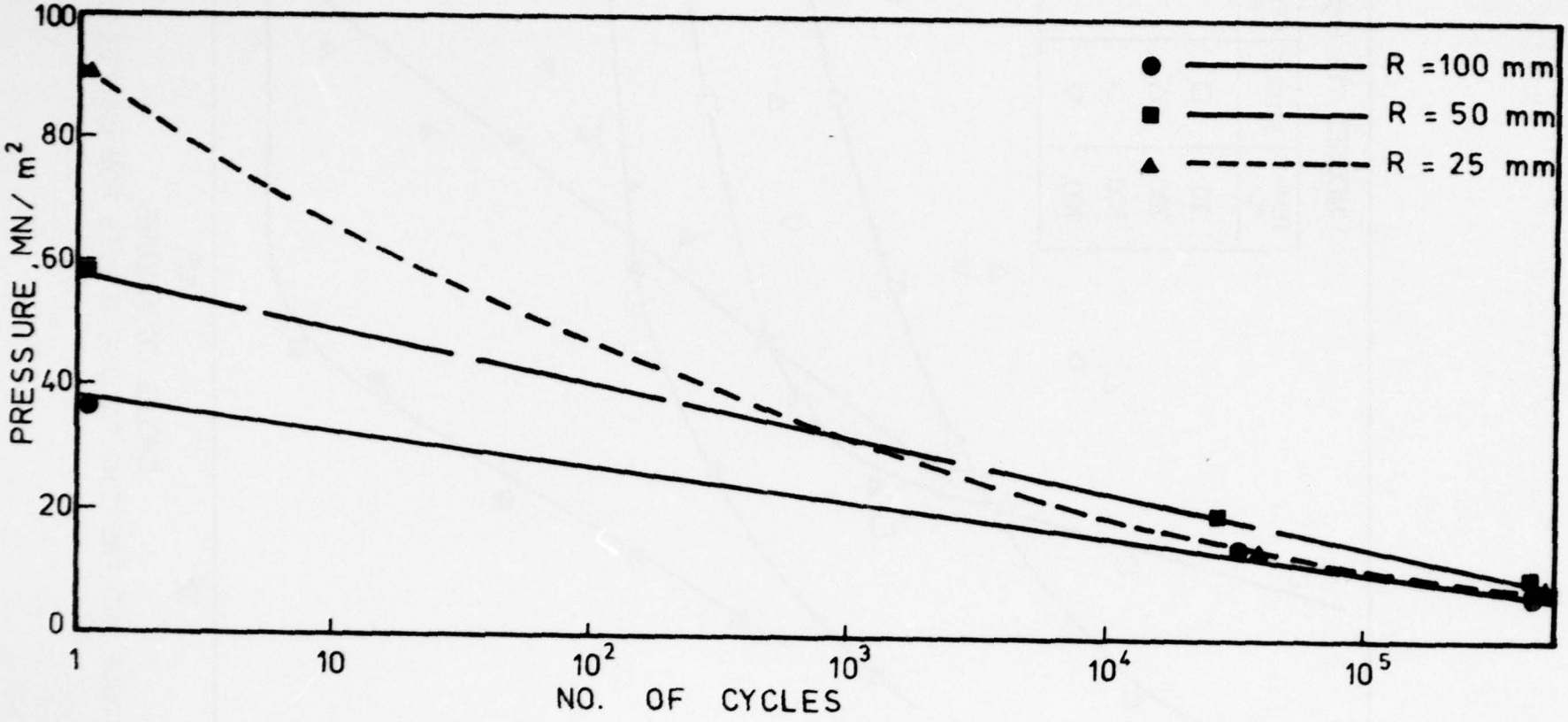

Fig.(32) PLOTS OF THE PRESSURE AGAINST NO OF CYCLES FOR DIFFERENT RADII.

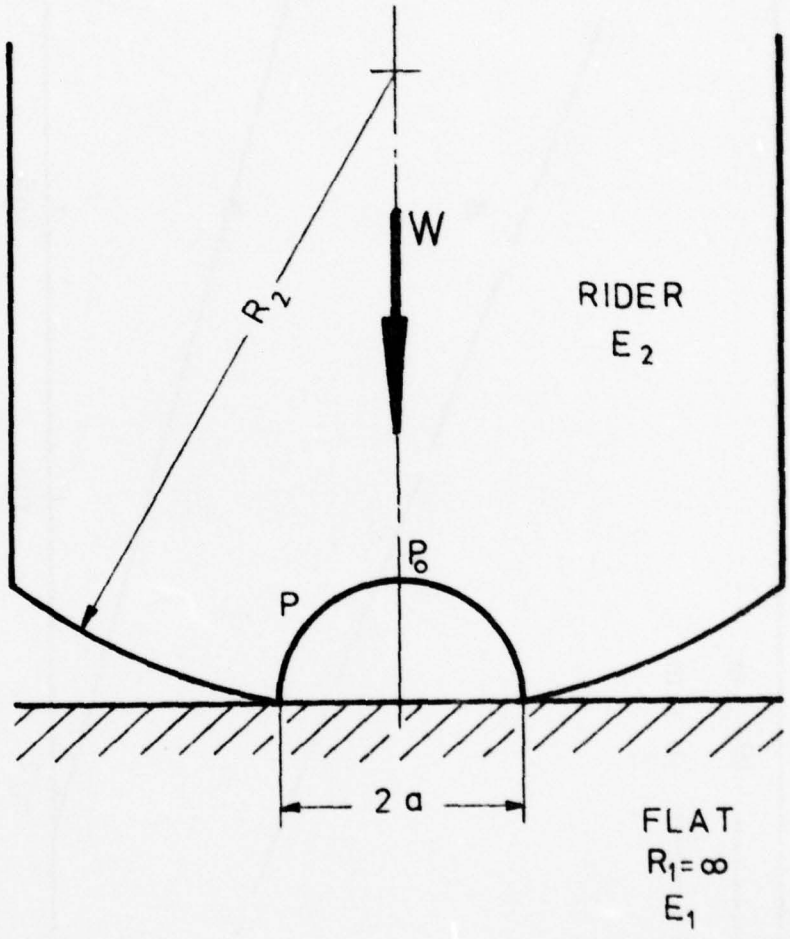

Fig. (33) CONTACT AREA BETWEEN A RIDER AND A FLAT.

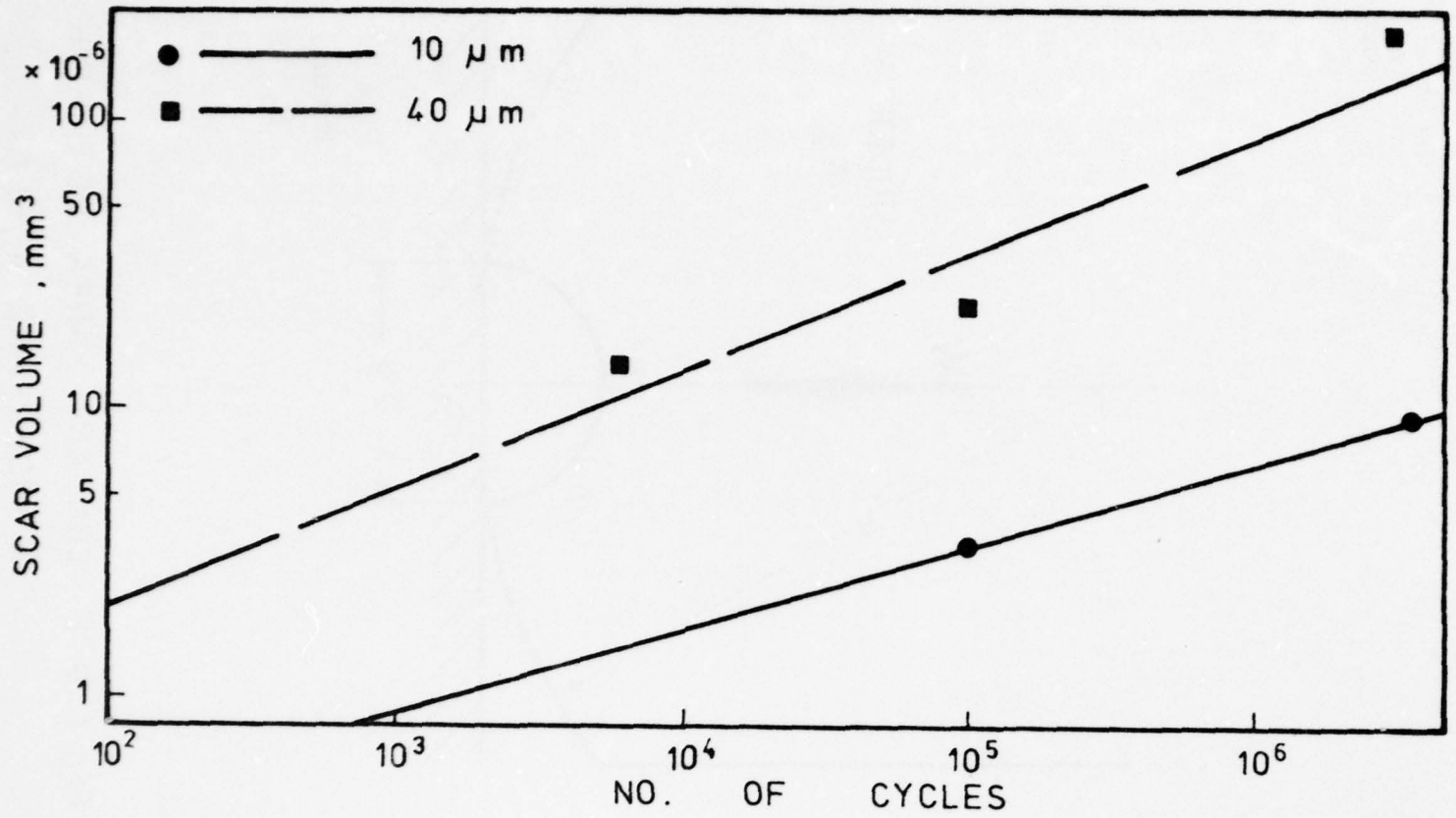

Fig. (34) PLOTS OF THE SCAR VOLUME AGAINST NO. OF CYCLES FOR Ti-6AL-4V ALLOY (AMMRC) AT 20 °C .

AD-A070 994 NOTTINGHAM UNIV (ENGLAND) DEPT OF METALLURGY AND MAT--ETC F/G 11/6
METALLURGICAL CHANGES IN THE HIGH TEMPERATURE FRETTING OF NI AN--ETC(U)
FEB 79 R B WATERHOUSE, M M HAMDY DAJA37-75-R-0649
UNCLASSIFIED NL

2 OF 2
AD A070994

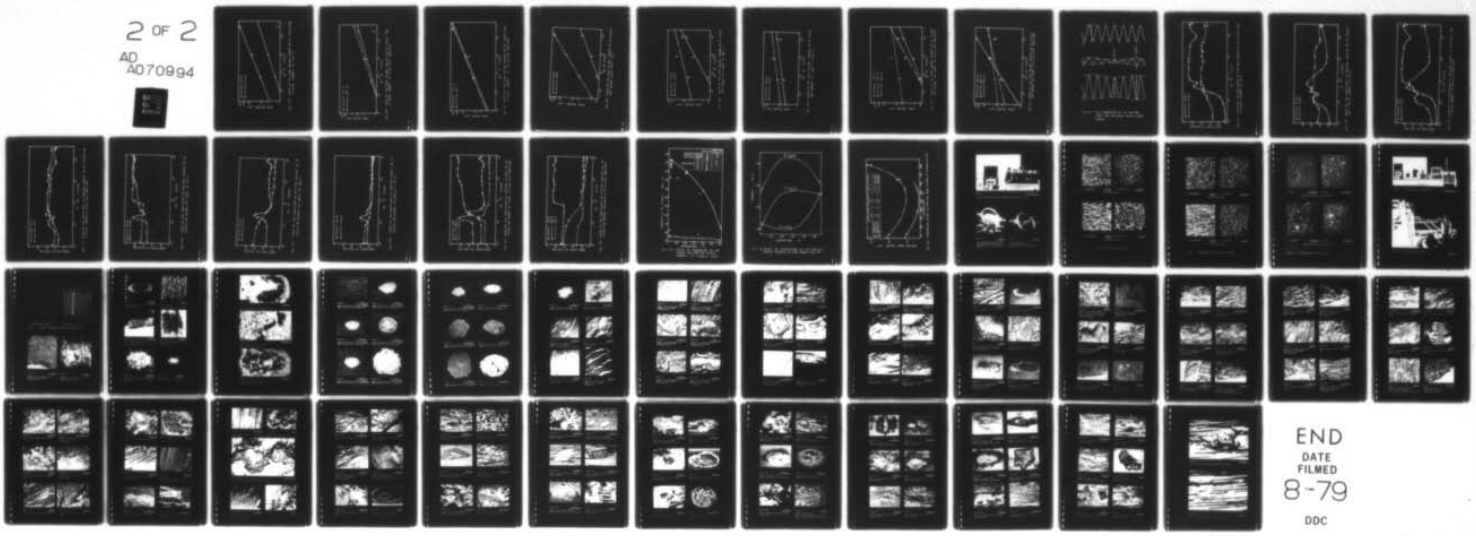

END
DATE FILMED
8-79
DDC

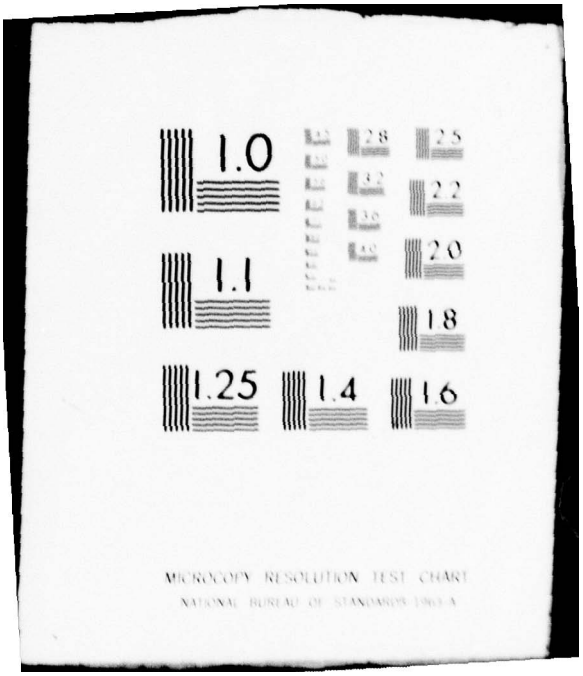
1.0
1.1
1.25
1.4
1.6
2.8
2.5
3.2
2.2
3.6
2.0
4.0
1.8
MICROCOPY RESOLUTION TEST CHART
NATIONAL BUREAU OF STANDARDS 1963-A

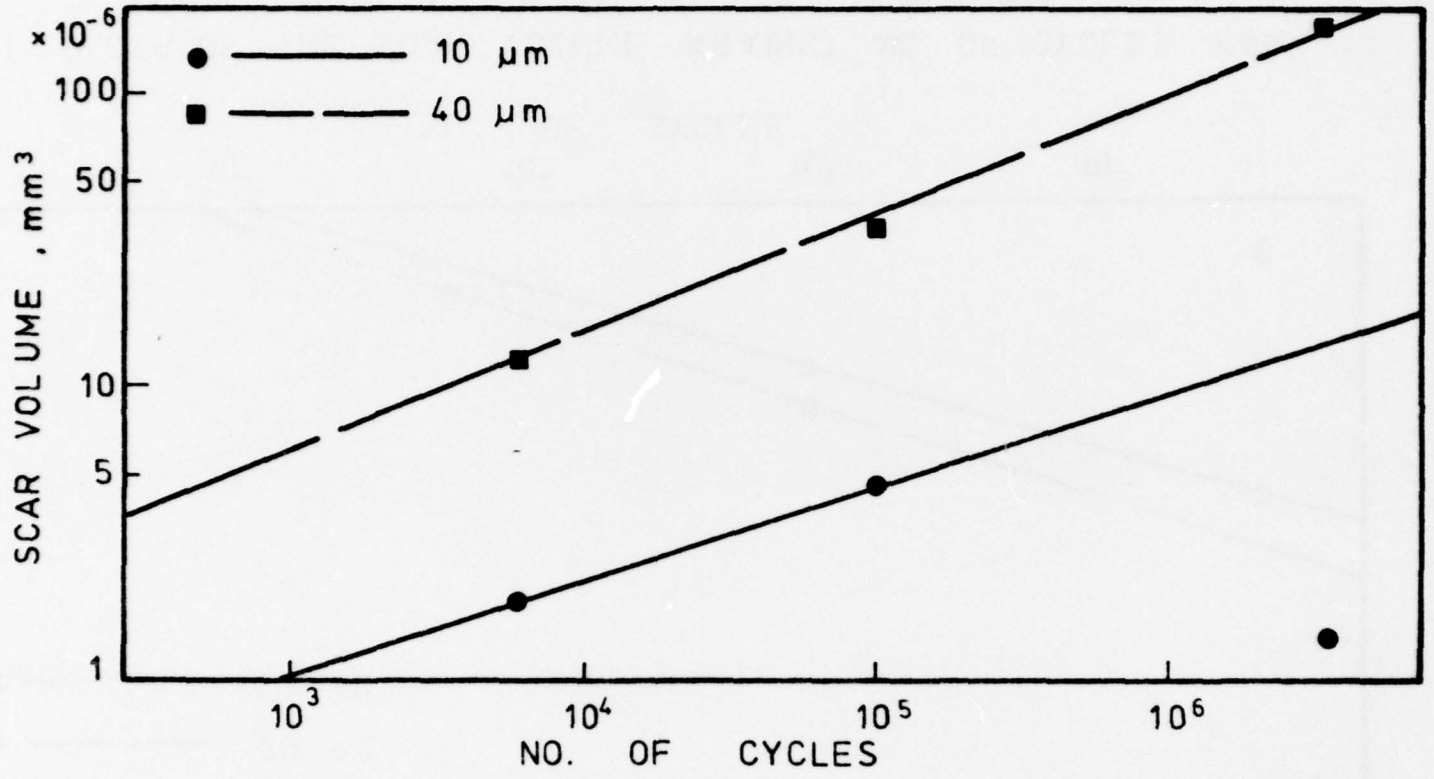

Fig. (35) PLOTS OF THE SCAR VOLUME AGAINST NO. OF CYCLES FOR Ti-ALLOY (AMMRC) AT 100 °C.

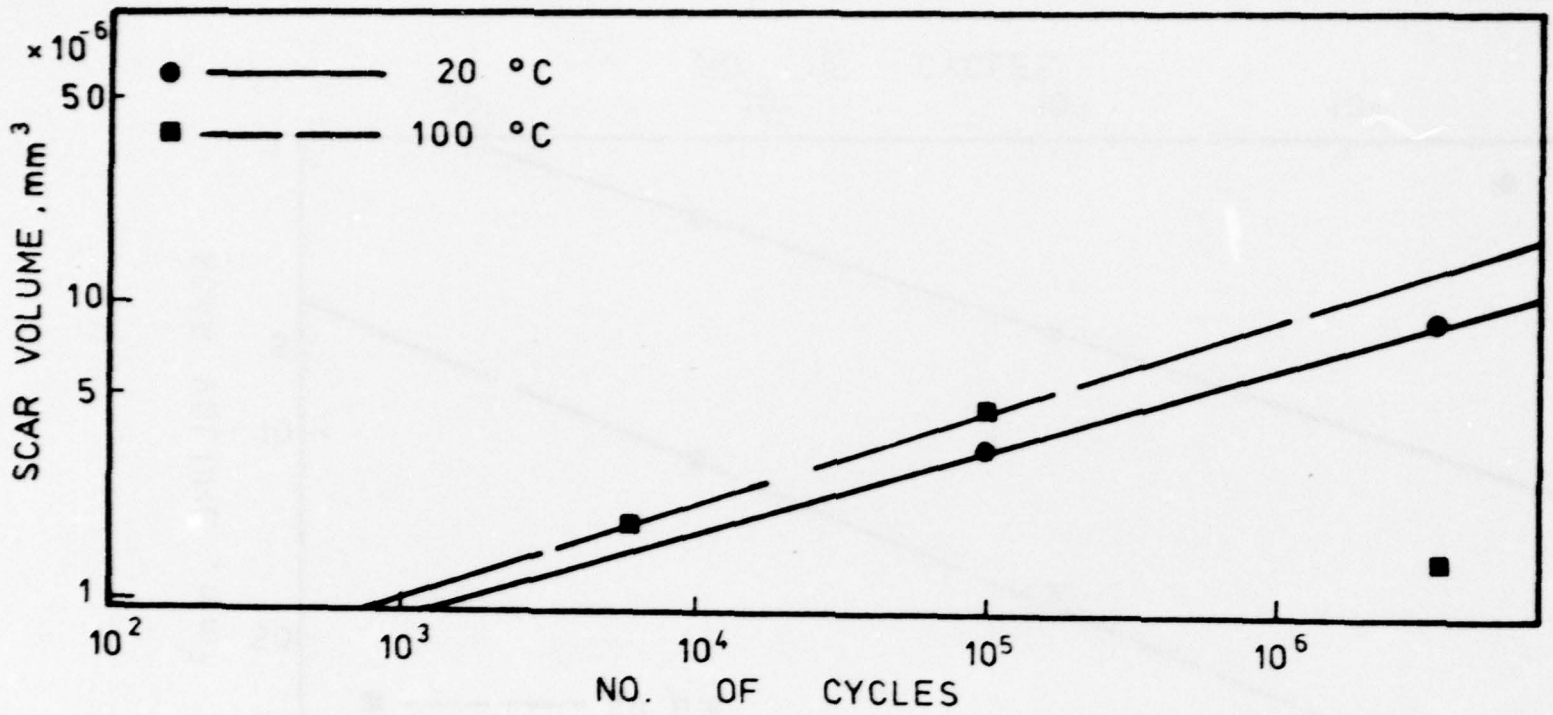

Fig.(36) PLOTS OF THE SCAR VOLUME AGAINST NO. OF CYCLES FOR Ti-ALLOY (AMMRC) AT 10 μm SLIP AMPLITUDE.

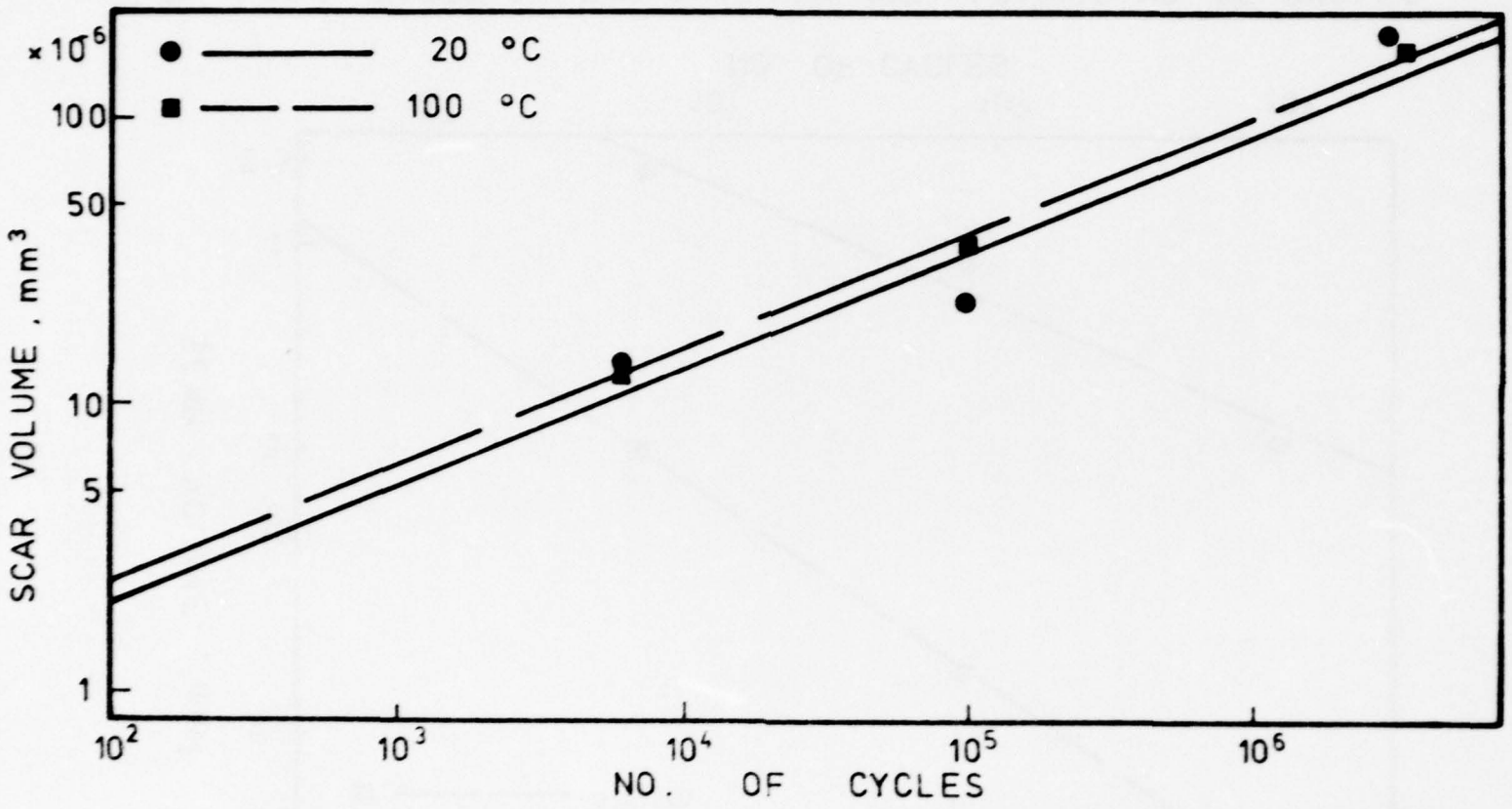

Fig. (37) PLOTS OF THE SCAR VOLUME AGAINST NO. OF CYCLES FOR Ti-ALLOY (AMMRC) AT 40 um SLIP AMPLITUDE.

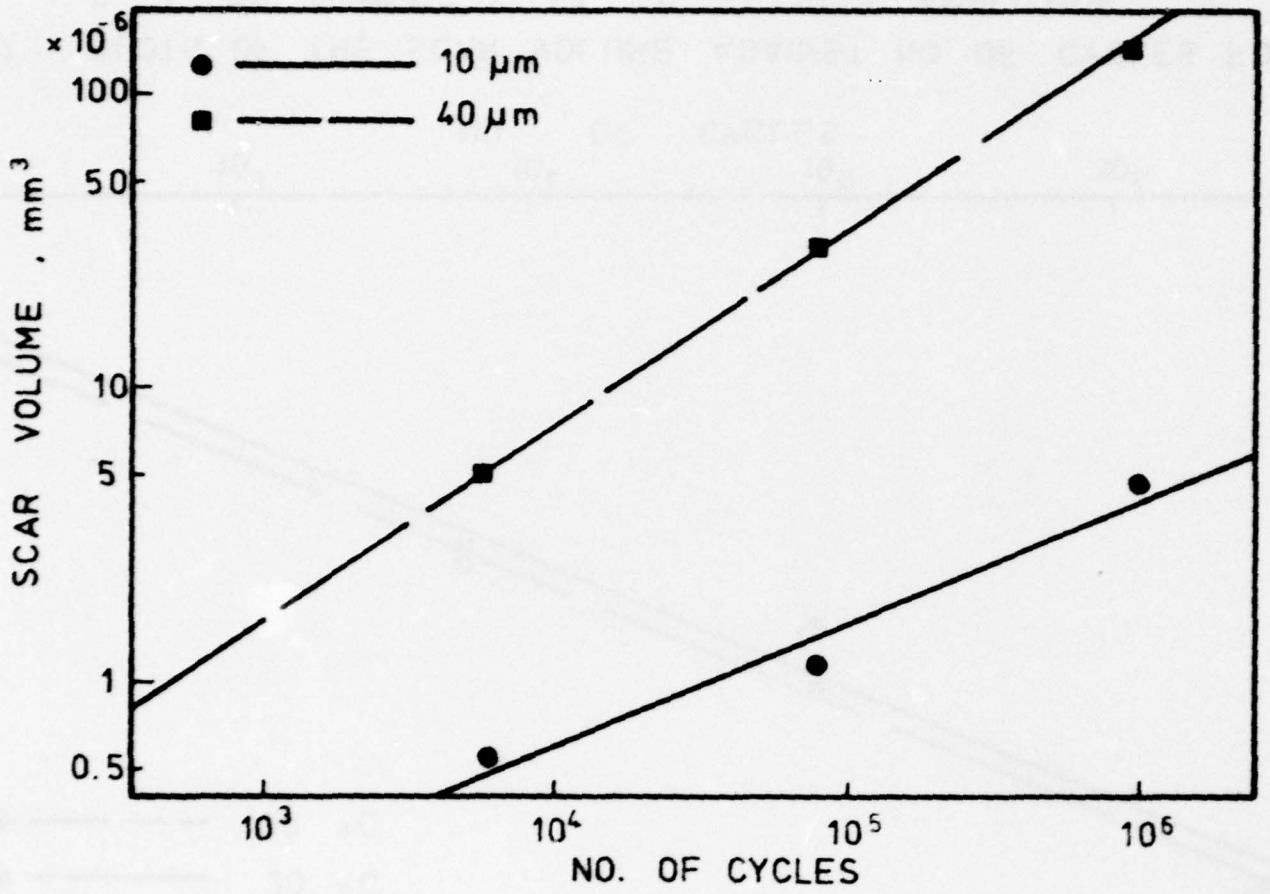

Fig. (38) PLOTS OF THE SCAR VOLUME AGAINST NO. OF CYCLES FOR INCONEL ALLOY 718 AT 20 °C.

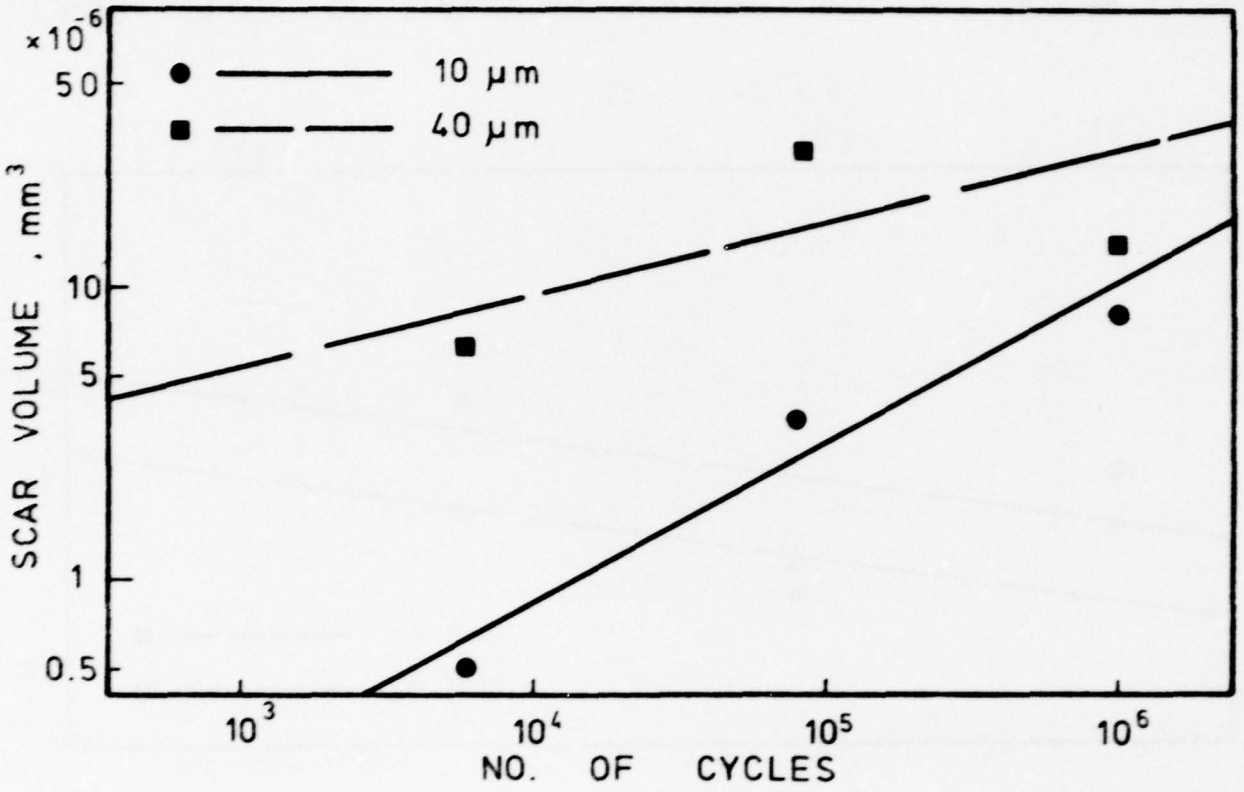

Fig. (39) PLOTS OF THE SCAR VOLUME AGAINST NO. OF CYCLES FOR INCONEL 718 (AGED) AT 280 °C.

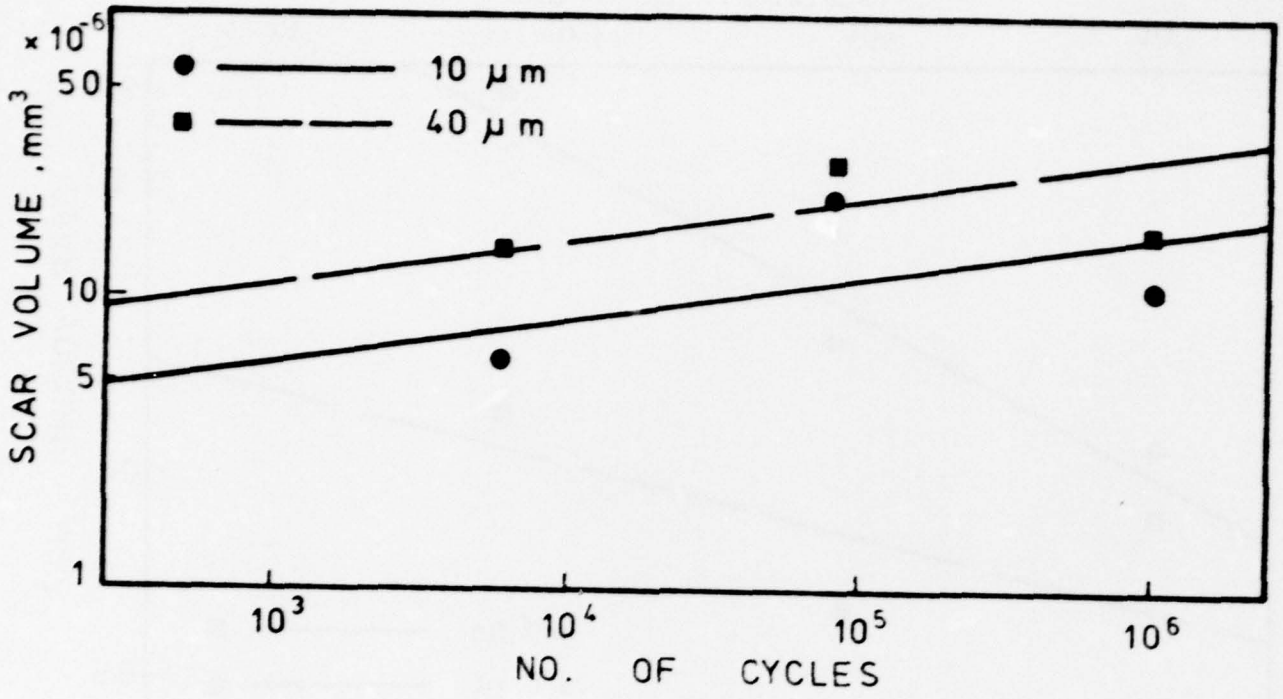

Fig. (40) PLOTS OF THE SCAR VOLUME AGAINST NO. OF CYCLES FOR INCONEL 718 (AGED) AT 540 °C .

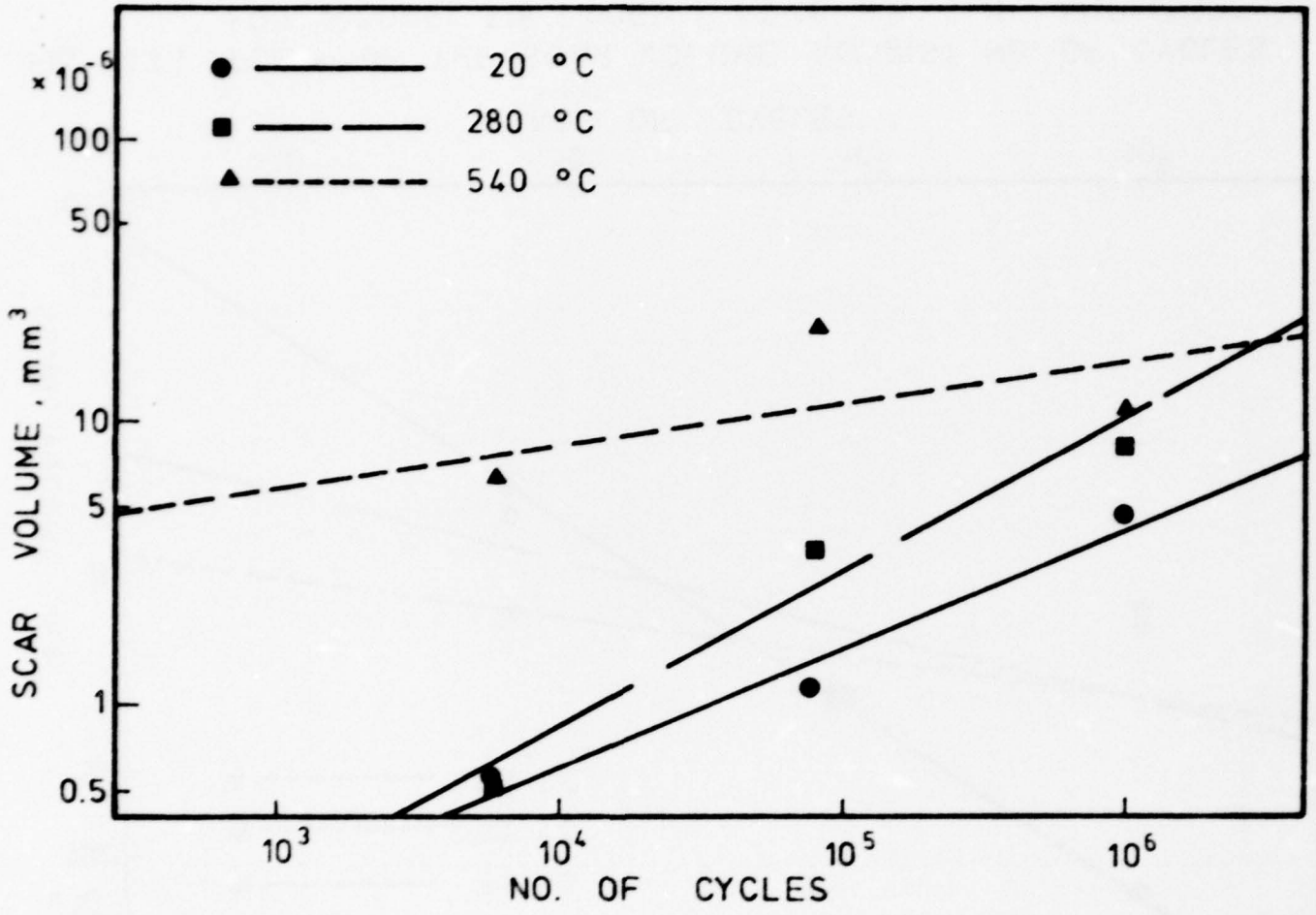

Fig. (41) PLOTS OF THE SCAR VOLUME AGAINST NO. OF CYCLES FOR INCONEL 718 (AGED) AT 10 μm SLIP AMPLITUDE.

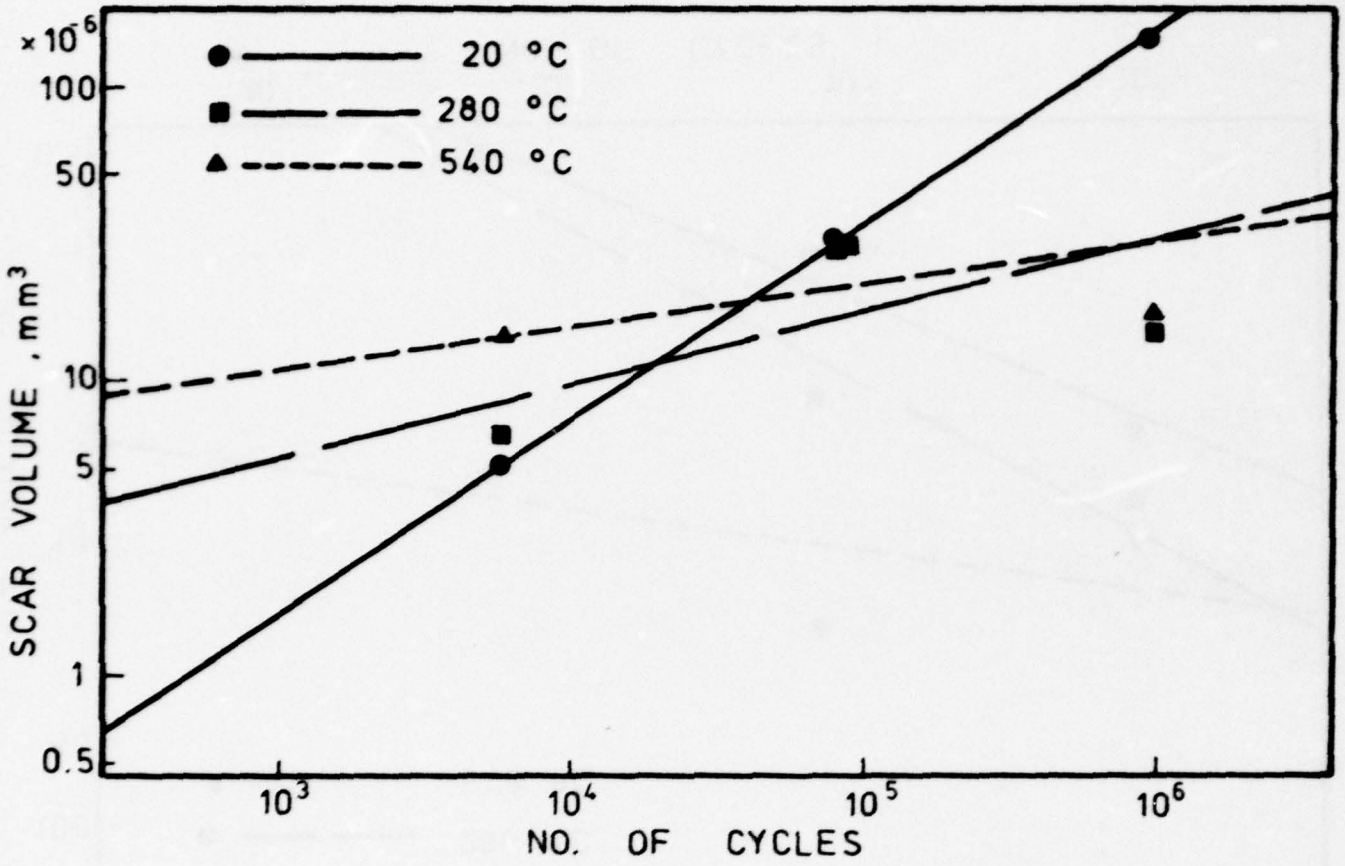

Fig. (42) PLOTS OF THE SCAR VOLUME AGAINST NO. OF CYCLES FOR INCONEL 718 (AGED) AT 40 μm SLIP AMPLITUDE .

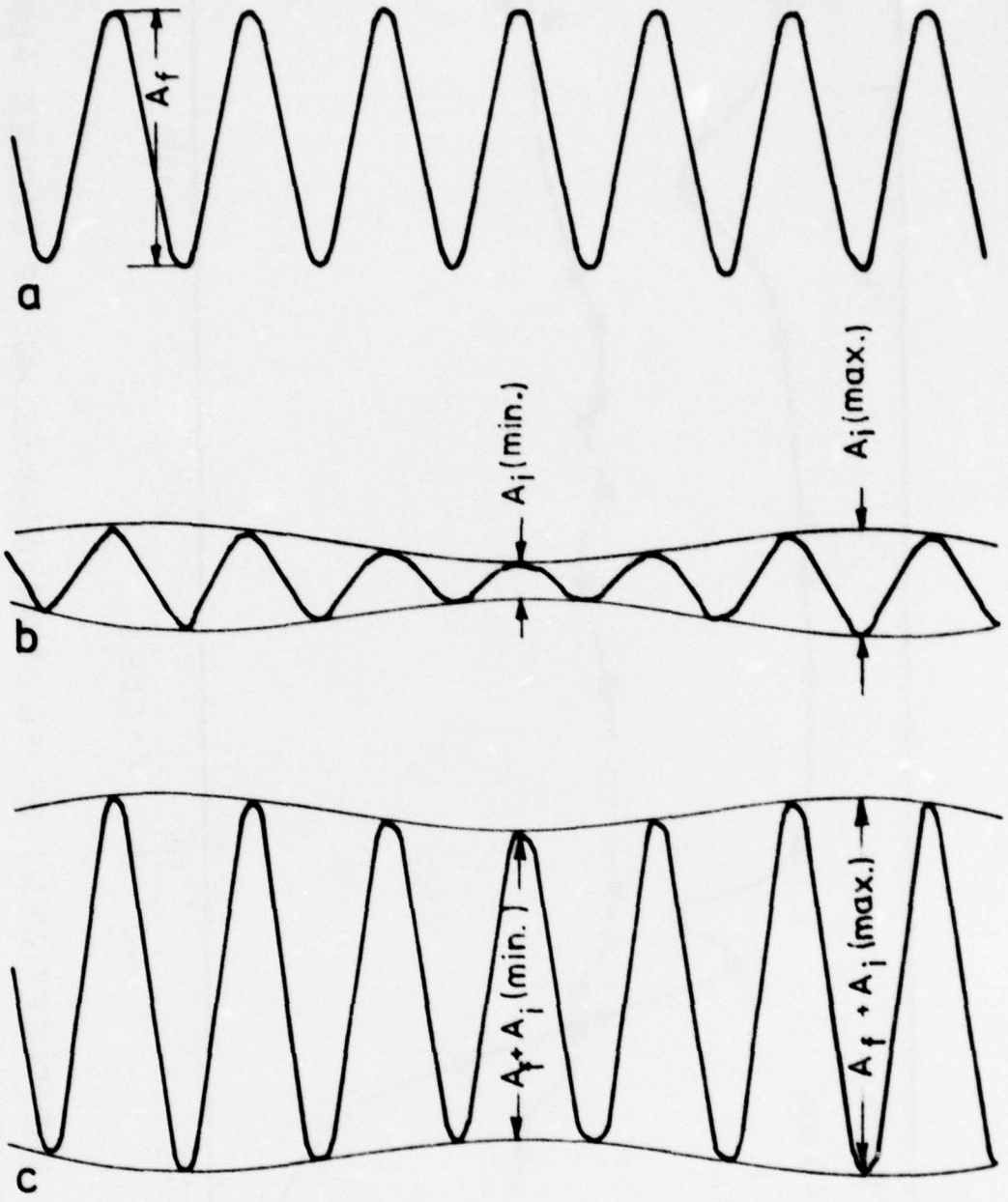

Fig. (43) THE COMBINATION OF THE FRICTION FORCE AND THE NOISE + INERTIA FORCE SIGNALS.

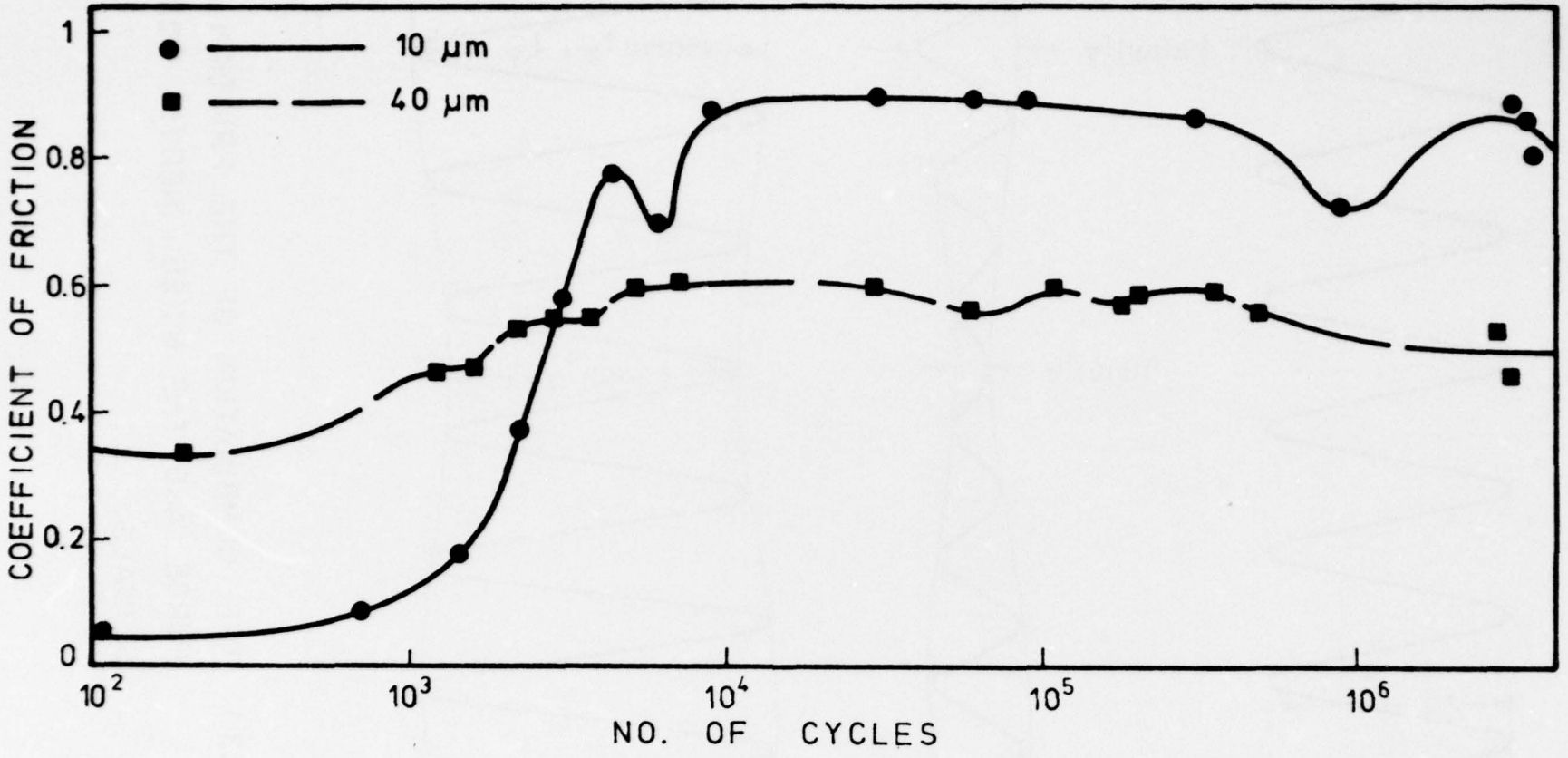

Fig. (44) PLOTS OF THE COEFFICIENT OF FRICTION AGAINST NO. OF CYCLES FOR Ti-ALLOY (AMMRC) AT 20 °C.

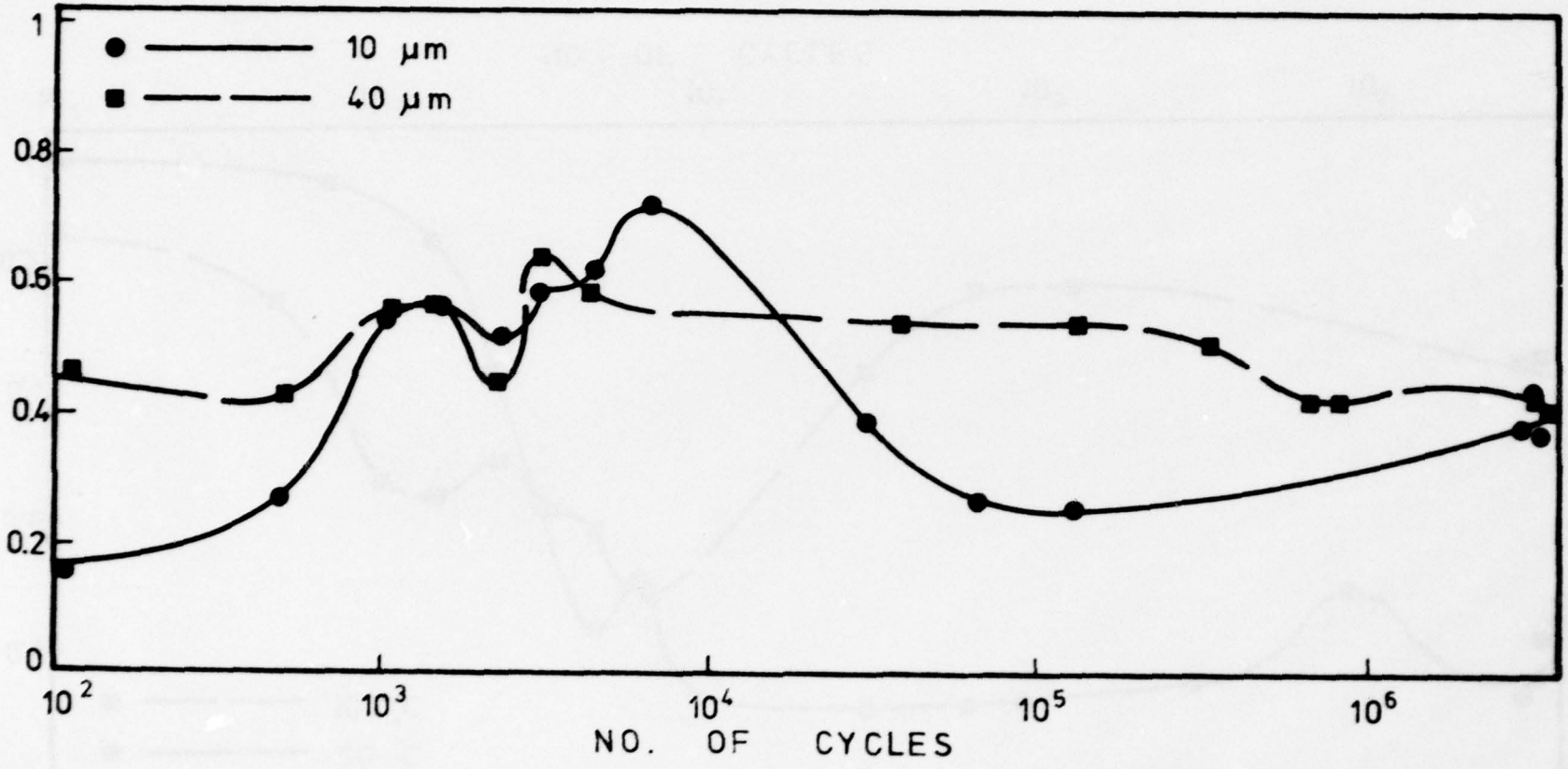

Fig. (45) PLOTS OF THE COEFFICIENT OF FRICTION AGAINST NO. OF CYCLES FOR Ti-ALLOY (AMMRC) AT 100 °C.

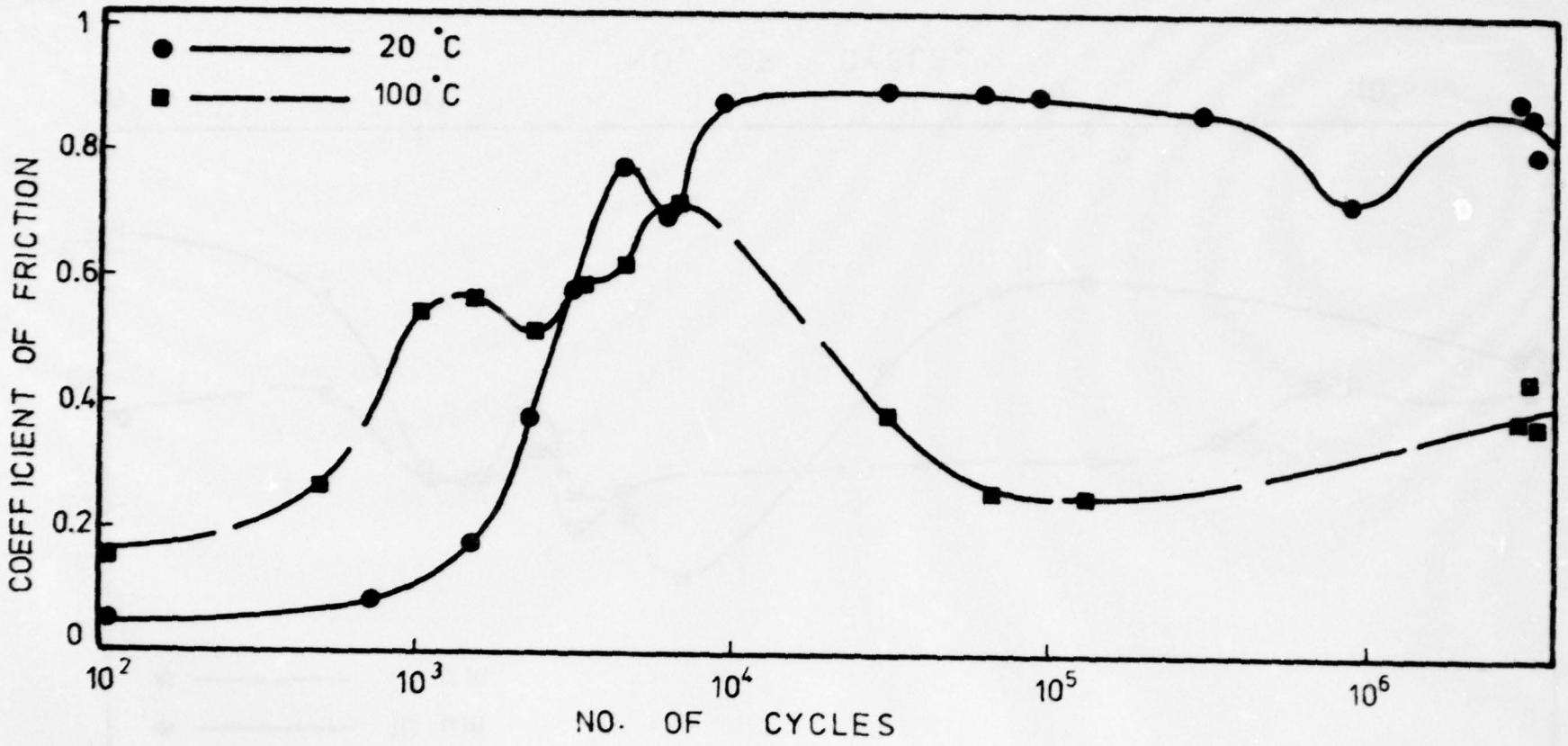

Fig. (46) PLOTS OF THE COEFFICIENT OF FRICTION AGAINST NO. OF CYCLES FOR Ti-ALLOY (AMMRC) AT 10 μm SLIP AMPLITUDE.

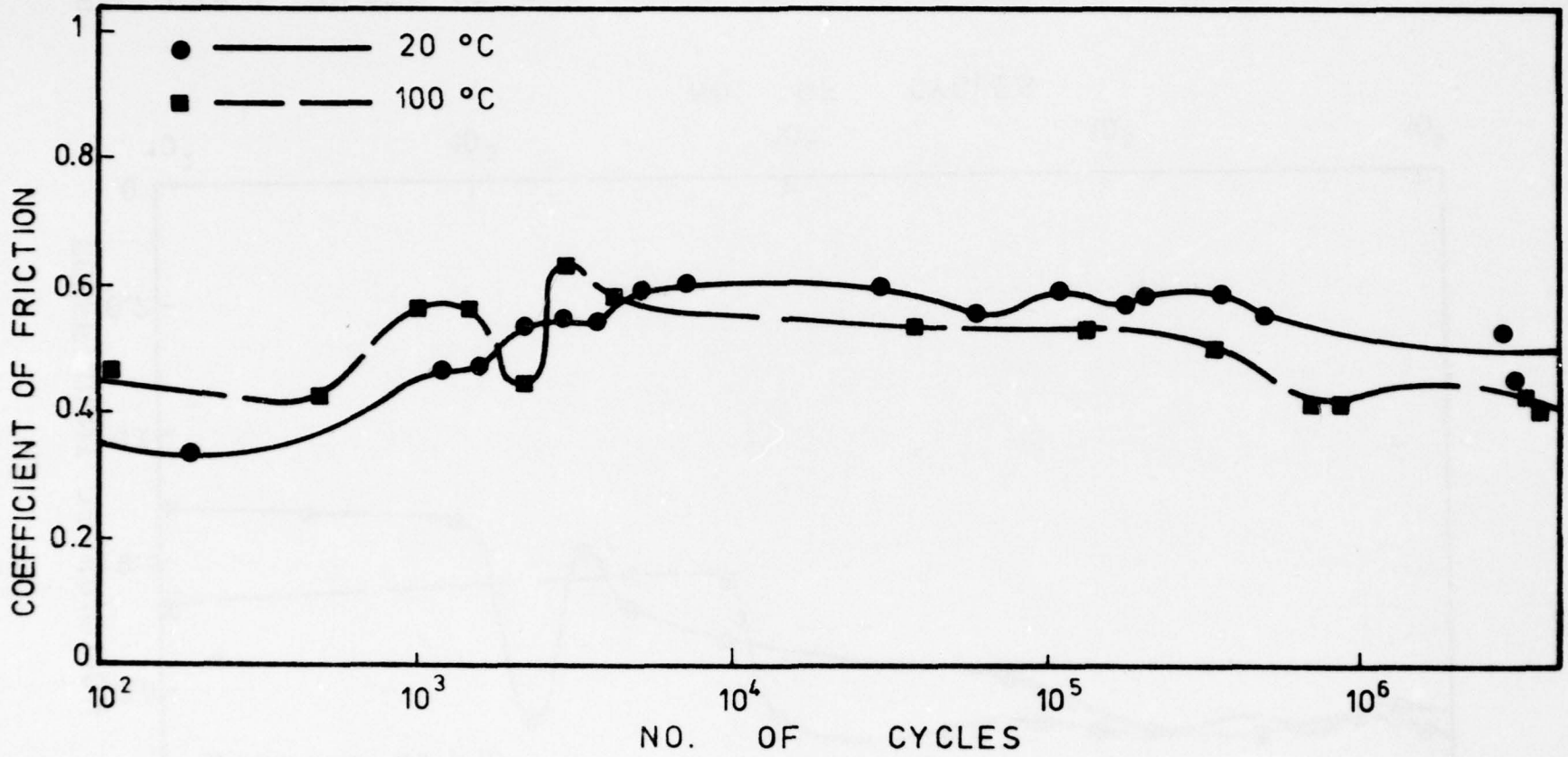

Fig. (47) PLOTS OF THE COEFFICIENT OF FRICTION AGAINST NO. OF CYCLES FOR Ti-ALLOY (AMMRC) AT 40 μm SLIP AMPLITUDE.

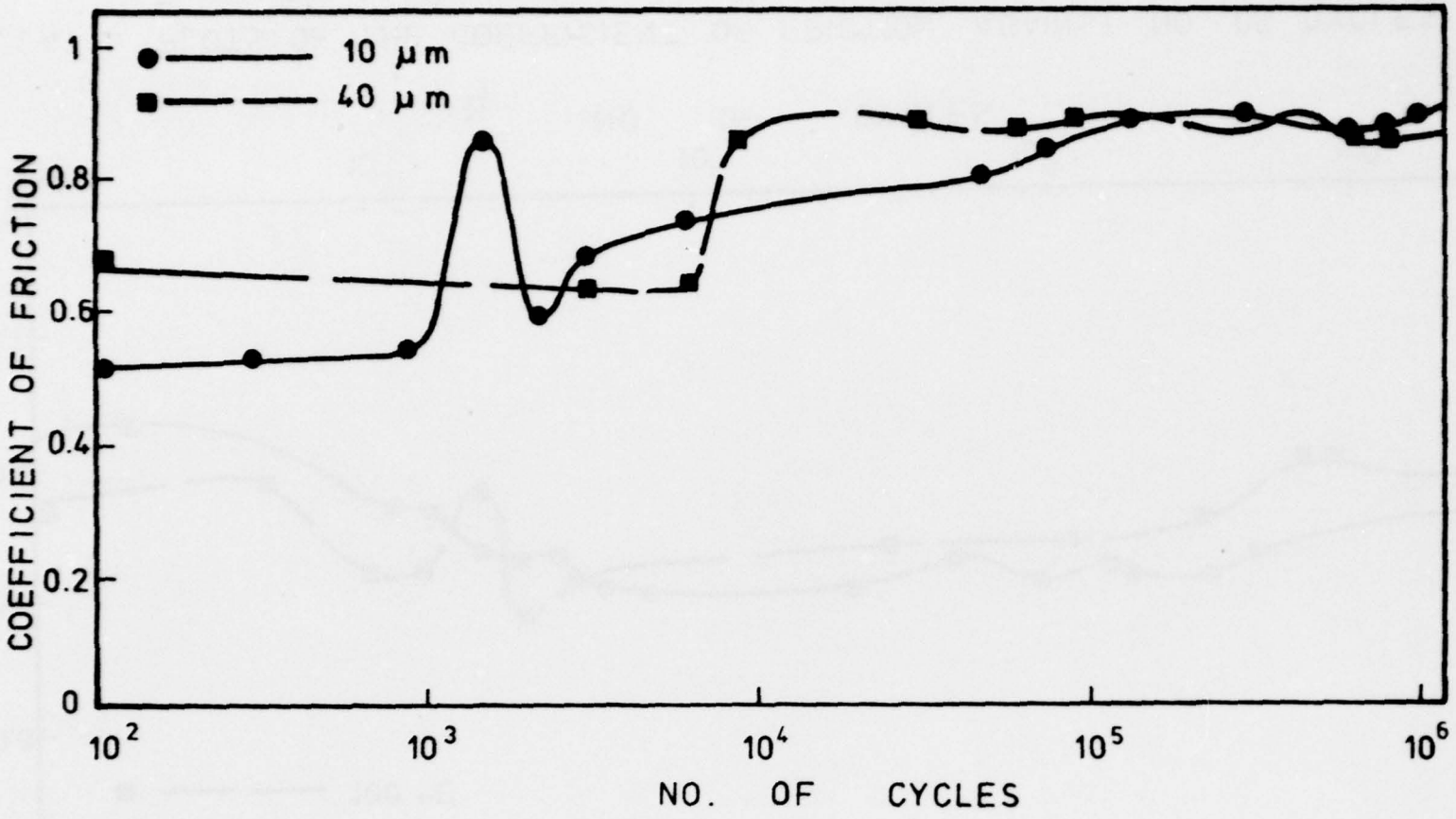

Fig. (48) PLOTS OF THE COEFFICIENT OF FRICTION AGAINST NO. OF CYCLES FOR INCONEL 718 (AGED) AT 20 °C .

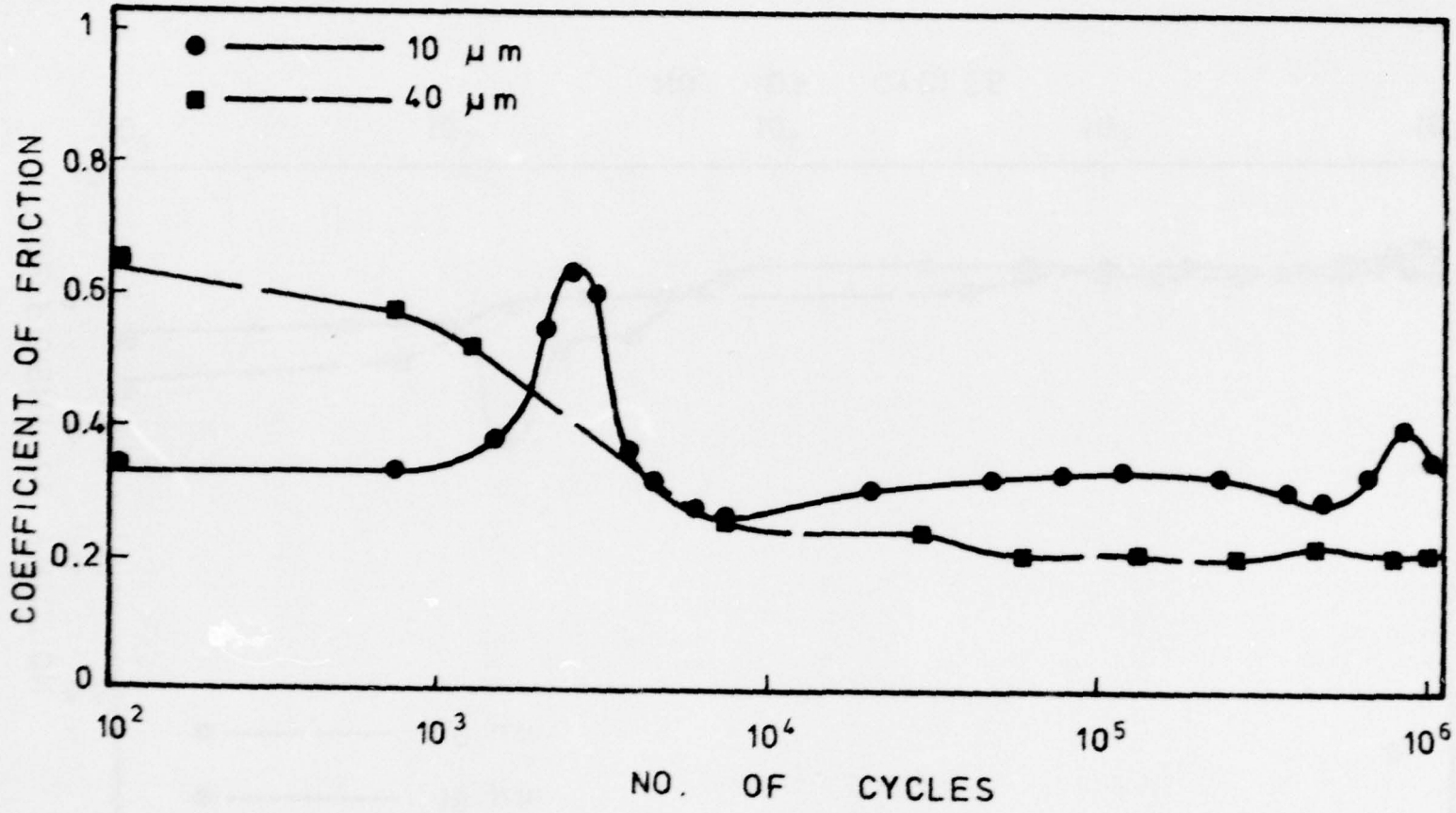

Fig. (49) PLOTS OF THE COEFFICIENT OF FRICTION AGAINST NO. OF CYCLES FOR INCONEL 718 (AGED) AT 280 °C .

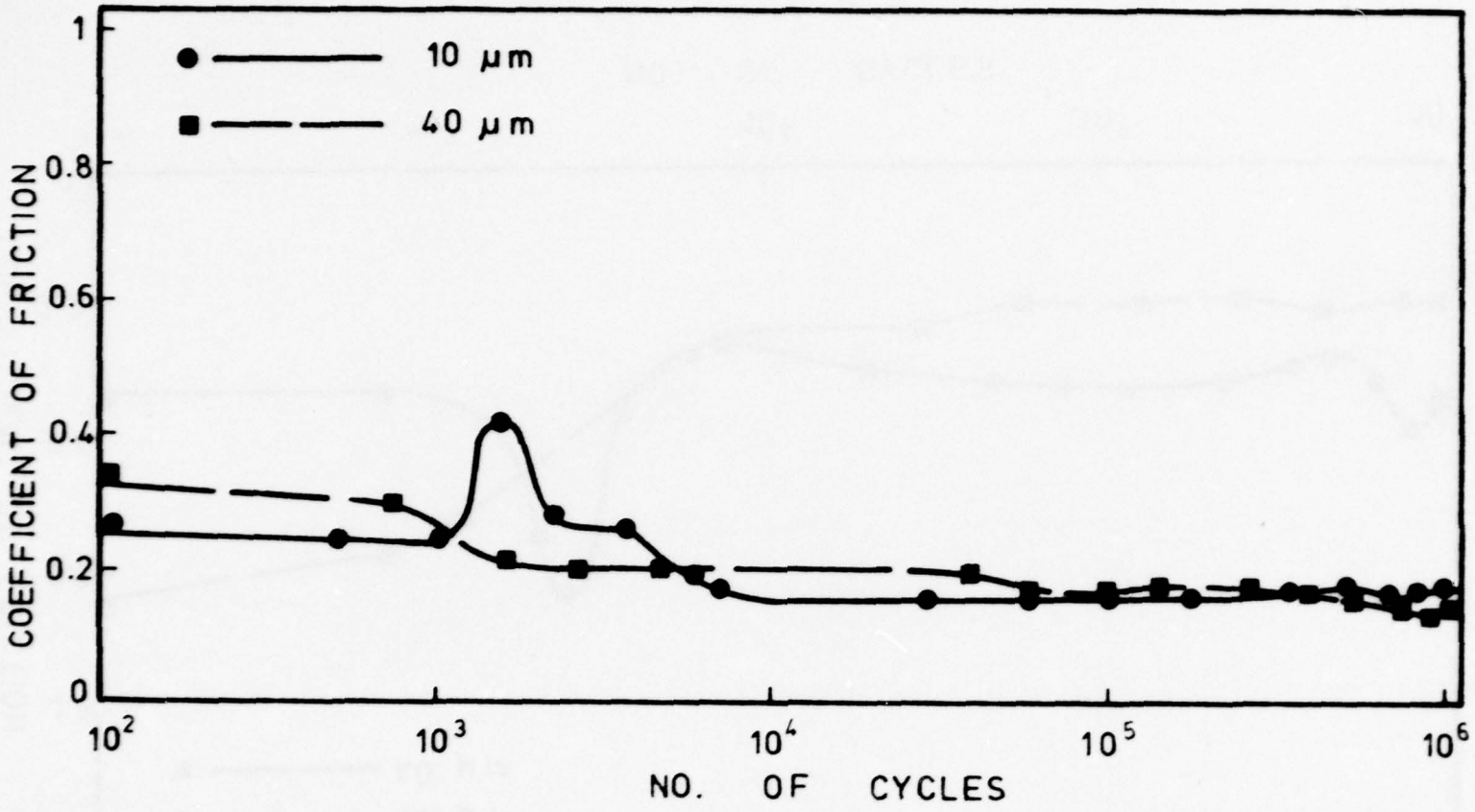

Fig. (50) PLOTS OF THE COEFFICIENT OF FRICTION AGAINST NO. OF CYCLES FOR INCONEL 718 (AGED) AT 540 °C .

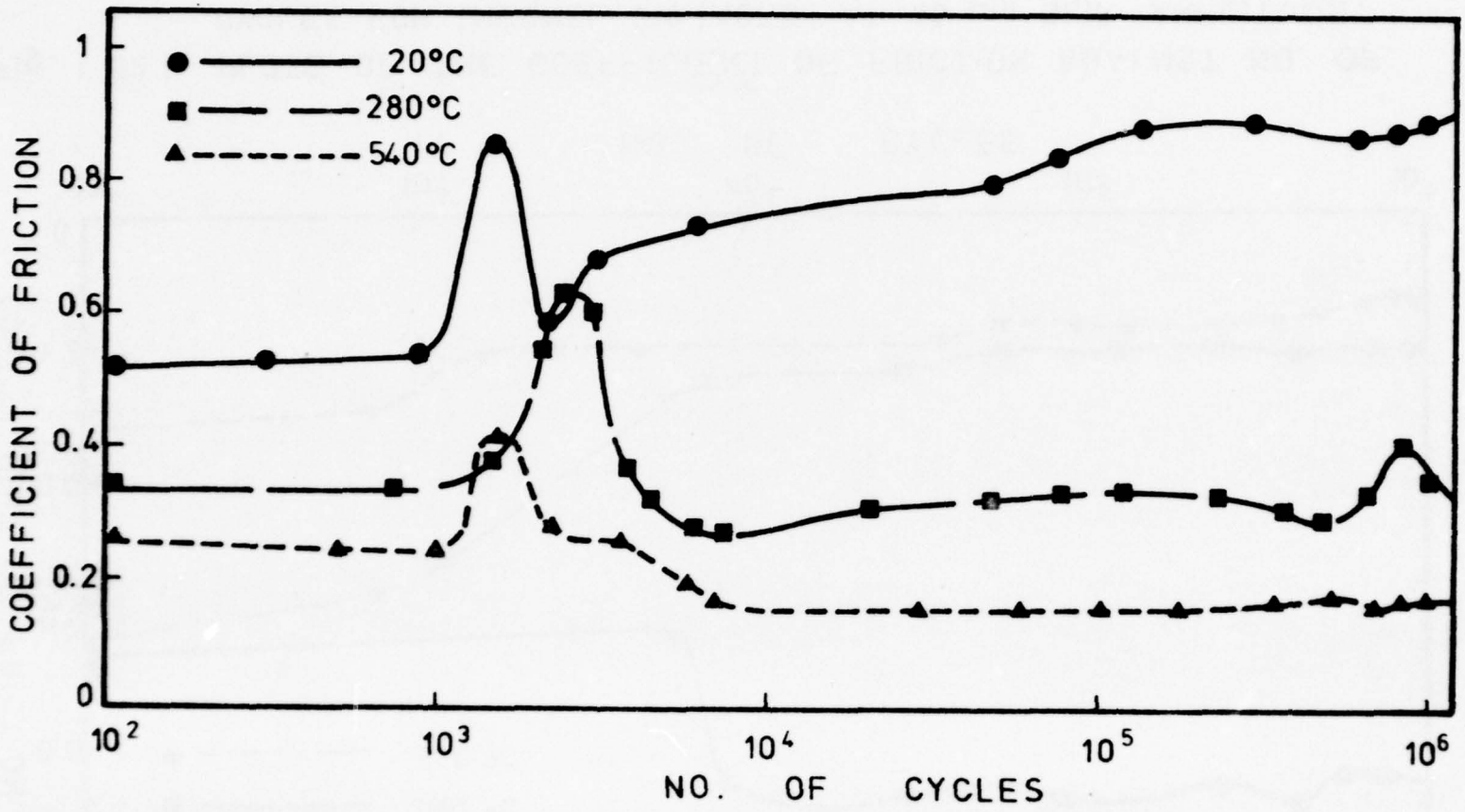

Fig. (51) PLOTS OF THE COEFFICIENT OF FRICTION AGAINST NO. OF CYCLES FOR INCONEL 718 (AGED) AT 10 μm SLIP AMPLITUDE.

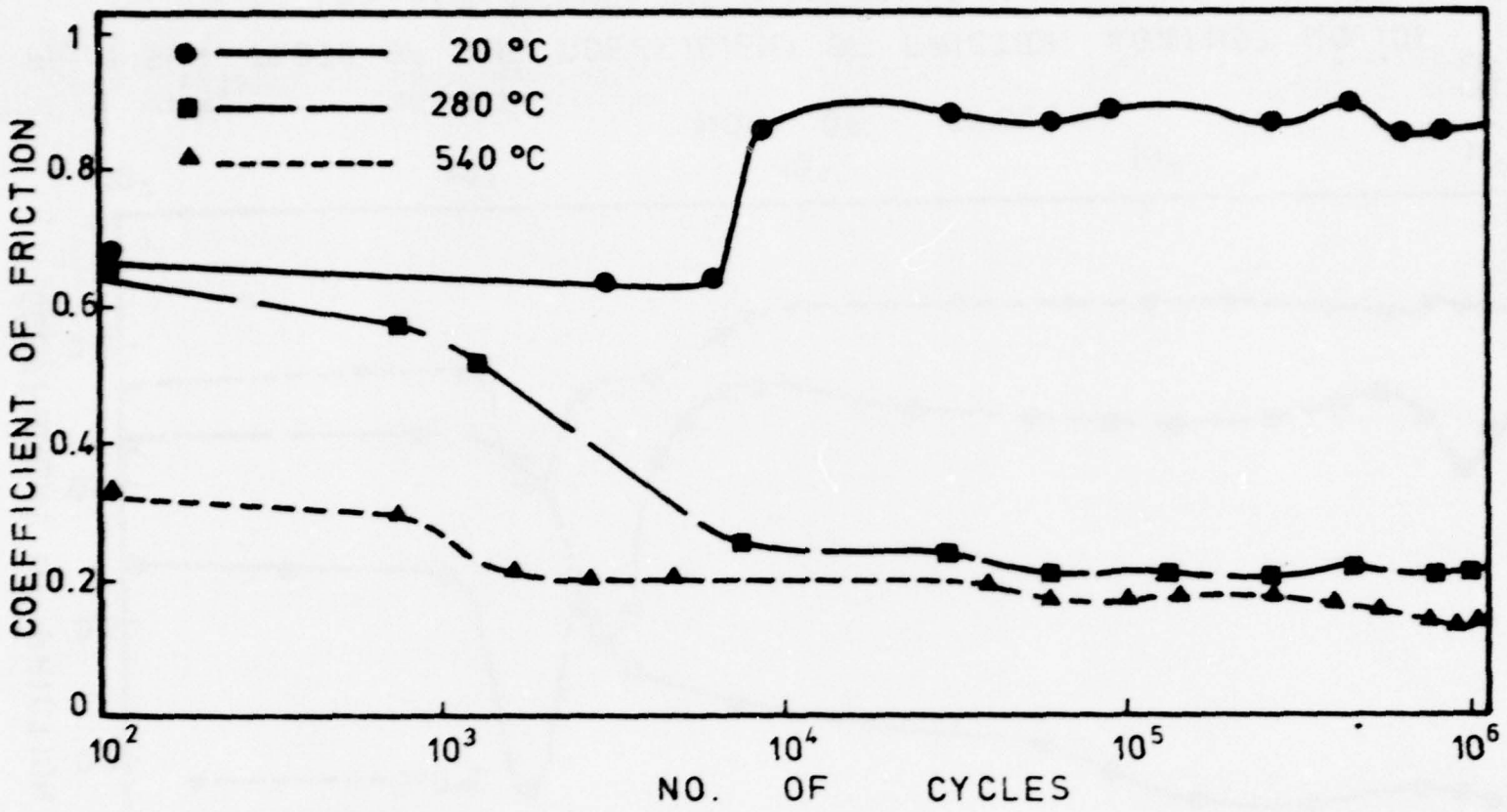

Fig. (52) PLOTS OF THE COEFFICIENT OF FRICTION AGAINST NO. OF CYCLES FOR INCONEL 718 (AGED) AT 40 μm SLIP AMPLITUDE.

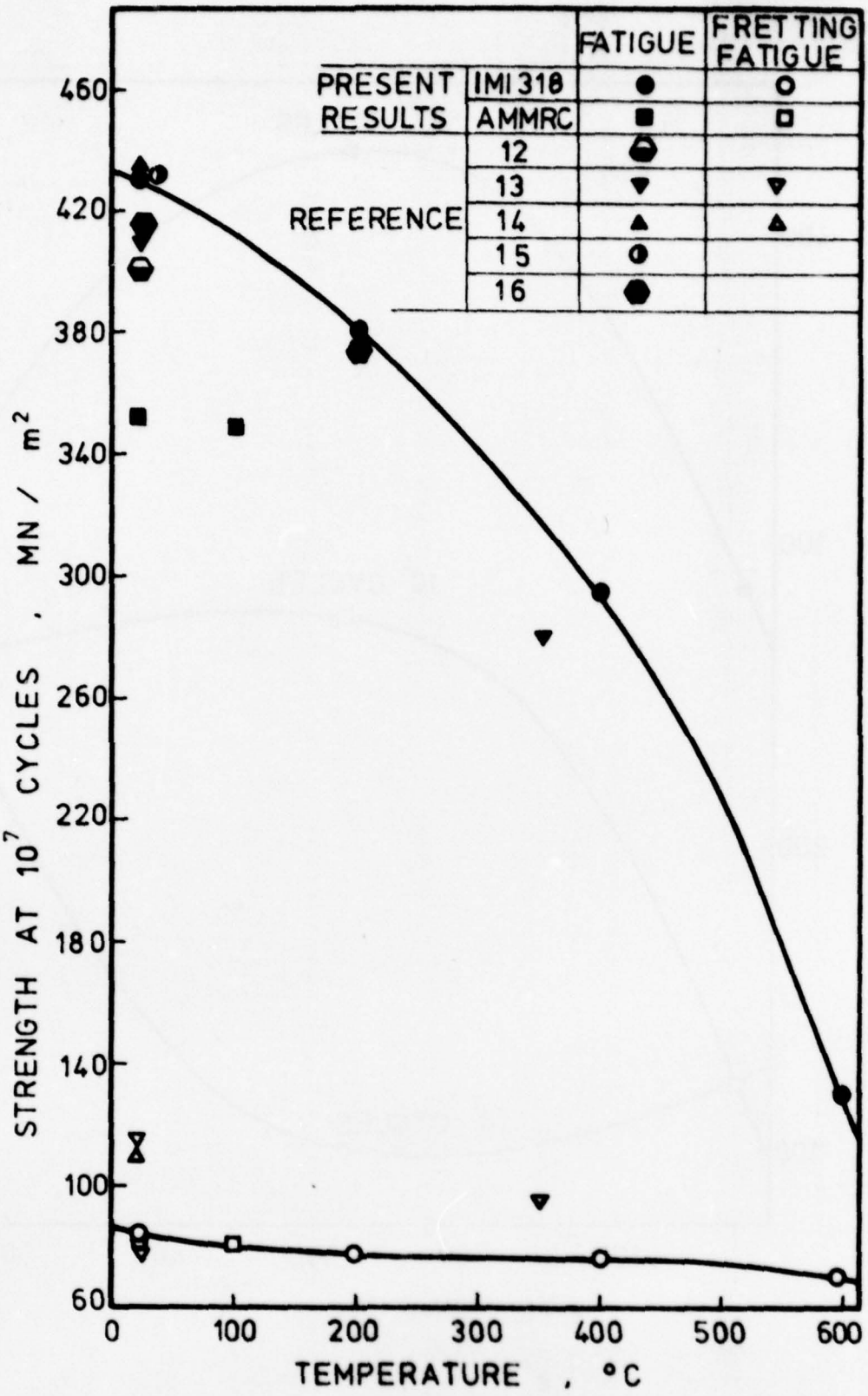

Fig. (53) EFFECT OF TEMPERATURE ON THE FATIGUE AND FRETTING FATIGUE STRENGTH OF Ti-6Al-4V ALLOY.

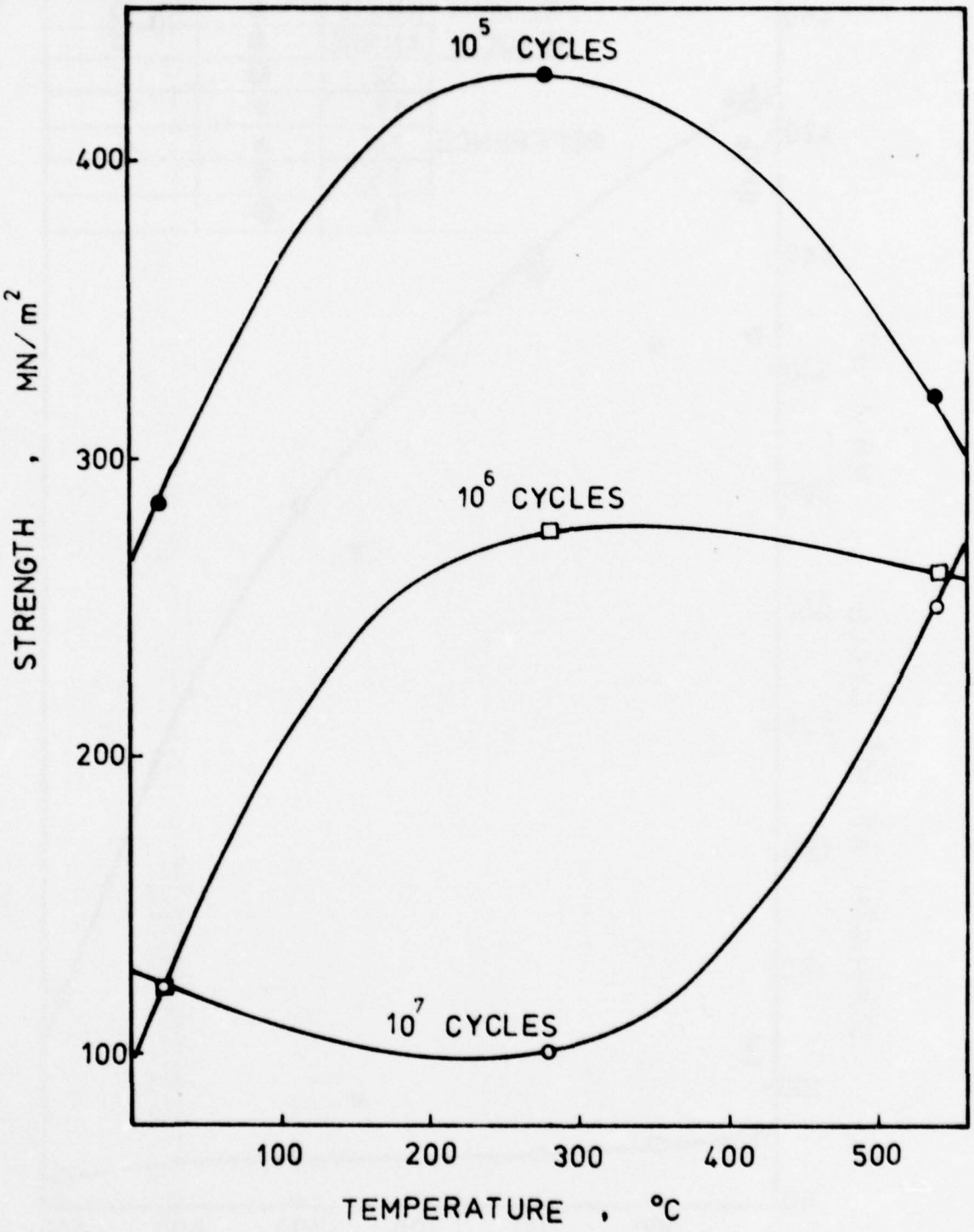

FIG. 54 EFFECT OF TEMPERATURE ON THE FRETTING FATIGUE STRENGTH OF AGED INCONEL ALLOY 718.

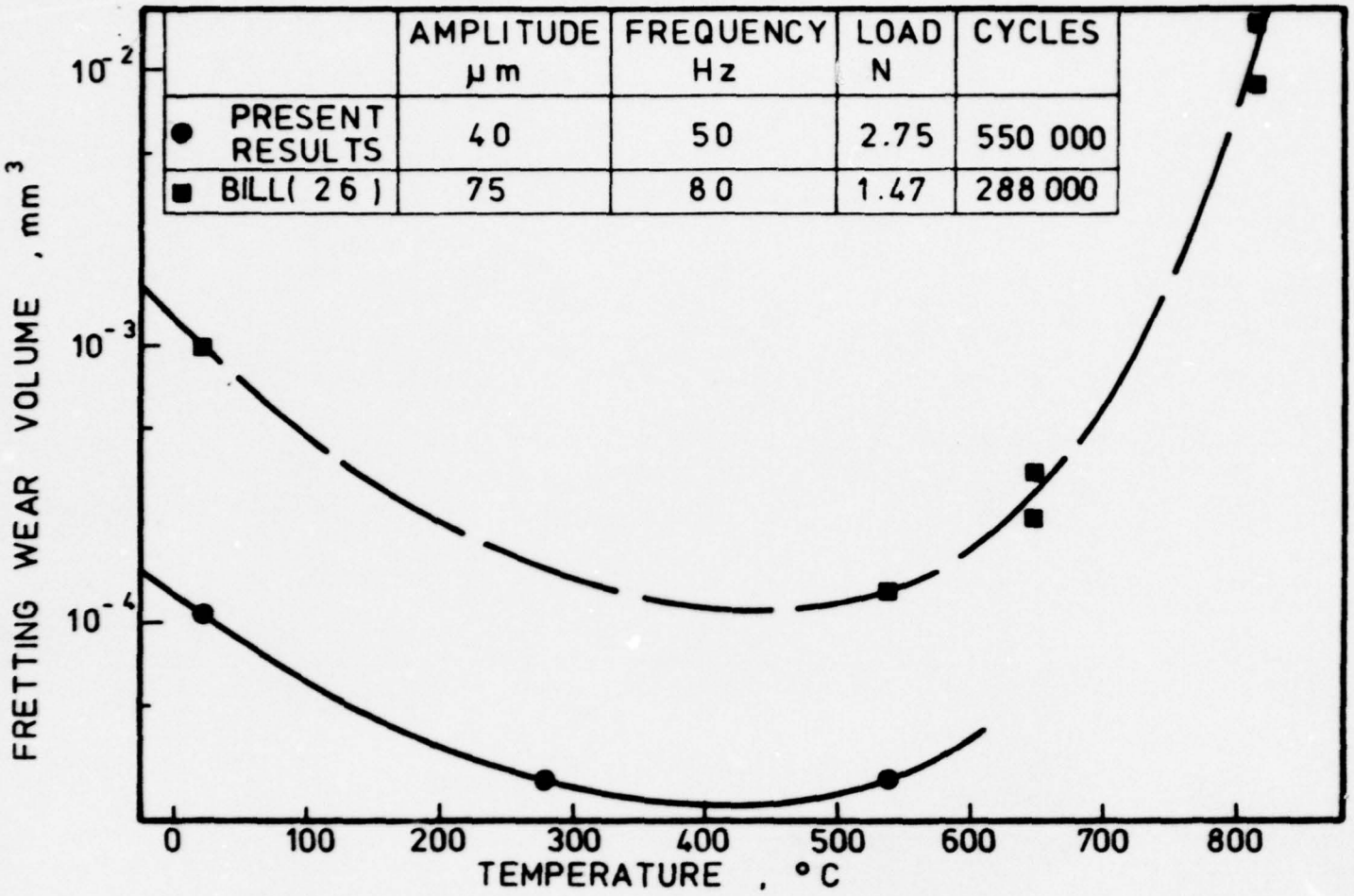

Fig.(55) TEMPERATURE EFFECT ON FRETTING WEAR VOLUME OF Ni-BASE ALLOYS.

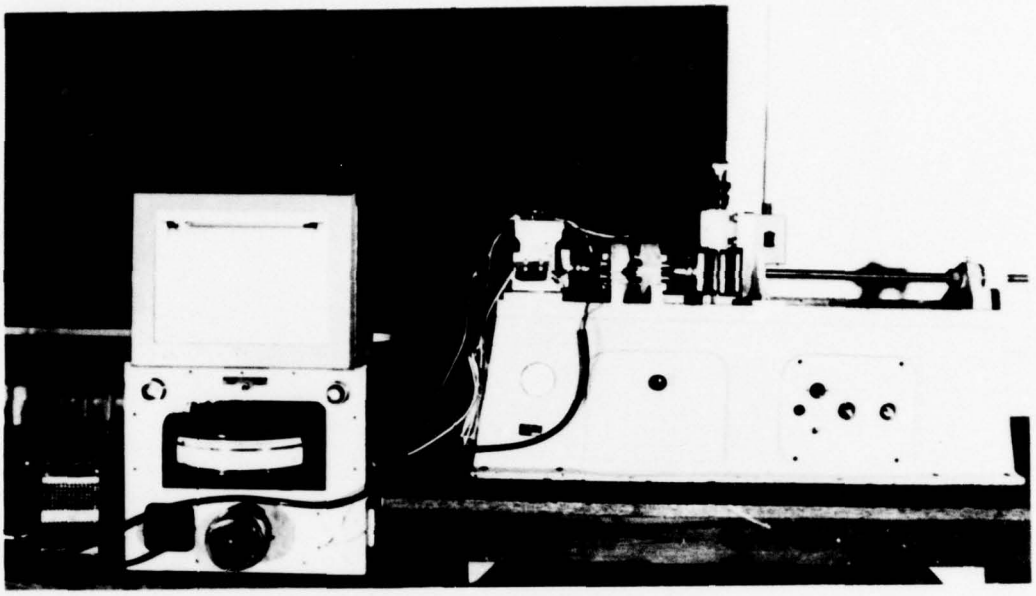

Plate 1

400 mm

Overall view of fatigue and fretting fatigue tests system.

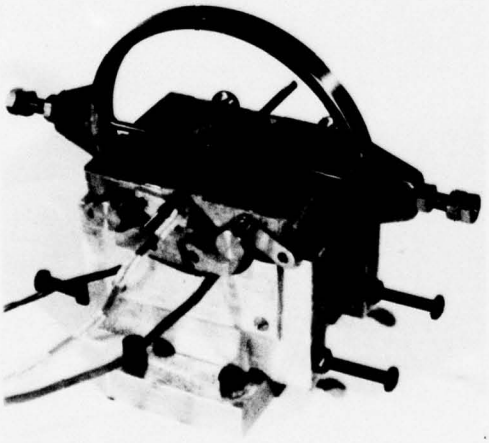

Plate 2

50 mm

The experimental arrangement with top half of the furnace removed showing specimen and fretting bridges.

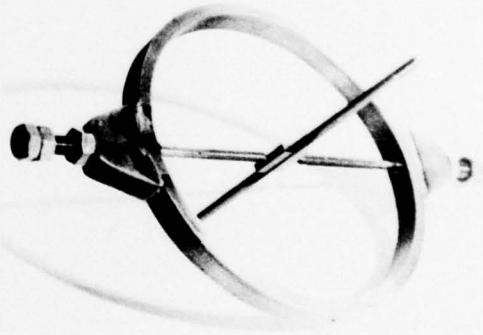

Plate 3

50 mm

The fretting fatigue device showing specimen and fretting bridges held by proving ring.

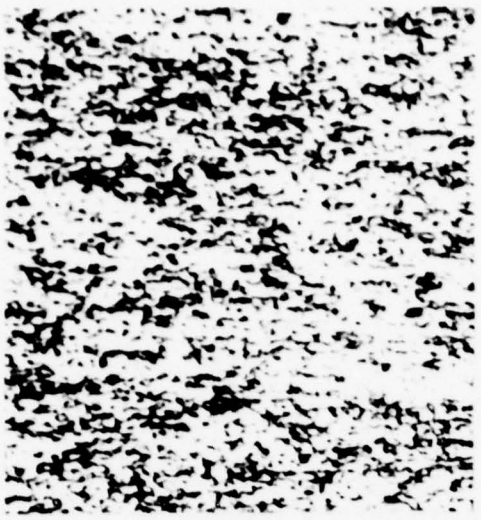

a - Longitudinal 40 μ

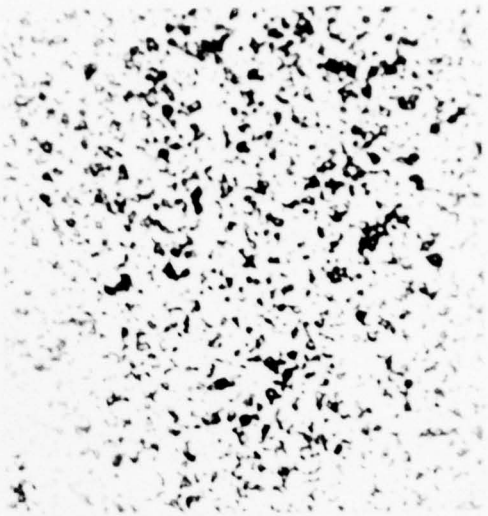

b - Transverse 40 μ

4.7 mm diameter rod

c - Longitudinal 40 μ

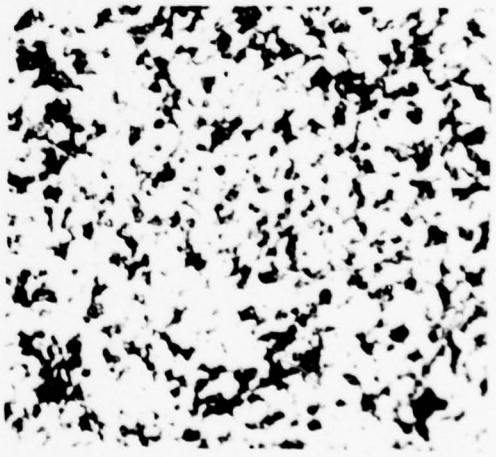

d - Transverse 40 μ

9.5 mm diameter rod

Plate 4 Microstructure of Ti-6Al-4V alloy (IMI 318).

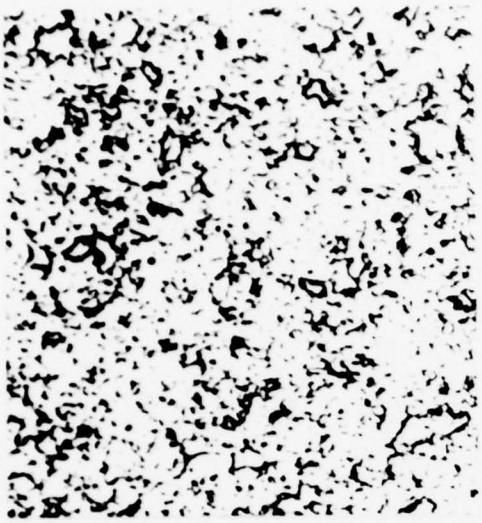

a - Longitudinal

40 μ

b - Transverse

40 μ

4.7 mm diameter rod

c - Longitudinal

40 μ

d - Transverse

40 μ

9.5 mm diameter rod

Plate 5 Microstructure of Ti-6Al-4V alloy (AMMRC).

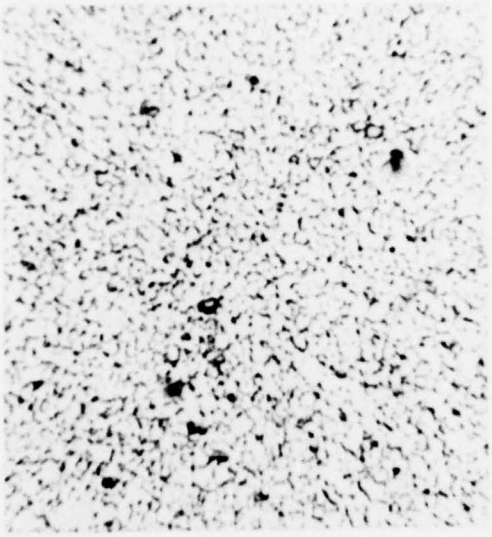

a - Aged 100 μ

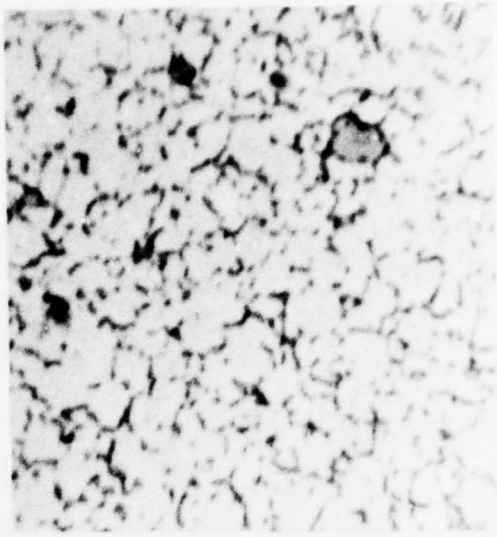

b - Aged 40 μ

Etched to reveal the grain boundaries

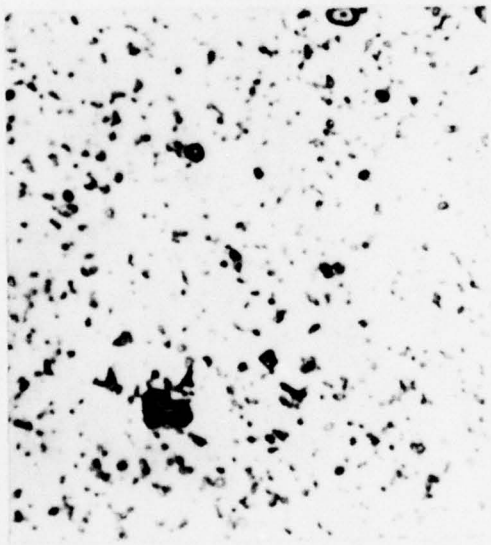

c - Annealed 40 μ

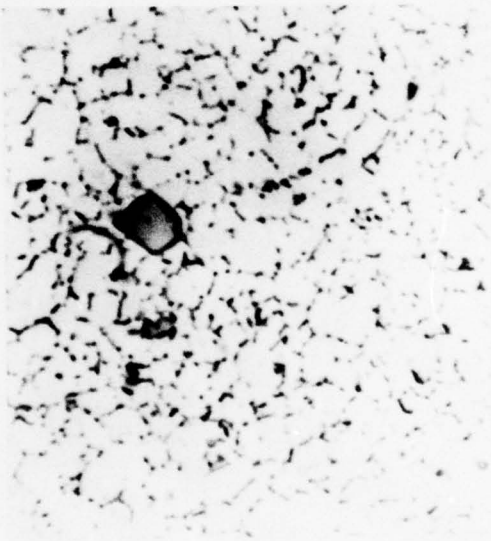

d - Aged 40 μ

Etched to reveal the precipitates

Plate 6 Microstructure of Inconel alloy 718.

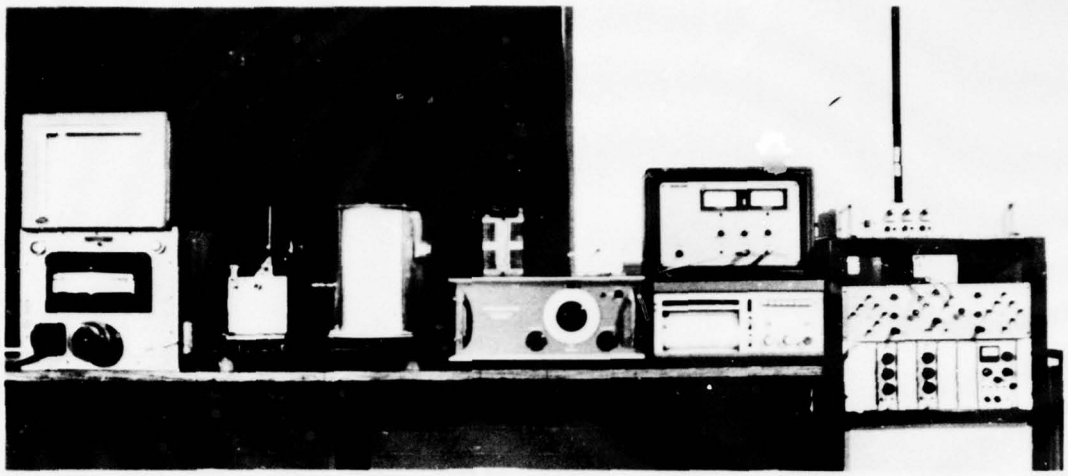

Plate 7 Fretting wear test arrangement.

500 mm

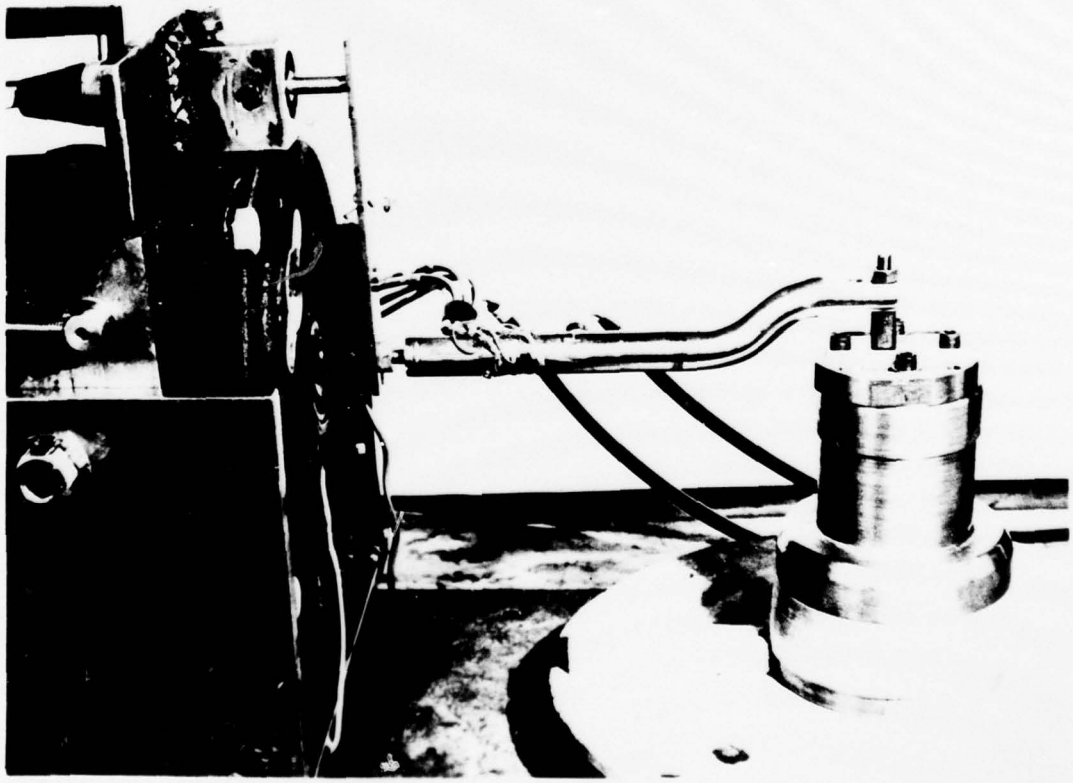

Plate 8 Oscillating movement system.

50 mm

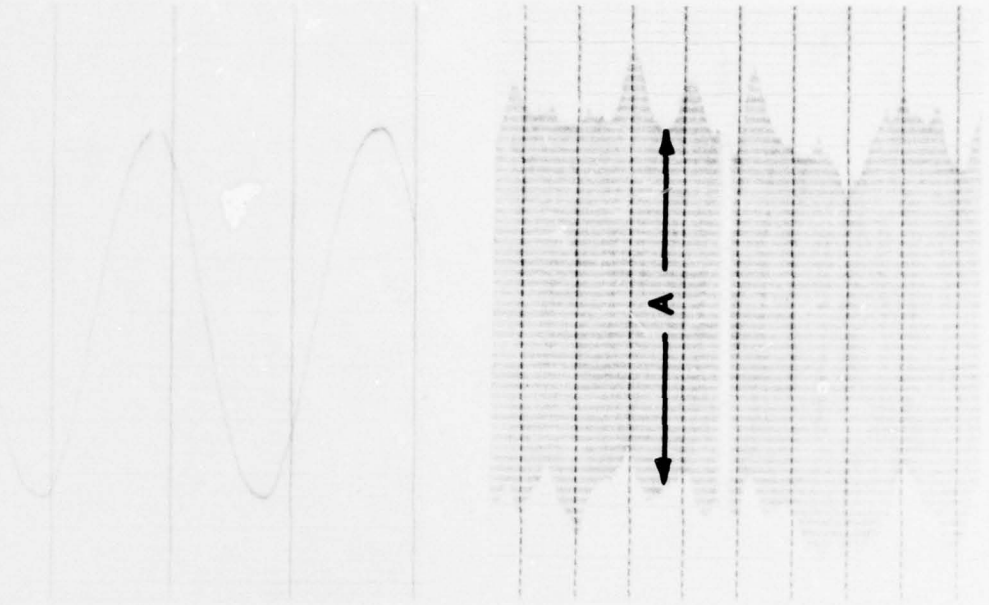

a - Chart speed = 200 cm/s

b - Chart speed = 1 cm/s

Plate 9 Typical recorded chart for the friction force.

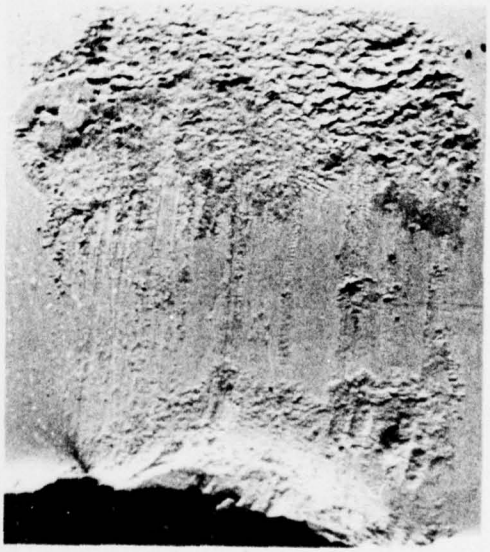

Plate 10 1 mm

S.E.M. of Ti-alloy (IMI 318)
200°C, 247 ± 170 MN/m²
272,000 cycles.

Plate 11 200 u

Optical picture of Ti-alloy (IMI 318)
400°C, 247 ± 93 MN/m²
759,000 cycles.

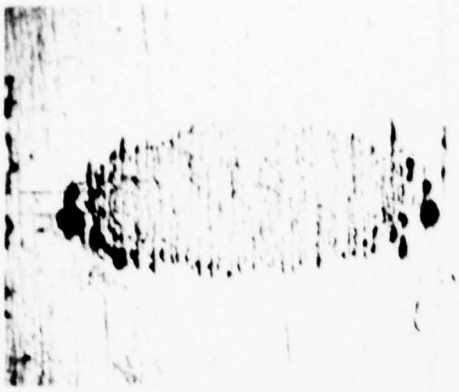

Plate 12 — 200 μ

Optical picture of Ti-alloy (AMMRC)
100°C, 400 ± 91 MN/m²
81 000 cycles.

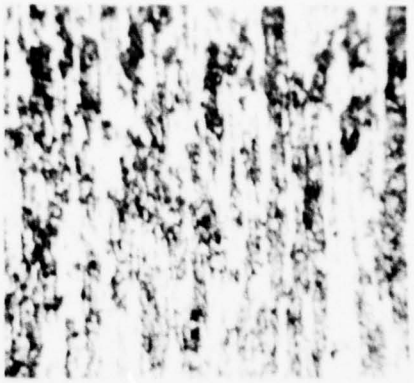

Plate 13 — 50 μ

Same as plate 12 but at higher magnification.

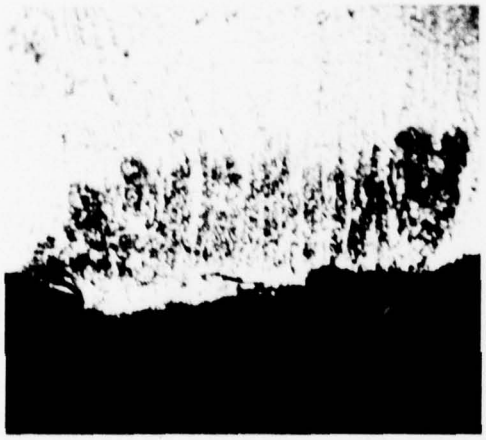

Plate 14 — 200 μ

Optical picture of Inconel 718 (aged)
280°C, 550 ± 114 MN/m²
12.6 × 10⁶ (unbroken specimen).

Plate 15 — 40 μ

Optical picture of Inconel 718 (aged)
540°C, 550 ± 260 MN/m²
981 000 cycles.

Plate 16 — 200 μ

Optical picture of Ti-alloy (AMMRC)
20°C, 10 μm slip, 3.5 × 10⁶ cycles
(sphere).

Plate 17 — 400 μ

Optical picture of Inconel 718 (aged)
20°C, 40 μm slip, 6000 cycles.

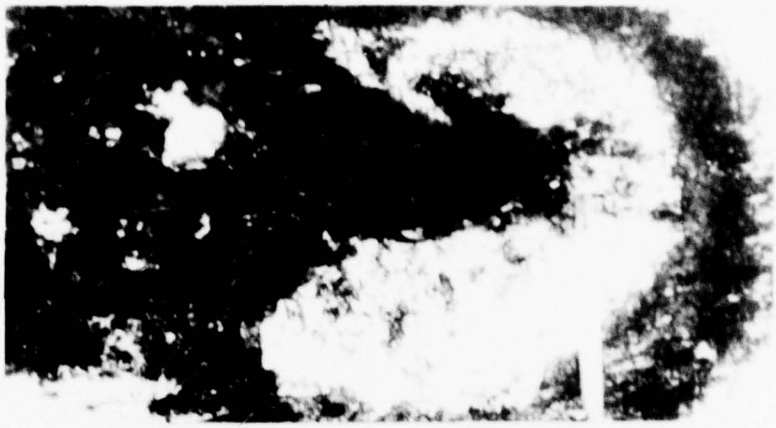

40 μ

Plate 18

Optical picture of Inconel 718
20°C, 10 μm slip, 8 x 10^4 cycles.

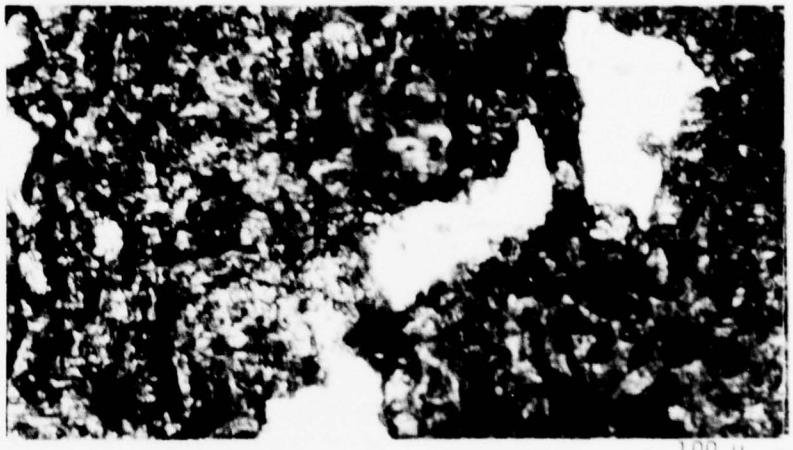

100 μ

Plate 19

Optical picture of Inconel 718
20°C, 40 μm slip, 10^6 cycles.

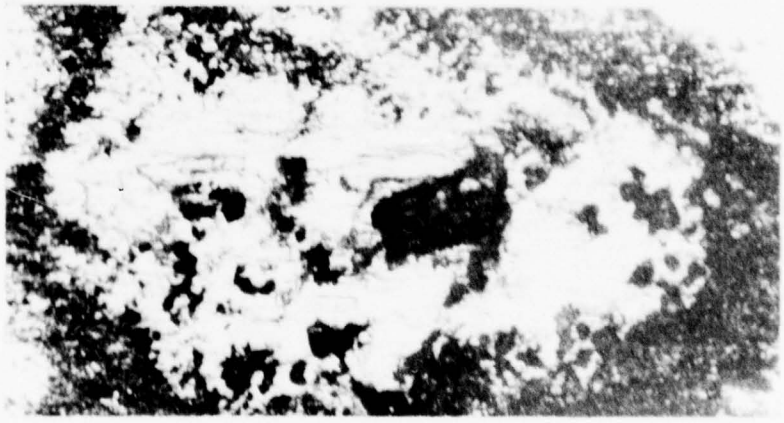

100 μ

Plate 20

Optical picture of Inconel 718
280°C, 40 μm slip, 10^6 cycles.

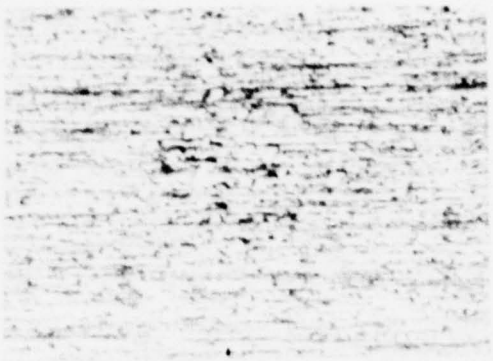

Plate 21 400 μ

Optical picture of Ti-alloy (AMMRC)
20°C, 10 μ m slip, 6000 cycles

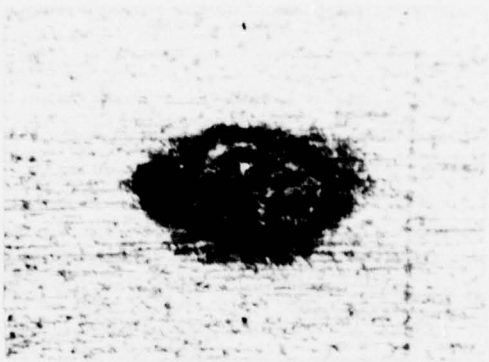

Plate 22 400 μ

Optical picture of Ti-alloy (AMMRC)
20°C, 10 μ m slip, 10^5 cycles

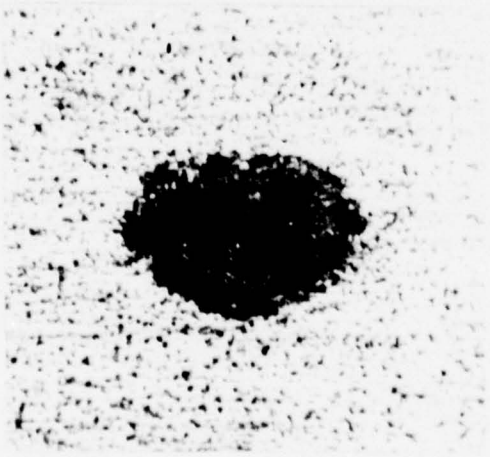

Plate 23 400 μ

Optical picture of Ti-alloy (AMMRC)
20°C, 10 μ m slip, 3.5×10^6 cycles

Plate 24 400 μ

Optical picture of Ti-alloy (AMMRC)
20°C, 40 μ m slip, 6000 cycles

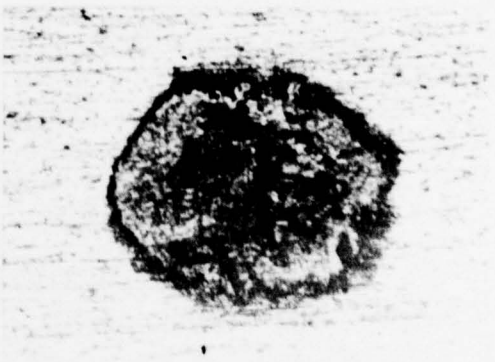

Plate 25 400 μ

Optical picture of Ti-alloy (AMMRC)
20°C, 40 μ m slip, 10^5 cycles

Plate 26 400 μ

Optical picture of Ti-alloy (AMMRC)
20°C, 40 μ m slip, 3×10^6 cycles

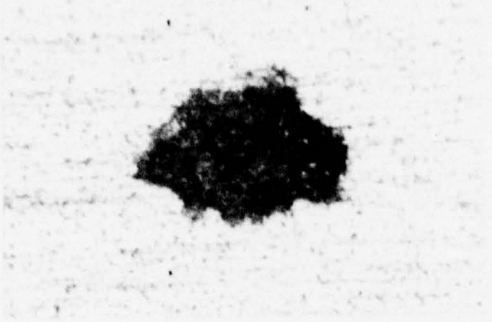

Plate 27 400 μ

Optical picture of Ti-alloy (AMMRC)
100°C, 40 μ m slip, 6000 cycles

Plate 30 400 μ

Optical picture of Incomel 718
20°C, 40 μ m slip, 6000 cycles

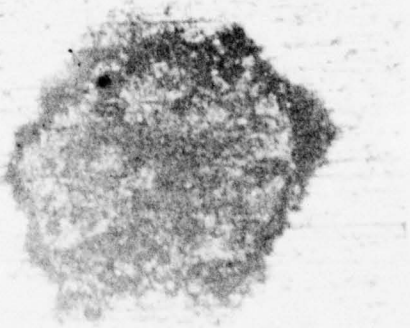

Plate 28 400 μ

Optical picture of Ti-alloy (AMMRC)
100°C, 40 μ m slip, 10^5 cycles

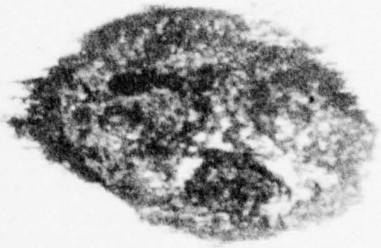

Plate 31 400 μ

Optical picture of Inconel 718
20°C, 40 μ m slip, 8×10^4 cycles

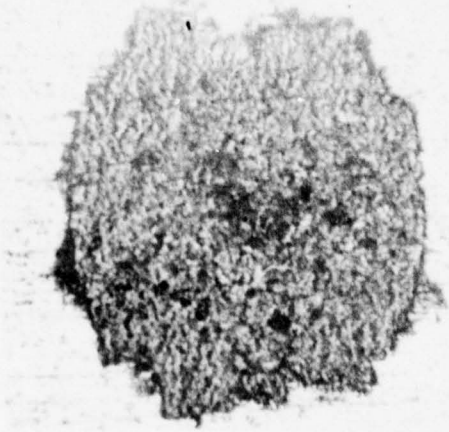

Plate 29 400 μ

Optical picture of Ti-alloy (AMMRC)
100°C, 40 μ m slip, 3.5×10^6 cycles

Plate 32 400 μ

Optical picture of Inconel 718
20°C, 40 μ m slip, 10^5 cycles

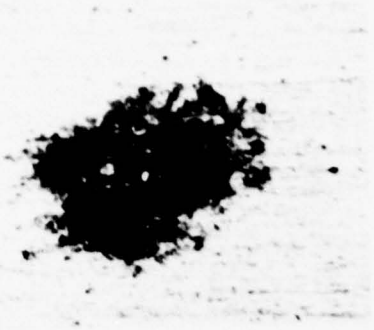

Plate 33 — 400 μ

Optical picture of Inconel 718
540°C, 40 μ m slip, 6000 cycles

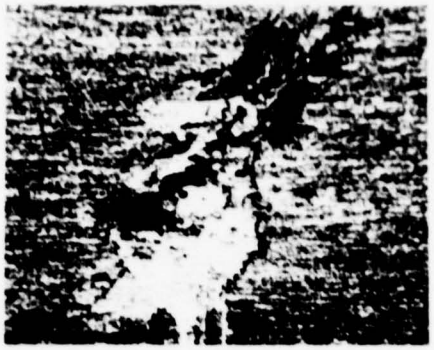

Plate 34 — 400 μ

Optical picture of Inconel 718
540°C, 40 μ m slip, 10^6 cycles

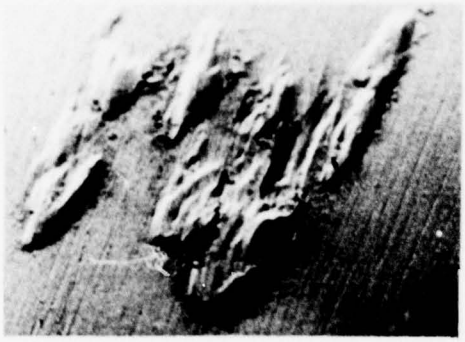

Plate 35 — 400 μ

S.E.M. of Ti-alloy (IMI 318)
600°C, 247 ± 62 MN/m²
10^6 cycles, (unbroken specimen)

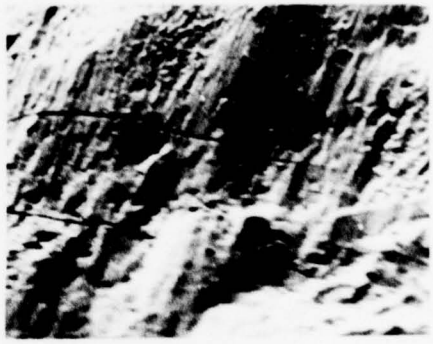

Plate 36 — 40 μ

Same as plate 35 but at higher magnification

Plate 37 — 400 μ

Same as plate 35 but for the bridge foot

Plate 38 — 10 μ

S.E.M. of Ti-alloy (IMI 318)
200°C, 247 ± 139 MN/m²
210 000 cycles

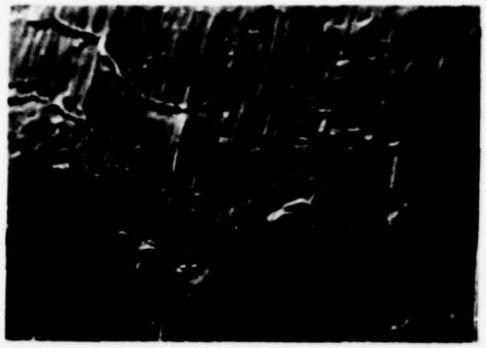

Plate 39 — 40 μ

S.E.M. of Ti-alloy (IMI 318)
400°C, 247 ± 93 MN/m²
750 000 cycles

Plate 40 — 10 μ

S.E.M. of Ti-Alloy (IMI 318)
600°C, 247 ± 124 MN/m²
119 000 cycles, (bridge foot)

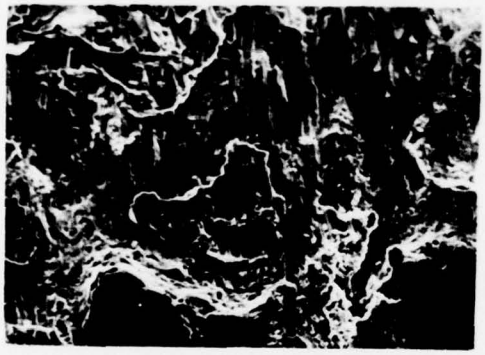

Plate 41 — 100 μ

S.E.M. of Ti-alloy (IMI 318)
400°C, 247 ± 108 MN/m²
222 000 cycles

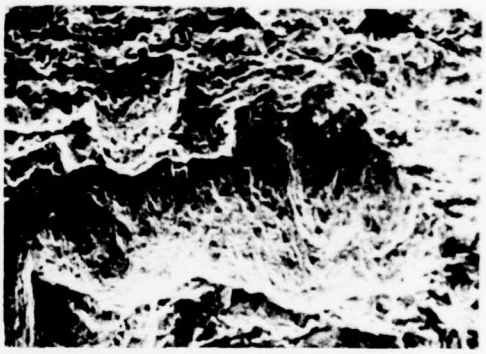

Plate 42 — 100 μ

S.E.M. of Ti-alloy (IMI 318)
400°C, 247 ± 154 MN/m²
137 000 cycles

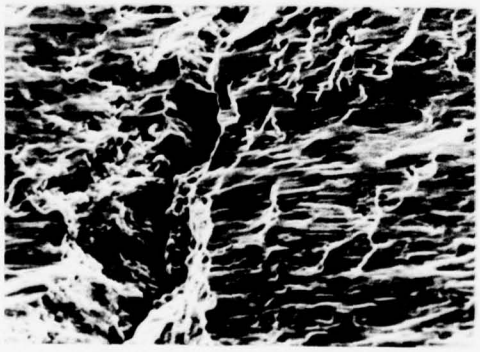

Plate 43 — 100 μ

S.E.M. of Ti-alloy (IMI 318)
400°C, 247 ± 170 MN/m²
118 000 cycles

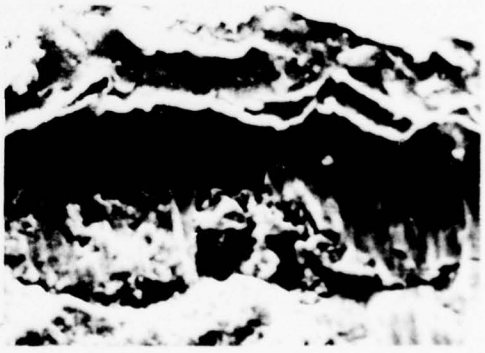

Plate 44 — 10 μ

S.E.M. of Ti-alloy (IMI 318)
400°C, 247 ± 124 MN/m²
183 000 cycles

Plate 45 — 40 μ

S.E.M. of Ti-alloy (IMI 318)
600°C, 247 ± 154 MN/m²
97 000 cycles, (bridge foot)

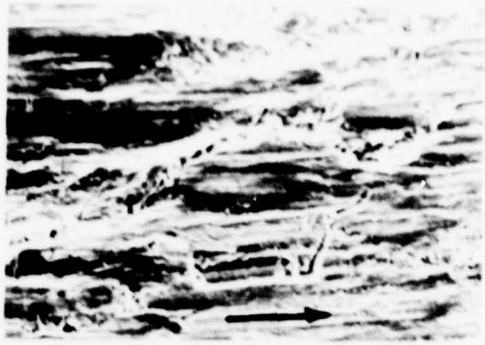

Plate 46 — 40 μ

Same as plate 45 but at another position

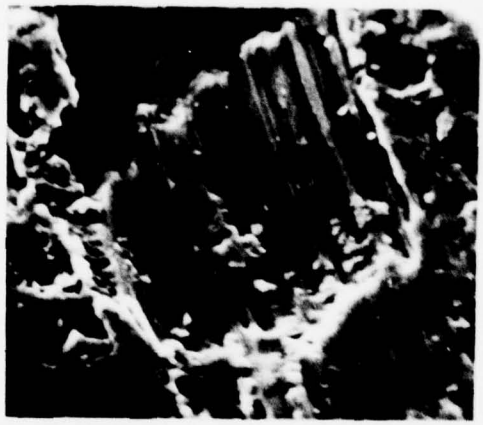

Plate 47 — 10 μ

S.E.M. of Ti-alloy (IMI 318)
400°C, 247 ± 77 MN/m²
11 x 10^6 cycles

Plate 48 — 10 μ

S.E.M. of Ti-alloy (IMI 318)
200°C, 247 ± 93 MN/m²
940 000 cycles

Plate 49 — 100 μ

S.E.M. of Ti-alloy (IMI 318)
400°C, 247 ± 93 MN/m²
5 814 000 cycles

Plate 50 — 20 μ

S.E.M. of Ti-alloy (IMI 318)
400°C, 247 ± 108 MN/m²
222 000 cycles

Plate 51 — 100 μ

S.E.M. of Ti-alloy (IMI 318)
400°C, 247 ± 93 MN/m²
479 000 cycles

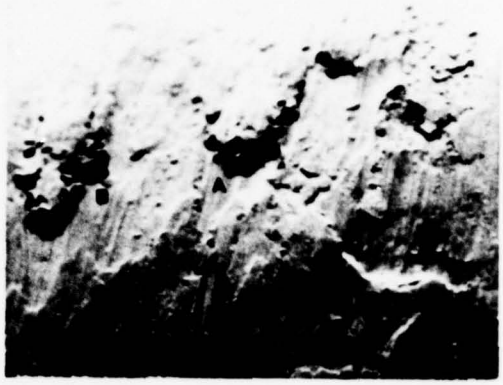

Plate 52 — 400 μ

S.E.M. of Ti-alloy (IMI 318)
600°C, 247 ± 170 MN/m²
24 000 cycles, (bridge foot)

Plate 53 — 40 μ

Same as plate 52 at site A

Plate 54 — 10 μ

Same as plate 53 but at higher magnification

Plate 55 — 10 μ

Same as plate 53 but at higher magnification

Plate 56 — 40 μ

S.E.M. of Ti-alloy (IMI 318)
600°C, 247 ± 139 MN/m²
45 000 cycles

Plate 57 — 10 μ

Same as plate 56 but at higher magnification.

Plate 58 — 400 μ

S.E.M. of Ti-alloy (AMMRC)
$20^{\circ}C$, 400 ± 84 MN/m^2
20×10^6 cycles (unbroken specimen).

Plate 59 — 100 μ

Same as plate 58 but at higher magnification for the bottom left-hand corner.

Plate 60 — 20 μ

Same as plate 58 but at higher magnification for the centre of the scar.

Plate 61 — 400 μ

S.E.M. of Ti-alloy (AMMRC)
$20^{\circ}C$, 400 ± 176 MN/m^2
81 000 cycles.

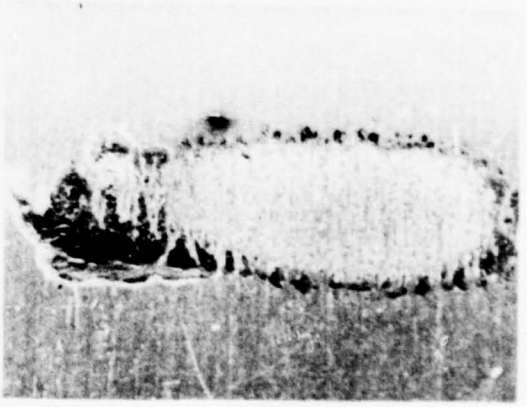

Plate 62 — 400 μ

S.E.M. of Ti-alloy (AMMRC)
$100^{\circ}C$, 400 ± 83 MN/m^2
12×10^6 cycles (unbroken specimen).

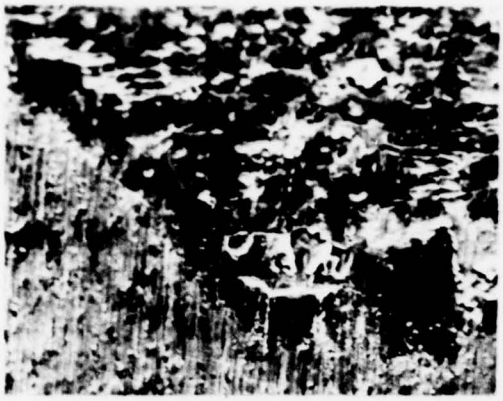

Plate 63 — 40 μ

S.E.M. of Ti-alloy (AMMRC).
Same as plate 61 but at higher magnification for the bottom left-hand corner.

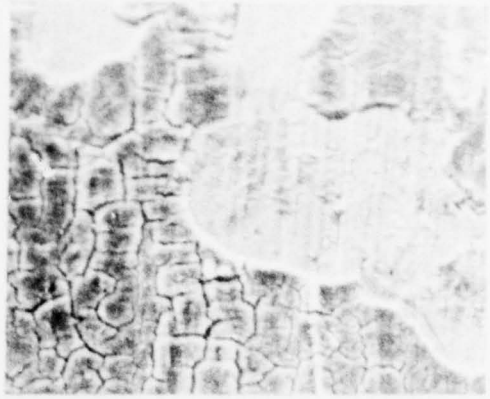

Plate 64 — 40 μ

S.E.M. of Ti-alloy (AMMRC)
100°C, 400 ± 164 MN/m²
86 000 cycles.

Plate 65 — 200 μ

S.E.M. of Ti-alloy (AMMRC)
20°C, 400 ± 151 MN/m²
141 000 cycles.

Plate 66 — 20 μ

Same as plate 65 but at higher magnification.

Plate 67 — 400 μ

S.E.M. of Ti-alloy (AMMRC)
100°C, 400 ± 152 MN/m²
122 000 cycles.

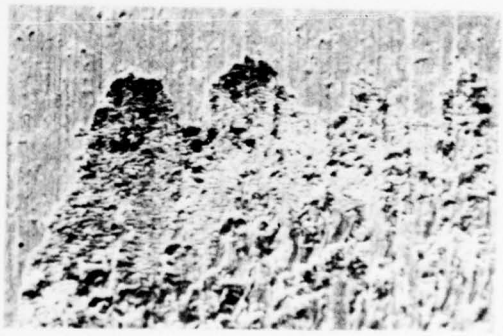

Plate 68 — 100 μ

Same as plate 67 but at higher magnification for the top left-hand corner of the scar.

Plate 69 — 40 μ

Same as plate 67 but at the fracture edge.

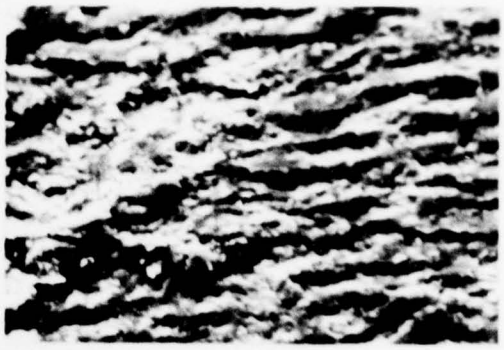

Plate 70 — 20 μ

Same as plate 69 but at higher magnification.

Plate 71 — 200 μ

S.E.M. of Inconel 718, aged
20°C, 550 ± 260 MN/m²
131 00 cycles.

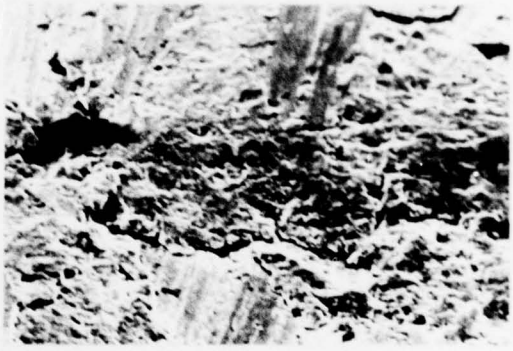

Plate 72 — 40 μ

S.E.M. of Inconel 718, aged
20°C, 550 ± 300 MN/m²
83 000 cycles.

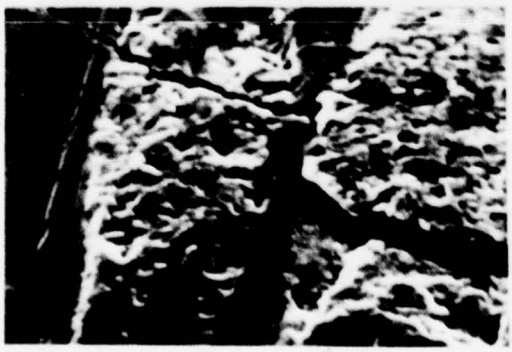

Plate 73 — 10 μ

Same as plate 72 but for another part of the scar.

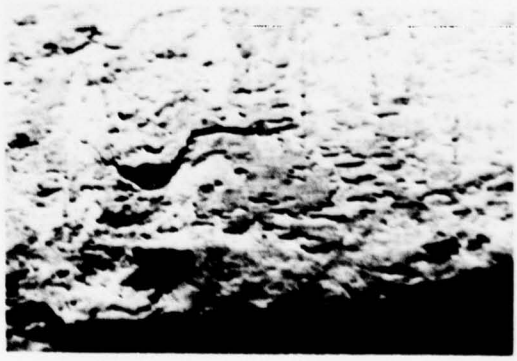

Plate 74 — 40 μ

S.E.M. of Inconel 718, aged
20°C, 550 ± 120 MN/m²
10^7 cycles (unbroken specimen).

Plate 75 — 10 μ

Same as plate 74 but at higher magnification.

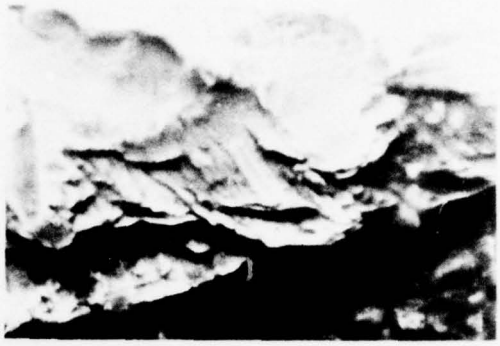

Plate 76 — 4 μ

S.E.M. of Inconel 718, aged $20^{o}C$, $550 \pm 132\ MN/m^2$
566 000 cycles.

Plate 77 — 10 μ

S.E.M. of Inconel 718, aged $280^{o}C$, $550 \pm 350\ MN/m^2$
212 000 cycles.

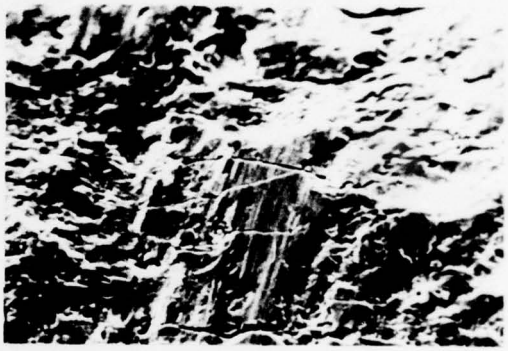

Plate 78 — 20 μ

Same as plate 77 but at another area.

Plate 79 — 20 μ

Same as plate 77 but at another area.

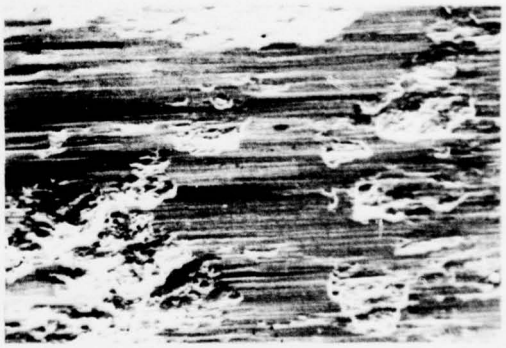

Plate 80 — 100 μ

S.E.M. of Inconel 718, aged $280^{o}C$, $550 \pm 260\ MN/m^2$
1 780 000 cycles.

Plate 81 — 100 μ

Same as plate 80 but for another area.

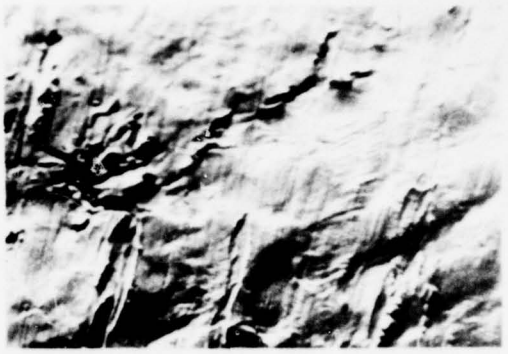

Plate 82 — 20 μ

Same as plate 80 but for another area.

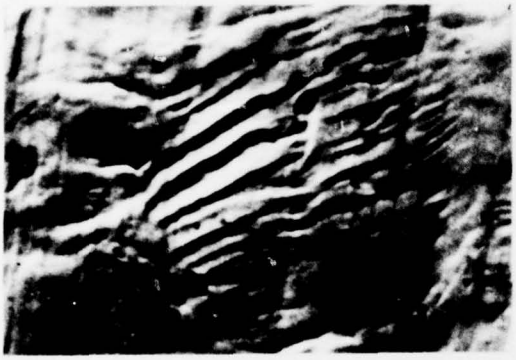

Plate 83 — 4 μ

Same as plate 82 but at higher magnification.

Plate 84 — 10 μ

Same as plate 80 but for another area.

Plate 85 — 10 μ

S.E.M. of Inconel 718, aged 280°C, 550 ± 114 MN/m^2
12 × 10^7 cycles (unbroken specimen).

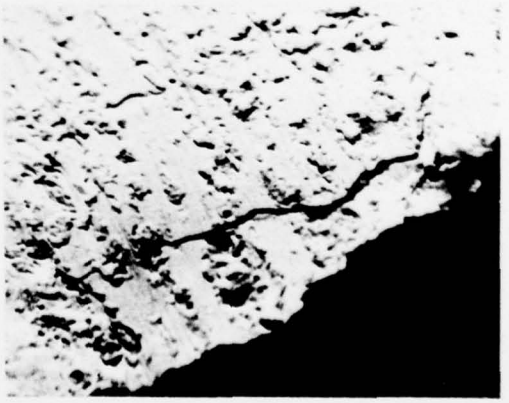

Plate 86 — 40 μ

S.E.M. of Inconel 718, aged 280°C, 550 ± 143 MN/m^2
4 600 000 cycles.

Plate 87 — 20 μ

Same as plate 86 but for another area.

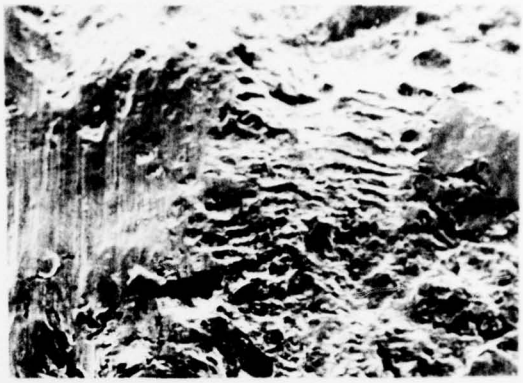

Plate 88 — 100 μ

S.E.M. of Inconel 718, aged 540°C, 550 ± 350 MN/m² 56 000 cycles.

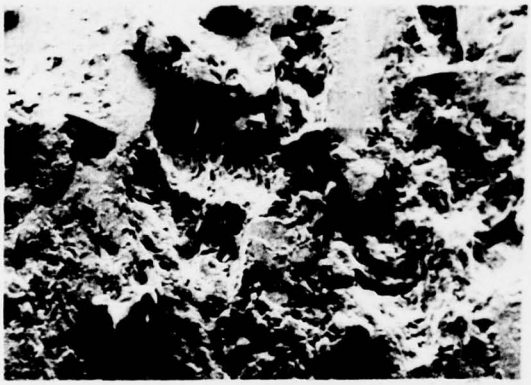

Plate 89 — 40 μ

Same as plate 88 but for another area.

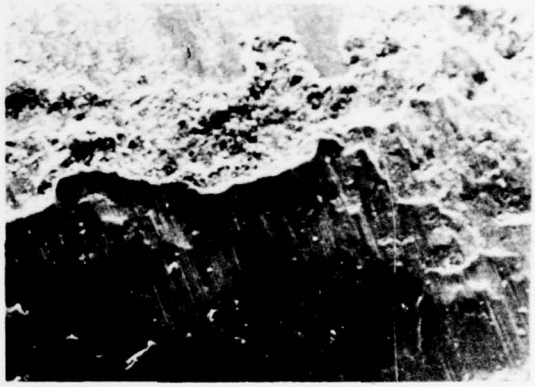

Plate 90 — 40 μ

Same as plate 88 but for the bridge foot.

Plate 91 — 40 μ

Same as plate 90 but for another area.

Plate 92 — 10 μ

Same as plate 90 but for another area.

Plate 93 — 40 μ

Same as plate 90 but for another area.

Plate 94 — 10 μ

Same as plate 93 but at higher magnification.

Plate 95 — 10 μ

Same as plate 93 but at higher magnification.

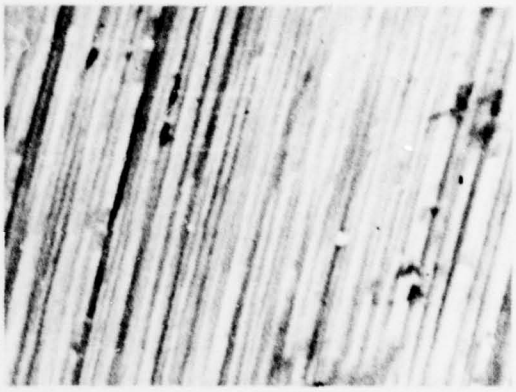

Plate 96 — 10 μ

S.E.M. of Inconel 718, aged 540°C, 550 ± 240 MN/m² 2 650 000 cycles (unbroken specimen).

Plate 97 — 100 μ

Same as plate 96 but for another area.

Plate 98 — 20 μ

Same as plate 97 but at higher magnification.

Optical picture of Inconel 718
280°C, 40 μm slip, 10^6 cycles.

Plate 99 — 10 u

Same as plate 96 but for the bridge feet.

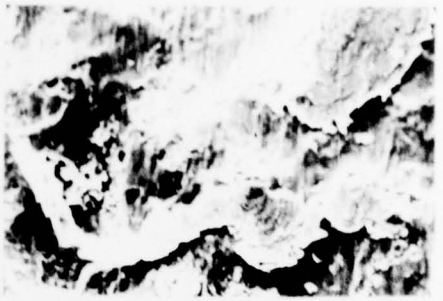

Plate 100 — 40 u

Same plate 99 but for another area.

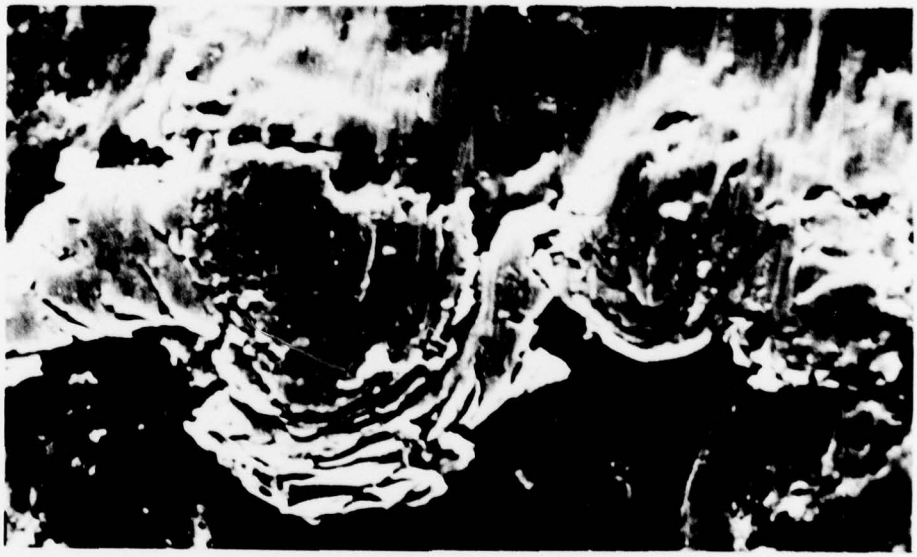

Plate 101 — 20 u

Same as plate 100 but at higher magnification.

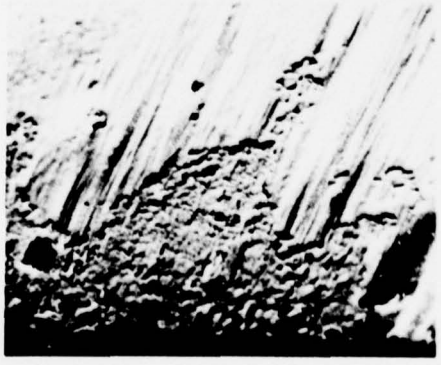

Plate 102 — 100 u

S.E.M. of Inconel 718, aged 700°C, 550 ± 228 MN/m²
4 160 000 cycles.

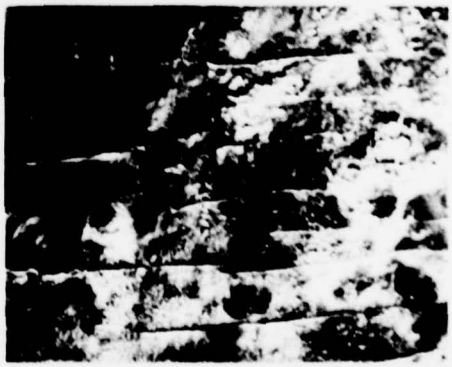

Plate 103 — 40 u

Same as plate 102 but for another area.

Plate 104 — 100 μ

Same as plate 102 but for another area.

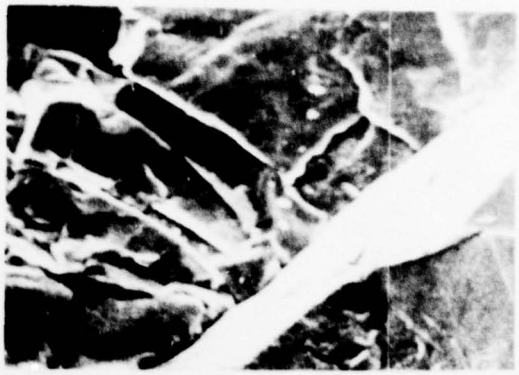

Plate 105 — 10 μ

Same as plate 104 but at higher magnification.

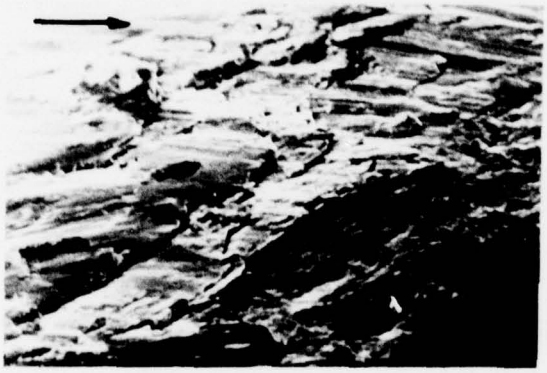

Plate 106 — 40 μ

S.E.M. of Inconel 718, annealed
$20^{o}C$, 256 ± 170 MN/m^2
673 000 cycles.

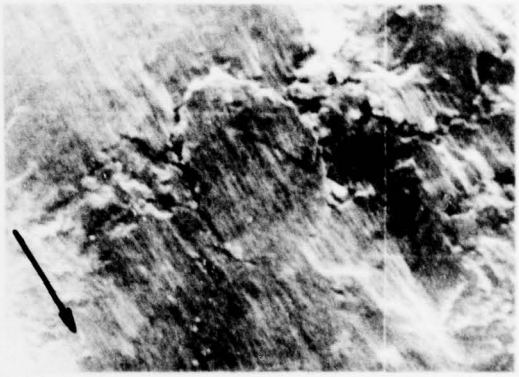

Plate 107 — 40 μ

S.E.M. of Inconel 718, annealed
$600^{o}C$, 256 ± 170 MN/m^2
249 000 cycles (unbroken specimen).

Plate 108 — 10 μ

Same as plate 107 but for another area.

Plate 109 — 200 μ

S.E.M. of Ti-alloy (AMMRC)
20^{o}, 40 μm slip, 6000 cycles.

Plate 110 — 100 μ

Same as plate 109 but at higher magnification.

Plate 111 — 10 μ

Same as plate 109 but at the edge of the scar at higher magnification.

Plate 112 — 200 μ

Same as plate 109 but after ultrasonic cleaning.

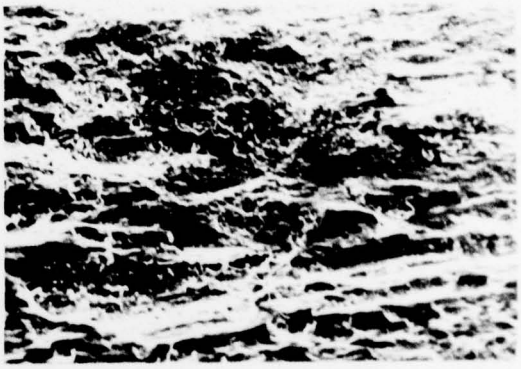

Plate 113 — 100 μ

Same as plate 112 but at higher magnification.

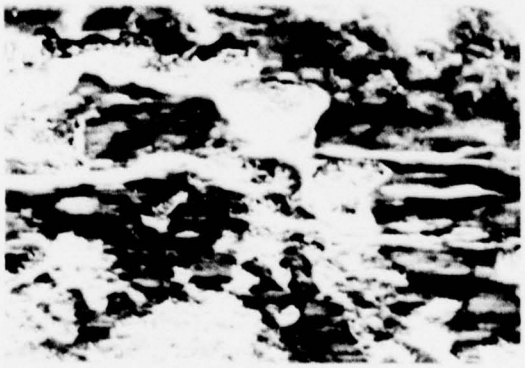

Plate 114 — 40 μ

S.E.M. of Ti-alloy (AMMRC)
20^{0}C, 40 μm slip, 10^{5} cycles.

Plate 115 — 200 μ

S.E.M. of Ti-alloy (AMMRC)
20^{0}C, 40 μm slip, 3×10^{6} cycles.

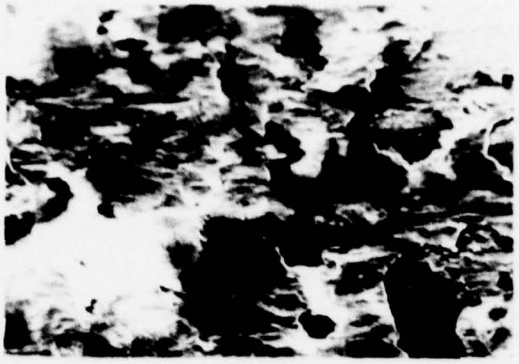

Plate 116 — 100 μ

Same as plate 115 but at higher magnification.

Plate 117 — 40 μ

S.E.M. of Ti-alloy (AMMRC)
20^{o}C, 10 μm slip, 6000 cycles.

Plate 118 — 20 μ

Same as plate 117 but at higher magnification.

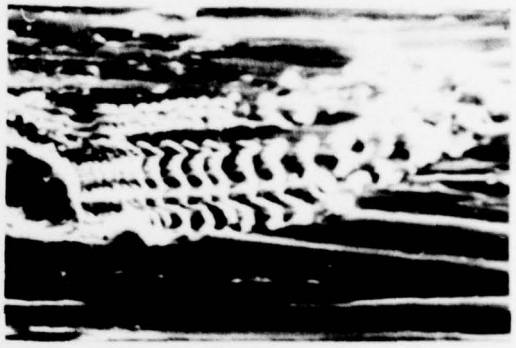

Plate 119 — 10 μ

Same as plate 118 but at higher magnification.

Plate 120 — 100 μ

S.E.M. of Ti-alloy (AMMRC)
100^{o}C, 40 μm slip, 3.5×10^{6} cycles.

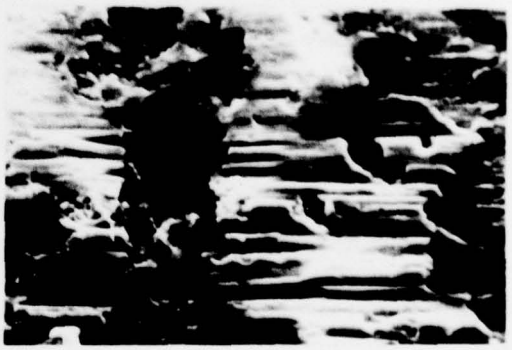

Plate 121 — 20 μ

Same as plate 120 but at higher magnification.

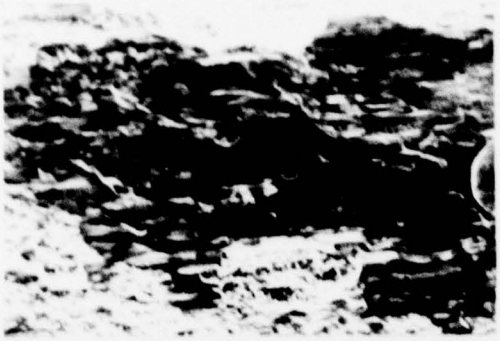

Plate 122 — 40 μ

S.E.M. of Ti-alloy (AMMRC)
100°C, 10 μm slip, 10^5 cycles.

Plate 123 — 100 μ

S.E.M. of Inconel 718
20°C, 10 μm slip, 6000 cycles.

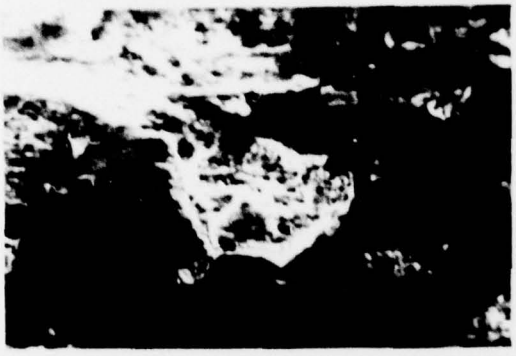

Plate 124 — 20 μ

Same as plate 123 but at higher magnification.

Plate 125 — 400 μ

S.E.M. of Inconel 718
20°C, 10 μm slip, 8×10^4 cycles.

Plate 126 — 20 μ

Same as plate 125 but at higher magnification.

Plate 127 — 200 μ

S.E.M. of Inconel 718
20°C, 10 μm slip, 10^6 cycles.

Plate 128 — 40 μ

Same as plate 127 but at higher magnification.

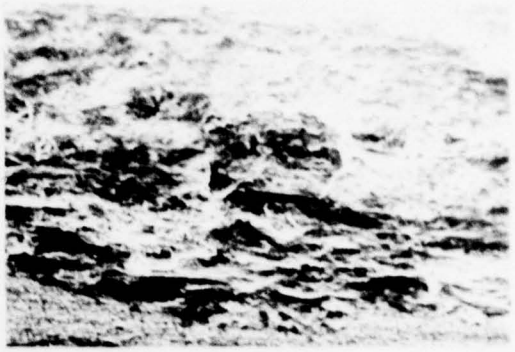

Plate 129 — 100 μ

S.E.M. of Inconel 718
$20^{o}C$, 40 μm slip, 6000 cycles.

Plate 130 — 400 μ

S.E.M. of Inconel 718
$20^{o}C$, 40 μm slip, 8×10^{4} cycles.

Plate 131a — 400 μ

S.E.M. of Inconel 718
$20^{o}C$, 40 μm slip, 10^{6} cycles.

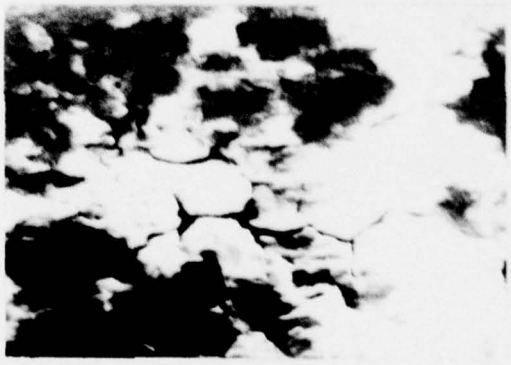

Plate 131b — 40 μ

Same as plate 131a but at higher magnification.

Plate 132 — 10 μ

S.E.M. of Inconel 718
Same as plate 130 but at the edge of the scar at higher magnification.

Plate 133 — 100 μ

S.E.M. of Inconel 718
280°C, 10 μm slip, 6000 cycles.

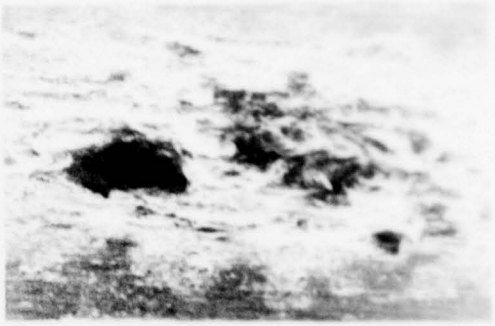

Plate 134 — 100 μ

S.E.M. of Inconel 718
280°C, 10 μm slip, 8×10^4 cycles.

Plate 135 — 20 μ

Same as plate 134 but at higher magnification.

Plate 136 — 100 μ

S.E.M. of Inconel 718
280°C, 10 μm slip, 10^6 cycles.

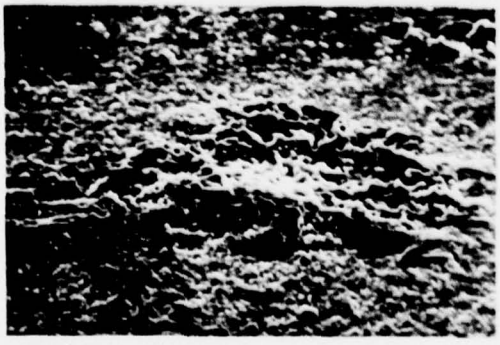

Plate 137 — 20 μ

Same as plate 136 but at higher magnification.

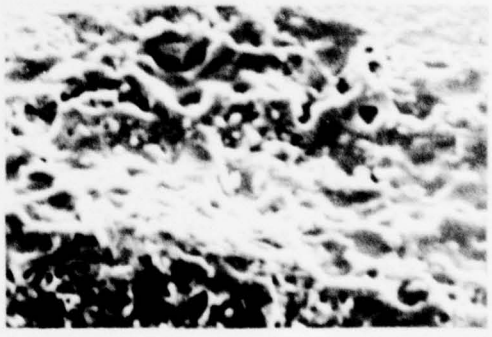

Plate 138 — 10 μ

Same as plate 137 but at higher magnification.

Plate 139 — 200 μ

S.E.M. of Inconel 718
280°C, 40 μm slip, 6000 cycles.

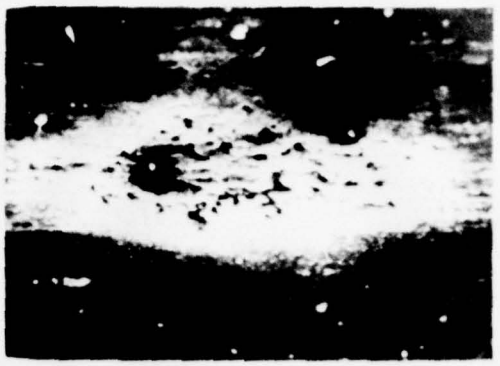

Plate 140 — 100 μ

S.E.M. of Inconel 718
280°C, 40 μm slip, 8×10^4 cycles.

Plate 141 — 200 μ

S.E.M. of Inconel 718
280°C, 40 μm slip, 10^6 cycles.

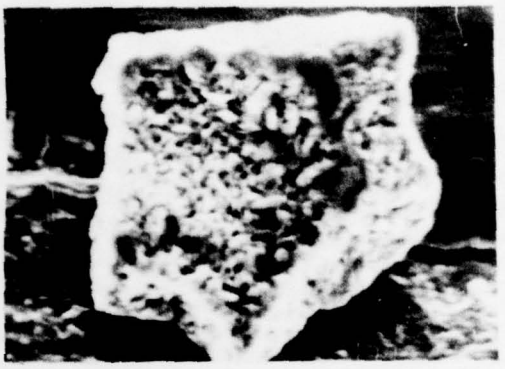

Plate 142 — 10 μ

Same as plate 139 but at higher magnification.

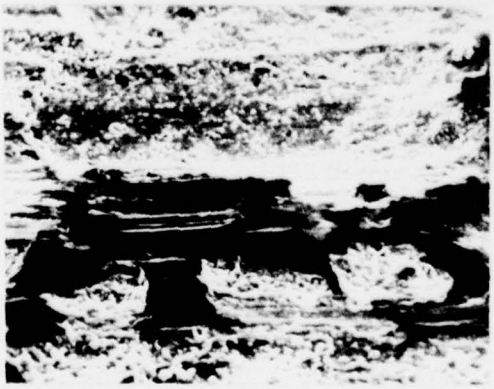

Plate 143 — 40 μ

Same as plate 140 but at higher magnification.

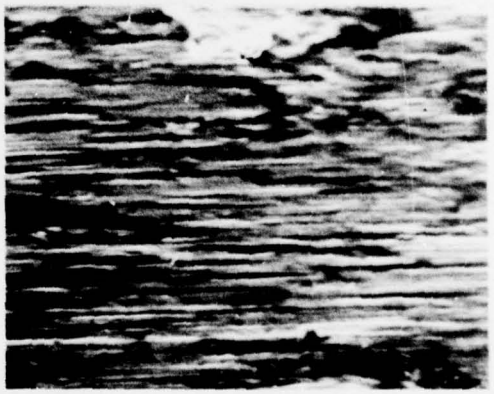

Plate 144 — 20 μ

Same as plate 141 but at higher magnification.

S.E.M. of Ti-alloy (AMMRC)
100°C, 400 ± 152 MN/m²
122 000 cycles.

Same as plate 67 but at higher magnification for the top left-hand corner of the scar.

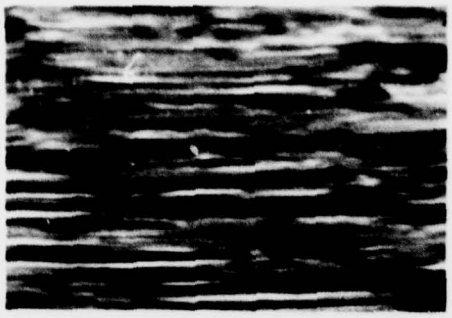

Plate 145 — 10 μ

Same as plate 144 but at higher magnification.

Plate 146 — 40 μ

Same as plate 141 but at higher magnification.

Plate 147 — 40 μ

S.E.M. of Inconel 718
540°C, 10 μm slip, 6000 cycles.

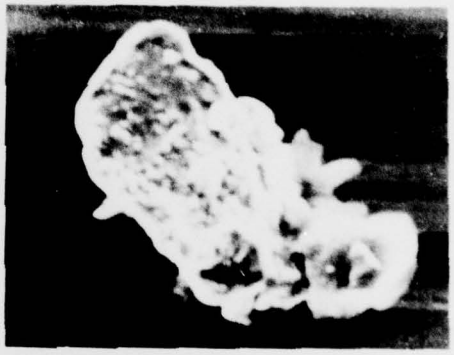

Plate 148 — 4 μ

S.E.M. of Inconel 718
540°C, 10 μm slip, 10^6 cycles.

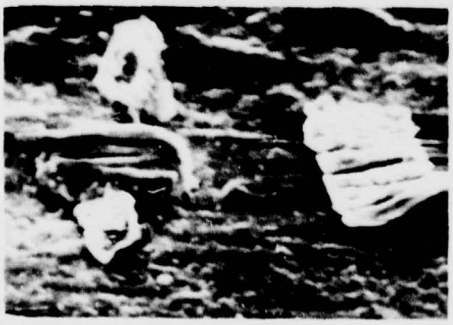

Plate 149 — 10 μ

Same as plate 148 but at another area of the scar.

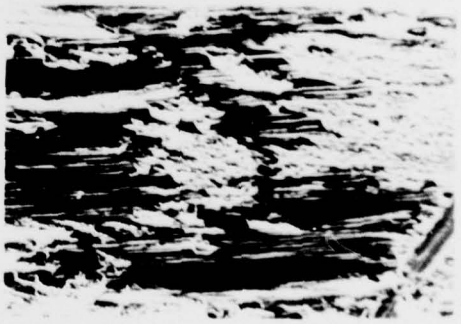

Plate 150 — 40 μ

S.E.M. of Inconel 718
540°C, 40 μm slip, 8×10^4 cycles.

Plate 151

4 μ

Same as plate 150 but at higher magnification.

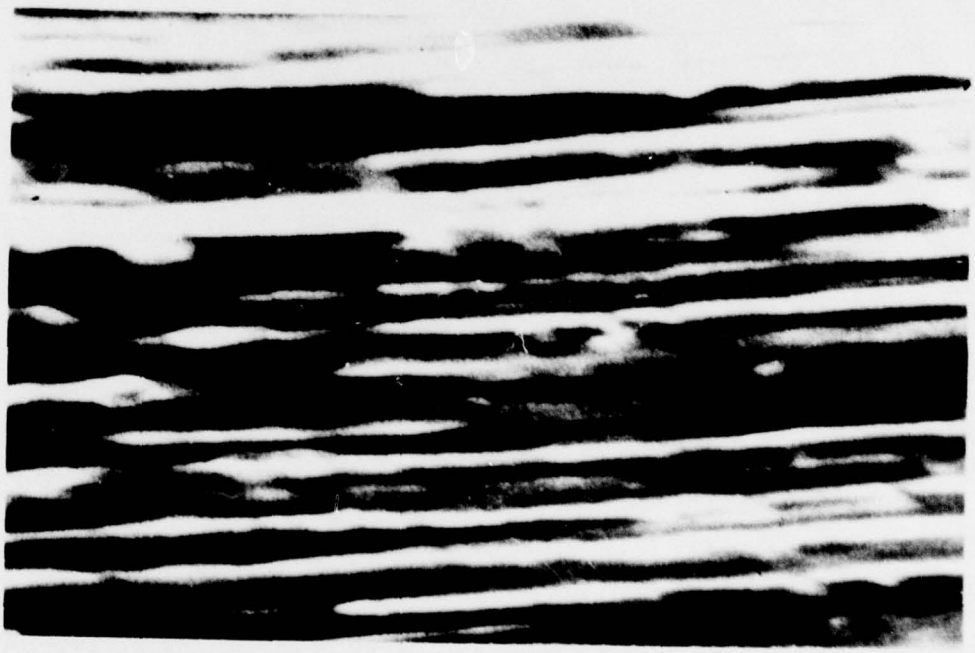

Plate 152

4 μ

Same as plate 150 but at higher magnification.